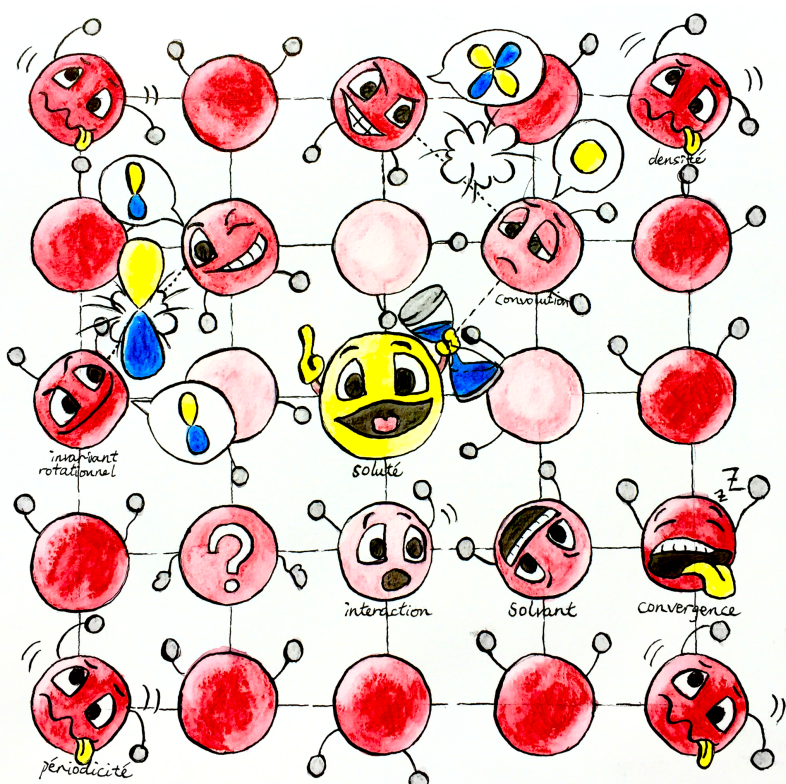


# MOLECULAR DENSITY FUNCTIONAL THEORY UNDER HOMOGENEOUS REFERENCE FLUID APPROXIMATION

LU DING

Under the direction of  
DANIEL BORGIS, LUC BELLONI & MAXIMILIEN LEVESQUE



SYSTEMATIC PREDICTION OF SOLVATION PROPERTIES  
WITH MOLECULAR-SCALE LIQUID THEORY



## ABSTRACT

---

In this thesis, two algorithms of excess energy functional evaluation are proposed, one is extension of the previous work, one is ... The new algorithm combines the molecular Ornstein-Zernike equation method with MDFT

It is shown that ...

The new method is able to calculate ...

## RÉSUMÉ

---



*When you are studying any matter, or considering any philosophy, ask yourself only,  
what are the facts and what is the truth that the facts bear out.  
Never let yourself be diverted either by what you wish to believe, or by what you think  
would have beneficent social effects if it were believed.  
But look only, and solely, at what are the facts.*

— Bertrand Russell

## ACKNOWLEDGEMENTS

---

First of all, I would like to express my most respectful gratitude to my thesis advisors, Daniel Borgis and Luc Belloni, who have developed the main theories used in this thesis and whose great knowledge of liquid theory as well as the genius way of thinking and explaining have given me a solid guide for doing this research. I would also like to thank them for their tireless work in correcting this manuscript.

I'm grateful to Maximilien Levesque, the other main developer of MDFT who joined the supervision of my thesis. Thanks for sharing some results and data that have proven useful to my research.

I wish to acknowledge all the great minds willing to evaluate and give ideas about my work: (**noms des jurés**), thank you for agreeing to be part of the jury of this thesis.

As a master student issue from pure chemistry speciality, a lack of knowledge about Informatics brought to me a lot of difficulties. I would like to express my sincere gratitude to my colleagues Pierre Kestener, Matthieu Haefele, and Yacine Ould-Rouis for their huge aid in Informatics and very useful advices during this thesis.

This thesis was produced at *Maison de la Simulation, CEA Saclay*, financially supported by the scholarship **IDEX-CEA**. I acknowledge all the organizations and staff that gave me the chance to have this three-year experience.

I am also grateful to Thomas Wiggins for help in correcting the huge amount of grammar faults in this manuscript.

I'm deeply indebted to my tutors during my bachelor and master, respectively Mr. Hongwei Tan and Mrs. Michelle Gupta, whose clear logic and warm encouragement gave me all that I needed to be in love with theoretical chemistry.

Finally I would like to thank my father, who made the right decision to send me here in France and support me in every aspect.



# CONTENTS

---

1	INTRODUCTION	1
1.1	Simulation of solvent effects,	1
1.2	Scope of this thesis,	3
I	STATE OF THE ART: SOLVATION, MODELS AND METHODS	5
2	MODEL OF SOLUTION SYSTEM	7
2.1	Continuum solvation models,	7
2.1.1	Poisson-Boltzmann methods,	8
2.1.2	Born / Onsager / Generalized Born models,	9
2.2	Model potential of explicit molecules,	10
2.2.1	Interaction of spherical particle,	11
2.2.2	Molecular fluid model,	12
2.2.3	Multipole and spherical harmonic expansion,	13
2.2.4	SPC/E water model,	13
2.2.5	Flexible and polarizable models,	14
2.3	Model of solute,	15
3	STATISTICAL MECHANICS OF CLASSICAL FLUIDS	17
3.1	Hamiltonian of a micro-state,	17
3.2	Time averages and ensemble averages / Partition functions and Thermo-dynamics,	18
3.3	Distribution functions,	19
4	INTEGRAL EQUATION THEORY	21
4.1	Ornstein-Zernike equation,	21
4.2	Closure,	22
4.3	RISM and 3D-RISM,	22
4.4	Molecular solvent,	22
4.5	Bulk properties and bridge function,	22
5	MOLECULAR DENSITY FUNCTIONAL THEORY	23
5.1	Equilibrium Classical DFT,	23
5.2	External Free energy,	25
5.3	Excess free energy,	25
5.3.1	Homogenous Reference Fluid Approximation,	26
5.3.2	nn_cs,	26
5.3.3	polarisation,	27
5.4	OZ Equation in MDFT and IEM Formalism,	27
5.5	Code MDFT,	27
5.5.1	Supercell discretization,	28
5.5.2	Minimizer L-BFGS-B,	28

5.5.3 Treatment to avoid unphysical density,	28
5.5.4 Evaluation of $V_{\text{ext}}$ ,	29
5.5.5 Evaluation of $V_{\text{exc}}$ ,	30
<b>6 MOLECULAR DYNAMICS &amp; MONTE CARLO SIMULATIONS</b>	<b>33</b>
6.1 Molecular Dynamics,	33
6.1.1 Principle,	33
6.1.2 Determination of free energy: umbrella sampling,	33
6.2 Monte Carlo Method,	33
6.3 Direct correlation function of water,	33
6.3.1 Dipole DCF from molecular dynamics simulation,	33
6.3.2 Extraction of DCF from bulk Monte Carlo simulation,	33
6.3.3 Conventions,	33
6.3.4 Comparison with non-coupling dipole DCF in MDFT ( $n_{\max} = 1$ ),	34
6.3.5 Comparison with respect to $n_{\max}$ ,	34
6.3.6 Transform between ck_angular and projections,	34
6.4 Umbrella sampling,	34
<b>II THEORY: HRF APPROXIMATION, FOR MOLECULAR SOLVENT</b>	<b>35</b>
<b>7 REDUCTION OF SPATIAL CONVOLUTION BY FFT</b>	<b>37</b>
7.1 Using intermolecular DCF,	38
7.1.1 Zero-order interpolation of DCF,	40
7.1.2 Linear interpolation of DCF,	40
7.2 Direct calculation of DCF from rotational invariant projections,	41
7.2.1 Using projections in form of $\hat{c}_{\mu\nu}^{mn}(k)$ ,	41
7.2.2 Using projections in form of $\hat{c}_{\mu\nu,\chi}^{mn}(k)$ ,	42
<b>8 ANGULAR CONVOLUTION, A BETTER ALGORITHM</b>	<b>43</b>
8.1 Angular convolution using Blum's reduction,	43
8.2 Fast generalized spherical harmonic transform,	44
8.2.1 Equivalence of order in angular quadratures and projections,	45
8.2.2 Integration of $\Phi, \Psi$ using FFT,	46
8.3 Operational algorithm,	48
8.3.1 Reduction by symmetry,	49
8.3.2 Commutativity between operations,	49
<b>9 FREE ENERGY AND RELATED THERMODYNAMIC QUANTITIES</b>	<b>53</b>
9.1 Free energy correction for single ions,	53
9.1.1 Correction of type B,	53
9.1.2 Correction of type C,	54
9.2 Some related thermodynamic quantities,	54
9.2.1 Solubility,	55
9.2.2 Pressure,	55
<b>10 SOLVATION STRUCTURE</b>	<b>57</b>

10.1 Radial distribution function and site-site distribution function,	57
10.2 Radial polarization functions,	57
10.3 Rotational invariant expansion,	57
10.4 Rebuilt of density in a certain orientation,	57
10.4.1 Radical distribution function of numeric density,	57
10.4.2 Radical distribution function of polarization,	57
<b>III IMPLEMENTATION</b>	<b>59</b>
<b>11 ALGORITHMS AND BRANCHES</b>	<b>61</b>
11.1 Branches "naive" ,	61
11.2 Branches "convolution",	62
11.3 Testing branches for nmax=1,	62
11.4 Other paths,	62
<b>12 NUMERICAL AND PHYSICAL ACCURACY</b>	<b>63</b>
12.1 Generalized spherical harmonics transform,	63
12.1.1 FFT,	63
12.1.2 $m_{\max}$ and $n_{\max}$ of projections,	63
12.1.3 From $\rho$ to $\gamma$ ,	63
12.2 Comparison between branches,	64
12.2.1 Error evaluation in $\hat{c}(\mathbf{k}, \Omega_1, \Omega_2)$ calculation,	64
12.2.2 A single k-kernel,	64
12.2.3 k-border effect,	65
12.3 Intrinsic variation of free energy,	66
12.3.1 Spatial grid: length and resolution,	66
12.3.2 Angular grid: effect of psi,	66
12.4 Series of charged LJ centre,	66
12.4.1 Box length dependance and charge dependance of free energy,	66
12.4.2 Comparison with IET,	67
12.4.3 Comparison with DM ,	67
12.5 Premier conclusion,	67
<b>13 COMPUTING PERFORMANCE OF SEQUENTIAL CODE</b>	<b>69</b>
13.1 FFT,	69
13.2 FGSHT,	70
13.2.1 Computing time of GSHT and FGSHT,	70
13.2.2 Performance with respect to $m_{\max}$ ,	70
13.2.3 Performance with respect to $n_{\max}$ ,	70
13.3 K-kernel,	70
13.3.1 Comparison between paths,	70
13.3.2 $m_{\max}$ and $n_{\max}$ dependance of OZ equation,	70
13.4 Entire iteration of $\mathcal{F}_{\text{exc}}$ evaluation,	70
13.4.1 Comparison between "naive_standard" and "convolution_pure-angular",	70
13.4.2 Comparison between "convolution_standard" and "convolution_asymm",	71
13.4.3 Comparison between "convolution_standard" and "convolution_pure-angular",	71

13.5 Global view of the sequential code performance,	71
<b>14 COMPUTING PERFORMANCE OF PARALLEL CODE</b>	<b>73</b>
14.1 Node-level Parallelization,	73
14.2 Parallelization on Several Nodes,	73
<b>IV APPLICATIONS</b>	<b>75</b>
<b>15 IONS AND SMALL MOLECULES COMPARED TO MD SIMULATION</b>	<b>77</b>
15.0.1 ions,	77
<b>16 HYDROGEN TRANSFER REACTION OF MN-OXO: ROLE OF SOLVENT IN REACTION SIMULATION</b>	<b>79</b>
16.1 Reinvestigation of the Manganese-oxo ,	79
<b>V CONCLUSION AND PERSPECTIVES</b>	<b>81</b>
<b>17 CONCLUSION</b>	<b>83</b>
<b>18 PERSPECTIVES</b>	<b>85</b>
18.1 Reduce memory use in MDFT,	85
18.1.1 Pass to simple precision,	85
18.1.2 MPI of the L-BFGS-B minimizer,	85
18.2 Polarisable solute,	85
18.3 MDFT Viewer,	85
18.4 Classical SCF method,	85
18.5 Other branches of development about MDFT,	85
<b>VI APPENDIX</b>	<b>87</b>
<b>A BASIC CONCEPTS ABOUT COMPUTING PERFORMANCE</b>	<b>89</b>
A.1 Algorithm complexity,	89
A.2 Roofline model and memory delay,	90
A.3 Scalability of parallelized code,	91
A.4 Profiling and tracing toolkits,	92
<b>B EQUIVALENCE OF QUADRATURE-PROJECTION ORDER</b>	<b>93</b>
B.1 Gaussian quadrature,	93
B.2 Angular integration in GSHT,	93
<b>C ROTATIONAL INVARIANT EXPANSION</b>	<b>95</b>
C.1 Orthogonality of $\Phi$ ,	95
C.2 Rotational invariance of $\Phi$ ,	96
C.3 Transform in local frame,	97
C.3.1 Transform between $F_{\mu\nu}^{mn}(r)$ and $F_{\mu\nu,\chi}^{mn}(r)$ ,	97
C.3.2 Rotational invariant transform with FFT-3D,	98

c.4	Transform in fixed frame,	99	
c.4.1	Expansion of $F(\mathbf{r}, \boldsymbol{\Omega})$ on rotational invariants,	99	
c.4.2	Rebuilding of $F(\mathbf{r}, \boldsymbol{\Omega})$ from projections,	100	
c.5	Symmetry,	100	
c.5.1	Symmetric rules of $F(\omega_1, \omega_2)$ in intermolecular form,	100	
c.5.2	Symmetric rules of rotational invariant projections,	101	
D	CALCULATION OF ROTATION MATRIX ELEMENTS $R_{\mu\mu'}^m$ BY RECURRENCE	103	
D.1	Case of $m_{\max} \leq 1$ ,	103	
D.2	Case of $m_{\max} > 1$ ,	104	
D.2.1	Recurrence relation for $-m + 1 \leq \chi' \leq m - 1$ ,	104	
D.2.2	Recurrence relation for $-m + 2 \leq \chi' \leq m$ ,	104	
D.2.3	Symmetries,	105	
E	PROPERTIES OF WIGNER 3J-SYMBOL AND GSH	107	
E.1	Properties of Wigner 3j-Symbol,	107	
E.2	Properties of GSH,	108	
F	ERROR EVALUATION OF INTERPOLATION STRATEGIES FOR DCF IN LOCAL FRAME	111	
G	ORIGINAL DATA OF MDFT IMPLEMENTATION	113	
G.1	Series of charged CH <sub>4</sub> center,	113	
G.1.1	Branch “naive” result,	113	
G.1.2	Branch “standard” result,	113	
	BIBLIOGRAPHY	115	

## LIST OF FIGURES

---

- Figure 1.1 The solvation process, 2  
Figure 2.1 Continuum solvent model, 7  
Figure 2.2 Definition of cavity surfaces, 8  
Figure 2.3 Euler angles, 10  
Figure 2.4 LJ pair potential, 12  
Figure 2.5 Water models, 13  
Figure 2.6 Direct interactions, 14  
Figure 2.7 Hierarchy of models, 15  
Figure 5.1 Flowchart of code MDFT, 25  
Figure 5.2 Main structure of code MDFT, 28  
Figure 5.3 Charge density projected onto grids. (a) Solute. (b) Solvent., 30  
Figure 7.1 Molecules 1 and 2 in different coordinate systems, 38  
Figure 7.2 Rotation matrices, 39  
Figure 7.3 Rotation to k-frame, 39  
Figure 7.4  $\phi_1 - \phi_2$  distribution, 40  
Figure 8.1 Indices arrangement in a complete forward-backward process of FFT-2D, 47  
Figure 8.2 mmax to nmax, 48  
Figure 8.3 Distribution of points to be calculated according to symmetry in a 2D plan, 49  
Figure 8.4 Commutativity of operations, 50  
Figure 9.1 IQ model and summation scheme, 54  
Figure 10.1 Structure of a POINCARE node, 59  
Figure 11.1 Possible algorithms for  $\gamma$  evaluation, 61  
Figure 12.1 Schema of a k-kernel test , 64  
Figure 12.2 k-border effet, 66  
Figure 12.3 structure of gamma in rotational invariants, 66  
Figure 12.4 free energy (without correction) of charged CH<sub>4</sub> centre (-1.0 to 1.0) with respect to the box length, 67  
Figure 12.5 Parabolic charge dependence of free energy of CH<sub>4</sub> centre series, 67  
Figure 12.6 Linear dependence of charge in the comparison to IET. Old algorithm / new algorithm, without correction, 68  
Figure 12.7 Comparison to IET. Old algorithm / new algorithm, with P-scheme correction, 68  
Figure 13.1 timing FFT, 69  
Figure 13.2 Computing time of GSHT and FGSHT (per 1000 times), 70  
Figure 13.3 , 70  
Figure 13.4 , 71  
Figure 13.5 , 71  
Figure A.1 Function growth, 89  
Figure A.2 The roofline model and performance pattern, 90  
Figure A.3 Memory usage in hardware level, 91  
Figure C.1 Symmetry operations of a 2-molecule system, 100

Figure F.1 Error of finding  $\hat{c}(\mathbf{k}, \Omega_1, \Omega_2)$  by interpolation compared to direct calculation, 111

## LIST OF TABLES

---

Table 1.1	Different solvation theories,	3
Table 2.1	Parameters for SPC and SPC/E water,	14
Table 8.1	Number of FE needed by OZ equation of different form,	45
Table 11.1	Branch option in MDFT,	61
Table 12.1	Maximum absolute error introduced by a forward-backward (real-complex-real) DFT1D process on a 100-value double precision array using FFTW3 package,	63
Table 12.2	Logarithm of maximum absolute error $\lg(E_a^{\max})$ introduced by a forward-backward GSHT process.,	64
Table 12.3	Maximum absolute error introduced by paths of a k-kernel test,	
	65	
Table 12.4	Error in $\gamma(\mathbf{r}, \Omega)$ and $\mathcal{F}_{\text{exc}}$ before border correction,	65
Table 12.6	Parameters of charged Lenard-Jones centre (modified from CH <sub>4</sub> ) ,	
	67	

## NOTATIONS

---

$\mathcal{F}[\rho]$	Solvation free energy functional [ $\text{kJ} \cdot \text{mol}^{-1}$ ] -
$\rho(\mathbf{r}, \Omega)$	Density of solvent [ $\text{\AA}^{-3}$ ]-
$\mathcal{F}_{\text{id}}[\rho]$	Ideal free energy functional [ $\text{kJ} \cdot \text{mol}^{-1}$ ] -
$\mathcal{F}_{\text{ext}}[\rho]$	External free energy functional [ $\text{kJ} \cdot \text{mol}^{-1}$ ] -
$\mathcal{F}_{\text{exc}}[\rho]$	Excess free energy functional [ $\text{kJ} \cdot \text{mol}^{-1}$ ]-
$\gamma(\mathbf{r}, \Omega)$	Gradient of excess free energy functional, []-
$q_e$	Elementary charge, $q_e = 1.602176565 \cdot 10^{-19}$ [C]
$\epsilon_0$	Vacuum permittivity, $\epsilon_0 = 8.854187817 \cdot 10^{-12}$ [ $\text{C}^2 \cdot \text{J}^{-1} \cdot \text{m}^{-1}$ ]
$N_A$	Avogadro constant, $N_A = 6.02214129 \cdot 10^{23}$ [ $\text{mol}^{-1}$ ].
$f_Q$	$f_Q = q_e^2 10^{-3} N_A / (4\pi\epsilon_0 10^{-10})$ , electrostatic potential unit so that $f_Q \cdot q^2 / r$ is in [ $\text{kJ} \cdot \text{mol}^{-1}$ ], where $q$ is the number charge without unity, $r$ in [ $\text{\AA}$ ].
$K_B$	Boltzmann constant, $K_B = 1.3806488 \cdot 10^{-23}$ [ $\text{J} \cdot \text{K}^{-1}$ ]
$\rho_0$	Bulk solvent angular density, $n_0 = \int d\Omega \rho_0 = 8\pi^2 \rho_0$ is the bulk solvent number density, both of unity [ $\text{\AA}^{-3}$ ]-
$\beta$	$\beta = (K_B T)^{-1}$ , reciprocal of the thermodynamic temperature [ $\text{mol} \cdot \text{kJ}^{-1}$ ]

## ACRONYMS

---

DCF direct correlation function

DFT discret Fourier transform, also refer to density functional theory

FGSHT fast generalized spherical harmonic transform

HRF homogeneous reference fluid (approximation)

IET integral equation theory

MC Monte Carlo

MD molecular dynamics

MDFT molecular density functional theory

OZ Ornstein-Zernike (equation)

QM quantum mechanics

RISM reference interaction site model

# INTRODUCTION

---

This thesis aims to develop an original numerical toolkit for physical chemists and structural biologists based on the molecular density functional theory (MDFT), which makes it possible to predict the solvation properties of arbitrary molecular objects in arbitrary molecular solvents (mainly water) efficiently and with microscopic accuracy. This introduction contributes to understand the objective of this thesis, it explains why the theorists are interested in the nature of solvation, what are the present computing trends in solvation simulations, and where our work situates in this frame of solvation theories.

## 1.1 SIMULATION OF SOLVENT EFFECTS

Solvation is a fundamental phenomenon in chemistry. The chemical behavior of numerous systems strongly depends on the nature of solvation; this is the case for example for the reaction mechanisms in metal-organic reacting centers [13, 46], or pharmaceutical studies [26, 47, 48]. The solvation properties demanded by scientific studies are highly diverse; they include such as the Gibbs free energy of solvation, solubility, concentration, partition coefficient, saturated vapor pressure, pH value, the 3D solvation structure, etc. Overall, the interest in these solvation properties touches many fields of study such as chemistry, biochemistry, as well as pharmaceutical, environmental, and agrochemical industries. Unlike the well-studied quantum mechanics (QM) for chemical interactions at a microscopic scale, and the finite element models for macroscopic physical processes, the theories of solvation are in between these description scales and are still under development, owing to the ambiguous compromise between accuracy and computing cost, and the rapid development of computer hardware which makes complicated calculations more and more accessible. In a word, the studies in this domain are quite vibrant.

To change a phenomenon into a model, we must first understand its process. Solvation is defined as the process of moving a molecule from the gas phase (or vacuum) to a condensed phase (figure 1.1), which builds a stabilizing interaction with the solute (or solute moiety, e. g., residues, interfaces, etc.) [42]. Such interactions are mostly classical interactions, involving electrostatic and van der Waals forces; but also with additional more specific chemical effects such as hydrogen bond formation, and quantic effects for some small solvent molecules whose vibrational or rotational energy states are at the same magnitude as  $k_B T$ , etc.

As not all kinds of interactions are important in applications, different models and methods have been developed according to the usage.

For most of the 20th century, the study of solvation effects has been dominated by continuum (implicit) models [9, 32], which mostly rely on the continuum dielectric description of the solvent and are not costly in terms of computation resources. They provide an accurate way to treat the strong, long-range electrostatic interactions which dominate many solvation phenomena, but lack detailed information on the first solvation shell. This information mainly includes the cavity formation energy and solute-solvent van der Waals interactions, that are often rudely treated by introducing an artificial form of cavity that links to the form of solute. The methods for testing electrostatic interactions include the

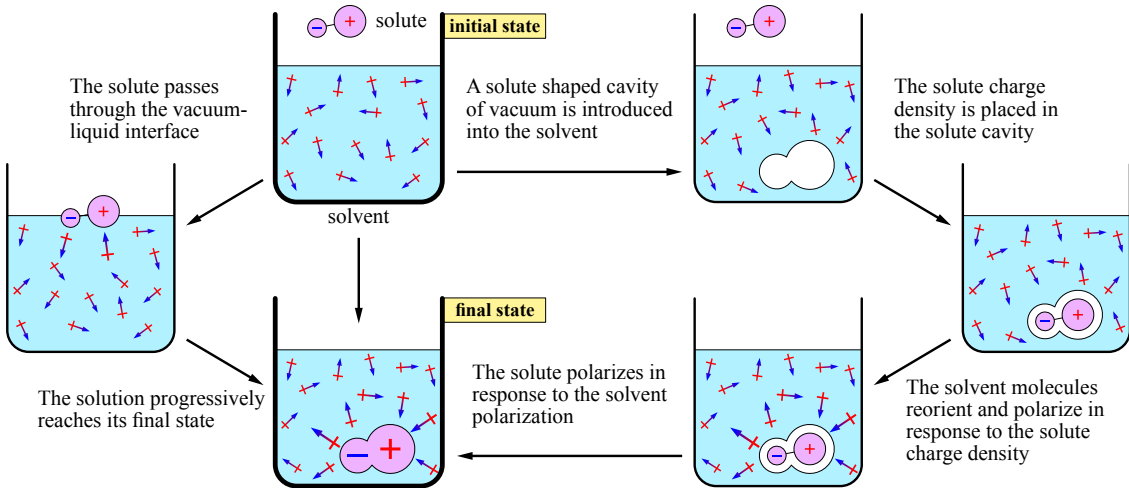


Figure 1.1: The solvation process. A thermodynamic system, whose properties only depend on the initial and final states, can go through different paths. The physical process of solvation (left path) takes the solute from vacuum into bulk solvent, progressively passing through the vacuum-liquid interface. Theoretically, the solvation energy is defined as the energy consumed in such a process. In theoretical studies, the process can be decomposed to some artificial unphysical process (right path), involving the growth of an uncharged solute-sized cavity within the bulk solvent, the transfer of the solute charge distribution from vacuum into cavity, and the interaction between the solute and solvent.

Generalized Born (GB) approximation or, for better estimates, Poisson-Boltzmann (PB) calculations. These are widely integrated within QM simulations by adding extra solvation terms onto the Fock or Kohn-Sham operator [58, 59]. However, the improper treatment of the first shell, where the microscopic interactions are primarily located, often introduces potentially huge errors in free energy evaluation, especially for polar solvents (such as water), despite the accuracy that the QM calculation alone can achieve. Therefore, classical molecular simulations, which describe the individual solvent molecules explicitly (explicit solvent), particularly the molecular dynamics (MD) and Monte Carlo method (MC), have become the alternative solution during the last few decades. They generate trajectories and configurations, and from there estimate free energy changes by statistical mechanical techniques, such as free energy perturbation (FEP) theory or thermodynamic integration (TI) [33]. These calculations are very demanding in computing cost, due to the need for very many (hundreds or thousands) solvent molecules to form a realistic model, and very many configurations (millions) to be statistically significant.

Recently, a third domain of theory to describe solvents based on the statistical mechanics of fluids has been growing rapidly. It mainly involves the integral equation theory (IET), and the classical density functional theory (cDFT) for liquids. These approaches are capable of giving the molecular nature of the first solvation shell, while without calculating all the instantaneous micro-states with respect to time, but rather by integrating over positions and momenta theoretically. Therefore, they are of orders of magnitude faster than the simulations done by micro-states.

The integral equation theory (IET) focuses on solving the Ornstein-Zernike (OZ) equation with a specific closure equation [19, 22]. It was firstly limited to so-called “simple liquids” - a system of spherical particles. The extension to molecular fluids, composed of polyatomic molecules with non-spherical shapes, was done in two different directions. On one hand, Chandler and Andersen in 1971 [6] developed the reference interaction site model (RISM), which discretizes the distribution and correlation functions into site-site

functions, and solves the OZ equation and the closure in a matrix [24]. On the other hand, Blum [3, 4], Fries and Patey [14] extend the OZ equation into a full molecular form, where the distribution and correlation functions depend on both position and orientation. In their theory, the orientation part of OZ equation is simplified by expanding the distribution and correlation functions onto Wigner generalized spherical harmonics.

The classical density functional theory approach deals with inhomogeneous liquids, and uses the same variation principle and minimization strategy [12, 21, 43] as electronic density functional theory (eDFT) for electron-electron interactions. The latter has received an immense success in computational chemistry. Classical DFT gives the Helmholtz free energy and the equilibrium solvent density by minimizing the free energy functional of the solvent density in the presence of a given external potential. Borgis and collaborators [18, 28–31, 38, 52, 53, 56, 61] have recently generalized it into the molecular case, leading to molecular density functional theory (MDFT), where the solvent density depends on both position and orientation,  $\rho(\mathbf{r}, \Omega)$ . The main theoretical difficulty lies in the definition of well-founded and reliable functionals of the excess free energy  $\mathcal{F}_{\text{exc}}[\rho]$ , accounting for the geometric complexity of the solvent molecule. Some recent research has shown that MDFT is capable to describe linear solvents like acetonitrile, but has still some caveats for the most complex solvent, i. e. water [61]. MDFT can be proven to be mathematically equivalent to the two-component molecular IET.

The majority of work of all these theories has been focused on water, since it is one of the most difficult systems to model due to its molecular geometry, unavoidable multi-body character, quantum effects, and hydrogen bonds, etc. The importance of including instantaneous polarization in potential functions is also an issue [10, 57]. However, since polarizable force fields are not yet in common use, the simulations by micro-states and the liquid theory which feed on force fields also have their own limits, compared to the continuum model which can be polarizable. The advantages and disadvantages of each branch of theory are listed in table 1.1.

THEORY	SPEED	LONG-RANGE	FIRST-SHELL	POLARIZABLE SOLVENT
Continuum model	fast	yes	no	fully
Simulation by time	costly	yes	yes	partially, very costly
Theory of liquids	fast	yes	yes	partially

Table 1.1: Different solvation theories

## 1.2 SCOPE OF THIS THESIS

This thesis aims to develop MDFT, focusing on the generalization and algorithmic acceleration of the excess free energy functional  $\mathcal{F}_{\text{exc}}$  evaluation under homogenous reference fluid (HRF) approximation, which will be discussed in detail in latter chapters.

Chapter I reviews a selection of models and methods to describe solvent effects. It includes the implicit and explicit models, the basics of liquid-state theory, as well as its two frontier research domains, IET and MDFT. The structure of the code named MDFT, associated to the MDFT approach, on which all the developments of this thesis are based, is also presented. There is also a brief introduction on how MD and MC simulations methods are used to generate the direct correlation functions (DCF) used in this thesis.

Chapter II presents all the theory developed and newly used in this thesis. Two algorithms for the excess energy functional evaluation are proposed. One is an extension of

the previous algorithm which can be only applied to linear solvent, to a full 3D molecular solvent case; while the other is a new algorithm, that combines the molecular OZ equation treatment of angular convolution with MDFT. The solvation properties that the actual code generates are also presented, mainly containing the free energy and solvent structure.

Chapter III reports all the implementation results, which are divided into two aspects: the “accuracy”, involves the error evaluations, comparisons between algorithms and with IET and MD results; and the “efficiency”, evaluates the computing cost of the code, of both in sequential and parallelized versions.

Chapter VI gives applications to ions and molecules. And some work undone due to the limit of time are put in the perspective.

## Chapter I

# STATE OF THE ART: SOLVATION, MODELS AND METHODS

This chapter gives a brief review of all the basic concepts and previous work that this thesis is based on.

In section 2, we begin by introducing the models used in our study, as well as some other examples of different description scale, by way of comparison to illustrate why we chose our models.

Once the model is chosen, all the theories become mathematical problems. Section 3 reviews some basic concepts of statistical mechanics for liquids (theory of liquids), which present some brief formalisms deduced from the model of the system. The following two sections, section 4 and 5 give two frontier domains of the theory of liquids: the integral equation theory (IET), and the molecular density functional theory (MDFT) that this thesis works upon. The clear mathematical equivalence between these two theories is presented in section 5, which gave us the idea to use the expansion technics in IET to serve MDFT.

Finally, we will give a brief introduction in section 6 to the bulk solvent direct correlation functions (DCF) we used in this thesis, which are generated by molecular dynamics (MD) and Monte Carlo (MC) simulations.



# 2

## MODEL OF SOLUTION SYSTEM

---

Computing models of solvents are broadly divided into two types: those treating the solvent as a continuous medium (implicit models) and those describing the individual solvent molecules (explicit models). In the continuum model, the solvent is characterized only by the dielectric constant  $\varepsilon$  and contains an artificial-shaped cavity. The explicit models can have more specific scales. Within the scope of classical mechanics, the solvent molecules are often described as rigid entities carrying distributed point charges; the most expensive methods involves flexible and polarizable explicit models. In computational chemistry, less precise models often have wider usage (the so-called coarse-grained models; for example, the proteins are treated in the unity of residues). As the theory of liquids was firstly established for spherical atom-like solvent particles, the model adopted by such theory is a rigid molecule model, only depending on its position and orientation, i. e. there is no relative movement within the solvent particles. This approximation has been proven reasonable [19]. In this section, we will give a brief introduction of the implicit model in order to facilitate later discussion on solvation free energy corrections. **We will then focus on the rigid solvent models and discuss the limits of each approximation.** The flexible and polarizable models will also be briefly mentioned.

### 2.1 CONTINUUM SOLVATION MODELS

Continuum models [9, 32, 59], which are popular in QM calculations, consider the solvent as a uniform polarizable medium with dielectric constant  $\varepsilon$ , with the solute  $M$  placed in the cavity within this medium (figure 2.1)

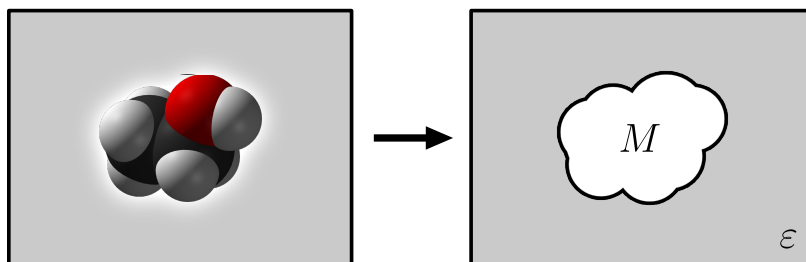


Figure 2.1: Continuum solvent model

*The dielectric constant  $\varepsilon$  is the only parameter characterizing the solvent. It is normally a constant value, but it can depend on the distance from the solute  $M$ . (see §2.1.1)*

The solvation Gibbs free energy according to this model is

$$\Delta G_{\text{solvation}} = \Delta G_{\text{cavity}} + \Delta G_{\text{dispersion}} + \Delta G_{\text{elec}} \quad (2.1)$$

where  $\Delta G_{\text{cavity}} > 0$  is the energy needed to create a hole in the medium, and  $\Delta G_{\text{dispersion}}$  is the dispersion interaction, which is roughly the van der Waals energy  $\Delta G_{\text{vdW}} < 0$  between the solvent and solute. In principle, there may also be a repulsive component, and the dispersion term is sometimes denoted dispersion / repulsion.  $\Delta G_{\text{elec}} < 0$  is the contribution of electrostatic interactions, introduced by electric charge distribution of  $M$  which polarizes the medium, and the action back of the medium on the molecule (reaction field).

The initial two terms in eq. (2.1) may be linked to the configuration of the first solvation shell (cavity). The definition of cavity varies from the simplest sphere or ellipsoid to the surface of the ensemble atomic surfaces defined by the van der Waals radii in the solute. It's somehow reasonable to consider the cavity area proportional to the number of solvent molecules in the first solvation shell. This number can be calculated as the area passing through the middle region of first shell solvent. This area, named as the solvent-accessible surface area (SASA) [23, 37], can be calculated by adding the radius of the probe solvent ball on the solvent excluded surface area (figure 2.2).

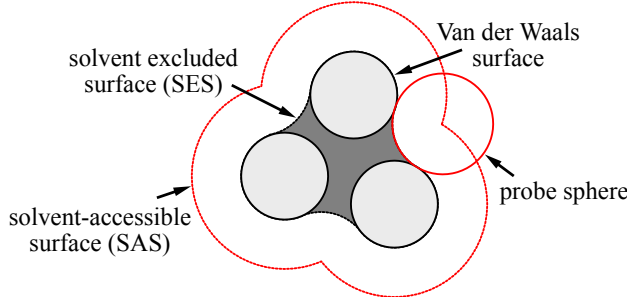


Figure 2.2: Definition of cavity surfaces. The solvent accessible surface (SAS) traced out by the center of the probe representing a solvent molecule. The solvent excluded surface (SES) is the topological boundary of the union of all possible probes that do not overlap with the molecule.

The energy required to create such a cavity and the stabilization due to van der Waals interactions between the solute and solvent, assumed to be proportional to the surface area of the cavity, is expressed as

$$\Delta G_{\text{cavity}} + \Delta G_{\text{dispersion}} = \gamma S_{\text{SASA}} + \beta \quad (2.2)$$

or parameterized by having a constant  $\xi$  specific for each atom type, with the  $\xi$  parameters being determined by fitting to experimental solvation data:

$$\Delta G_{\text{cavity}} + \Delta G_{\text{dispersion}} = \sum_i^{\text{atoms}} \xi_i S_i \quad (2.3)$$

The models and methods to calculate the electrostatic contribution  $\Delta G_{\text{elec}}$  have varied greatly according to their usage. The sections below list the most common examples. By the way, the integration of continuum models into QM calculations is also important, which will not be detailed as it does not link to our theory. Such kind of methods are called the self-consistent reaction field (SCRF) models, which treat the calculation of the solute-solvent interaction in addition to the solute wave function by an iterative procedure. Some examples are presented in the list of Gaussian keyword SCRF [17], and well reviewed by for example Tomasi [58, 59] and Jensen [32].

### 2.1.1 Poisson-Boltzmann methods

The Poisson-Boltzmann equation (PBE) [25] permits to calculate the electrostatic potential  $V_{\text{elec}}$  in the continuum model, such that the electrostatic component of the free energy can be written as

$$\Delta G_{\text{elec}} = \frac{1}{2} \int d\mathbf{r} \rho_q(\mathbf{r}) V_{\text{elec}}(\mathbf{r}) \quad (2.4)$$

where  $\rho_q$  is the charge distribution of the continuous medium.

The Maxwell-Gauss equation in SI units convention gives

$$\nabla \cdot D(\mathbf{r}) = \frac{\rho_q(\mathbf{r})}{\varepsilon_0} \quad (2.5)$$

where  $D(\mathbf{r}) = \varepsilon_0 E(\mathbf{r}) + P(\mathbf{r})$  is the electric displacement field,  $P(\mathbf{r})$  is the system polarization,  $E(\mathbf{r})$  the electric field,  $\varepsilon_0$  the vacuum permittivity.  $D(\mathbf{r})$  can also be expressed in term of the position-dependent dielectric constant  $\varepsilon(\mathbf{r})$ ,  $D(\mathbf{r}) = \varepsilon(\mathbf{r})E(\mathbf{r})$ , thus gives

$$\nabla \cdot \varepsilon(\mathbf{r})E(\mathbf{r}) = \frac{\rho_q(\mathbf{r})}{\varepsilon_0} \quad (2.6)$$

or in terms of electrostatic potential

$$\nabla \cdot [\varepsilon(\mathbf{r})\nabla V_{\text{elec}}(\mathbf{r})] = -\frac{\rho_q(\mathbf{r})}{\varepsilon_0} \quad (2.7)$$

This second-order differential equation (2.7) is called the Poisson equation.

This equation cannot be solved analytically for complex geometries (such as protein), therefore, it is done numerically using numerical methods. Such methods are mentioned in, for example, the article of Roux and Simonson [54] or Holst [25]. A density functional approach based on the minimization of the polarization density can be equally used to solve this equation [39, 40].

If the solvent is ionic, the Poisson equation can be modified by taking into account a (thermal) Boltzmann distribution of ions in the solvent, leading to the Poisson-Boltzmann Equation:

$$\begin{aligned} \nabla \cdot (\varepsilon(\mathbf{r})\nabla\phi(\mathbf{r})) - \kappa^2 \left( \frac{kT}{q} \right) \sinh \left( \frac{qV_{\text{elec}}(\mathbf{r})}{kT} \right) &= -\frac{\rho(\mathbf{r})}{\varepsilon_0} \\ \kappa^2 &= \frac{8\pi q^2 I}{kT} \end{aligned} \quad (2.8)$$

Here  $q$  is the ion charge,  $I$  is the ion strength of the solution, and the  $\kappa^2$  factor is inversely related to the Debye-Hückel length. [Unity?]

### 2.1.2 Born / Onsager / Generalized Born models

For simple geometries, the Poisson equation (2.7) can be solved analytically.

The simplest model is a spherical cavity. For a net charge  $q$  in a cavity of radius  $a$ , the electrostatic free energy of a medium with a dielectric constant of  $\varepsilon$  is given by the Born model:

$$\Delta G_{\text{elec}}(q) = -\frac{1}{8\pi\varepsilon_0} \left( 1 - \frac{1}{\varepsilon} \right) \frac{q^2}{2a} \quad (2.9)$$

However, the Born model is not fully capable to predict the solvent behavior in a lot of cases [32]. Other similar models include Onsager model, in which a dipole point (characterized by momentum  $\mu$ ) is put in a spherical cavity; and the Kirkwood model refers to a general multipole expansion in a spherical cavity; while the Kirkwood-Westheimer model arises for an ellipsoidal cavity.

The generalized Born (GB) model is the superposition of several net charges in spherical cavities as Born model describes, with a similar formalism: (Unity?)

$$\Delta G_{\text{elec}} = -\frac{1}{8\pi\varepsilon_0} \left( 1 - \frac{1}{\varepsilon} \right) \sum_i \sum_j \frac{q_i q_j}{f_{ij}} \quad (2.10)$$

where the function  $f_{ij}$  depends on the internuclear distance and Born radii for each pair of atoms,  $a_i$  and  $a_j$ :

$$f_{ij} = \sqrt{r_{ij}^2 - a_i a_j \exp\left(\frac{r_{ij}^2}{4a_i a_j}\right)} \quad (2.11)$$

$r_{ij}$  being the distance between the centers of atom  $i$  and  $j$ .

The GB model provides a very fast method, with rather the same accuracy compared to Poisson-Boltzmann calculations. That makes it widely used to perform optimization and simulations.

## 2.2 MODEL POTENTIAL OF EXPLICIT MOLECULES

The model potential frequently used in the theory of liquids is a classical, rigid, pairwise additive model [19, 22]. It is based on three assumptions.

- Firstly, the quantum effect of solvent should have been ignored. It is assumed that the rotational and transitional motion of solvent particles are continuous and classical, that means the separation of both transitional and rotational states are largely inferior of  $k_B T$ . For light molecules, that is not always convincing. Some molecules containing hydrogen (e. g. H<sub>2</sub>O, NH<sub>3</sub>, and particularly H<sub>2</sub>) exhibit obvious quantum effects at low temperature in liquid state. Gaseous H<sub>2</sub>O and NH<sub>3</sub> also need quantum effect corrections. However, in which we are interested the most, the liquid H<sub>2</sub>O at room temperature, the contribution of this effect is enough small. And obviously, there should not be any chemical interaction of solvent with the solute.
- Secondly, the intramolecular movement (vibration and internal rotation) should be either independent of transitional and rotational movement or absent. This rigid molecule approximation assumes that the intermolecular potential  $\mathcal{U}(\mathbf{r}^N, \Omega^N)$  only depends on the positions of the  $N$  molecular centers  $\mathbf{r}^N \equiv \mathbf{r}_1 \mathbf{r}_2 \dots \mathbf{r}_N$  and on their orientation  $\Omega^N$ , where  $\Omega \equiv (\Theta, \Phi, \Psi)$  represents the Euler angles (figure 2.3).

Compared to atomic models that only depend on  $\mathbf{r}^N$ , the angular correlations can give influence on both structural and thermodynamics proprieties. That is why our theory is extended to linear case ( $\Omega \equiv (\Theta, \Phi)$ ) then molecular case ( $\Omega \equiv (\Theta, \Phi, \Psi)$ ).

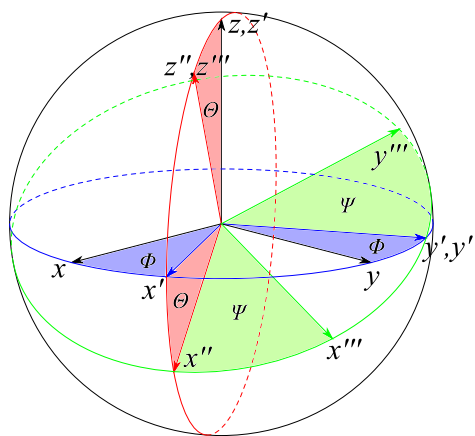


Figure 2.3: Euler angles. The result basis vectors of the new orientation are obtained by 3 sequential operations: (1) A rotation  $\phi$  ( $0 < \phi < 2\pi$ ) about the  $z$ -axis, bringing the frame of axes from the initial position  $\mathbf{S}$  into the position  $\mathbf{S}'$  (2) A rotation  $\theta$  ( $0 < \theta < \pi$ ) about the  $y$ -axis of the frame  $\mathbf{S}'$ , which is transformed into  $\mathbf{S}''$  (3) A rotation  $\psi$  ( $0 < \psi < 2\pi$ ) about the  $z$ -axis of the frame  $\mathbf{S}''$ .

(The choice of molecular centre?)

This approximation is quite realistic for molecules in which the separation of vibrational states largely exceed  $k_B T$ , and implies that the solvent molecule stays in

its ground vibrational state. (**Why?**) For many small molecule solvents such as N<sub>2</sub>, CO<sub>2</sub>, C<sub>6</sub>H<sub>6</sub>, it is the case, except of water. (...) **The non-rigidity of water should be studied in the cases of (...)**

3. Finally, the intermolecular forces have been assumed to be pairwise additive:

$$\mathcal{U}(\mathbf{r}^N, \Omega^N) = \frac{1}{2} \sum_{i \neq j} u(\mathbf{r}_{ij}, \Omega_i, \Omega_j) = \sum_{i < j} u(\mathbf{r}_{ij}, \Omega_i, \Omega_j) \quad (2.12)$$

That means the model potential only depends on the intermolecular separation  $\mathbf{r}$  and on the molecular orientations  $\Omega_1$  and  $\Omega_2$ . This approximation is quasi-exact for low density gases, where the three and more body terms decrease rapidly, but for dense fluids, in most of cases the multi-body potential can not be ignored, but it is often taken into account by an effective pair potential (measured by experiments or calculated by simulations) due to computational cost. Three-body omission can cause surface tension problem, (...)

The complete model potential with higher order corrections can be written in the form of

$$\mathcal{U}(\mathbf{r}^N, \Omega^N) = \sum_{i < j} u(ij) + \sum_{i < j < k} u(ijk) + \sum_{i < j < k < l} u(ijkl) + \dots \quad (2.13)$$

where  $u(ijk) = u(\mathbf{r}_{ij}, \mathbf{r}_{jk}, \mathbf{r}_{ki}, \Omega_i, \Omega_j, \Omega_k)$ .

**For water, most of the publications have already shown... at the approximation level in this thesis...**

In the test below we will present some common models from the most simple to the most complicate.

### 2.2.1 *Interaction of spherical particle*

The simplest model of a fluid is the hard sphere model. With  $d$  is the hard-sphere diameter, the pair potential

$$u(r) = \begin{cases} \infty & r < d \\ 0 & r > d \end{cases} \quad (2.14)$$

**This model can represent some physical systems, such as ... However, the absence of attractive force ... .**

More realistic neutral particle models, like Lenard-Jones (LJ) model, have a potential energy curve that has the same shape as the real interaction of rare gas, as shown in figure 2.4.

The Lennard-Jones (LJ) interaction gives

$$u_{LJ}(r) = 4\epsilon \left[ \left( \frac{\sigma}{r} \right)^{12} - \left( \frac{\sigma}{r} \right)^6 \right] \quad (2.15)$$

where  $r$  (of unity [Å]) is the distance from central to central,  $\sigma$  (of unity [Å]) is the collision diameter is the separation of particles where  $u(r) = 0$ , and  $\epsilon$  is the well depth of the potential (of unity kJ/mol). This well (the minimum) occurs at  $r_{\min} = 2^{1/6}\sigma$  and  $u(r_{\min}) = -\epsilon$ . The parameters  $\sigma$  and  $\epsilon$  can be measured by experimentation.

Theoretically, all terms in the multipole series represent attractive contributions to the potential. The leading term, varying as  $r^{-6}$ , describes the dipole-dipole interaction.

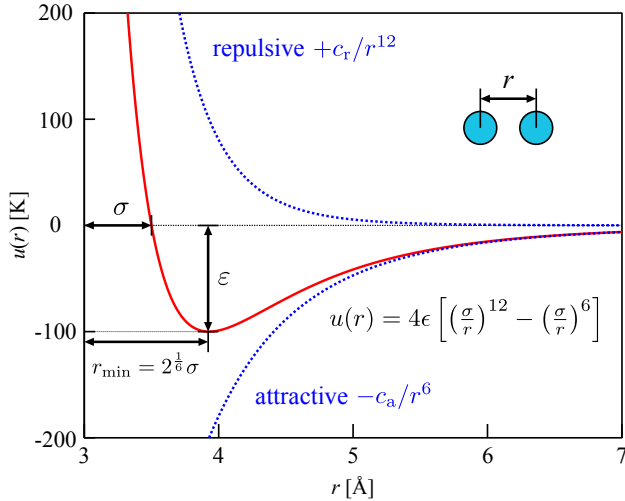


Figure 2.4: LJ pair potential. The plot gives the potential energy  $u(r)$  versus internuclear distance  $r$  of two particles. At large distances, both attractive and repulsive interactions are small. As the distance between the atoms decreases, the attractive electron-proton interactions dominate, and the energy of the system decreases. At the observed bond distance, the repulsive electron-electron and proton-proton interactions just balance the attractive interactions, preventing a further decrease in the internuclear distance. At very short internuclear distances, the repulsive interactions dominate, making the system less stable than the isolated atoms.

Higher-order terms represent dipole-quadrupole ( $r^{-8}$ ), quadrupole-quadrupole ( $r^{-10}$ ) interactions, and so on, but these are negligible compared to  $r^{-6}$ . The short-range interaction is difficult to calculate, and it is defined as  $r^{-12}$  in the LJ model.

The electrostatic interaction between two charged particles 1 and 2 is described by the Coulomb point charge interaction:

$$u_{\text{Coul}}(r) = \frac{q_1 q_2}{4\pi\epsilon_0 r} \quad (2.16)$$

Generally, the pair potential for atomic particles  $u(r)$  used is a sum of LJ and Coulomb interactions.

### 2.2.2 Molecular fluid model

As discussed before, atomic description of interactions is not sufficient to well describe solvation properties. For polar liquids, the dipole-dipole interaction should be mainly taken into account. It can be superposed onto the spherically symmetric potential:

$$u(1, 2) = u_0(r) - \boldsymbol{\mu}_1 \cdot \mathbf{T}(\mathbf{r}) \cdot \boldsymbol{\mu}_2 \quad (2.17)$$

where  $\mathbf{r}$  is the vector separation of the molecular centers,  $u_0(r)$  is the spherically symmetric term as discussed above,  $\boldsymbol{\mu}_i$  is the dipole moment vector of particle  $i$  and  $\mathbf{T}(\mathbf{r})$  is the dipole-dipole interaction tensor:

$$\mathbf{T}(\mathbf{r}) = \nabla^2 \left( \frac{1}{r} \right) = 3\mathbf{rr}/r^5 - \mathbf{I}/r^3 \quad (2.18)$$

where  $\mathbf{I}$  is the unit tensor.

The site-site model is a further extension of atomic model, in which the solvent molecule is represented by a set of discrete interaction sites. The total potential energy is a sum of spherical interaction potentials:

$$u(1, 2) = \frac{1}{2} \sum_{\alpha} \sum_{\beta} u_{\alpha\beta}(|\mathbf{r}_{2\beta} - \mathbf{r}_{1\alpha}|) \quad (2.19)$$

where  $\mathbf{r}_{is}$  is the coordinates of site  $s$  in molecule  $i$ ,  $u_{\alpha\beta}(r)$  the interatomic potential energy of pair of sites  $\alpha, \beta$ , as discussed above. This model is the mostly adopted, as well as in this thesis.

The full formalism of molecular fluid is  $u(\mathbf{r}_{12}, \Omega_1, \Omega_2)$  as in eq. (2.12). It can be without any supplementary approximation, with in the frame of pair-additive assumption.

### 2.2.3 Multipole and spherical harmonic expansion

The molecular model potential is often expanded to multipole, owing to the fast convergence of  $u$  with respect to the expansion order:

In this thesis we  
use ???

$$u(1, 2) = q\mathbf{T}^{(0)}(\mathbf{r}) - \boldsymbol{\mu} \cdot \mathbf{T}^{(1)}(\mathbf{r}) + \frac{1}{2}\mathbf{Q} : \mathbf{T}^{(2)}(\mathbf{r}) - \frac{1}{6}\mathbf{O} : \mathbf{T}^{(3)}(\mathbf{r}) + \dots \quad (2.20)$$

where  $\mathbf{T}^{(l)}(\mathbf{r}) = \nabla^l \left( \frac{1}{r} \right)$ , and  $q$ ,  $\boldsymbol{\mu}$ ,  $\mathbf{Q}$ ,  $\mathbf{O}$  are the monopole, dipole, quadrupole and octopole moments. (Physical meaning and magnitude of each term.) Other forces such as magnetic, multipolar, dispersion and induction intermolecular forces are usually negligible compares to the dipole interaction.

The molecular model potential can also be expanded to spherical harmonics:

$$u(1, 2) = \sum_{lm} u_m^l Y_m^l(\Omega) \quad (2.21)$$

Potentials of the same order in multipole or **GSH!** are mathematically equivalent to each other. (When  $\psi = 0$ ?)

### 2.2.4 SPC/E water model

As water can't be perfectly described by the pair potential due to multi-body effects, quantum effects, hydrogen bond, etc., there develops various models to fit certain properties. The models contain several sites, which can be placed elsewhere other than the center of atom (figure 2.5). The more sites the model has, the more precise it can be. There is a great work done by Martin Chaplin [7], which summarized all frequent water models.

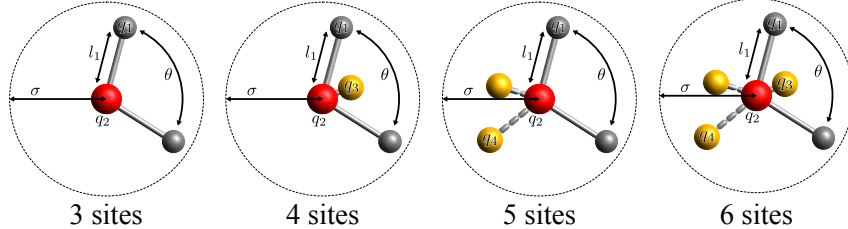


Figure 2.5: Water models

In this thesis, we use the extended simple point charge model (SPC/E) of water [2] as the solvent though all this thesis. It is a 3-site model, the electrostatic interaction is modeled using Coulomb's Law and the dispersion and repulsion forces using the Lennard-Jones potential.

The SPC/E model adds an polarization correction term to the SPC potential energy function:

$$E_{\text{pol}} = \frac{1}{2} \sum_i \frac{(\mu - \mu^0)^2}{\alpha_i}$$

It should be noted  
that any rigid  
solvent model is  
compatible with  
the theory of  
liquids, e. g.  
acetonitrile used  
in [61].

where  $\mu$  is the dipole of the effective pair model,  $\mu^0$  is the dipole moment of an isolated water molecule, and  $\alpha_i$  is an isotropic scalar polarizability [2]. The SPC/E model gives a better radial distribution function and diffusion constant than the SPC model, **and it is successful in ... (applications)**

The parameters are listed in table 2.1, compared with its relative SPC model. As the numerical density, dielectric constant, etc. vary with temperature, we fix the temperature at 298K. **(Which properties needed?)**

MODEL	$\sigma$ [ $\text{\AA}^6$ ]	$\varepsilon$ [ $\text{kJ} \cdot \text{mol}^{-1}$ ]	$l_1$ [ $\text{\AA}$ ]	$q_1$ [e]	$q_2$ [e]	$\theta$ [ $^\circ$ ]
SPC[94]	3.166	0.650	1.0000	+0.410	-0.8200	109.47
SPC/E[3]	3.166	0.650	1.0000	+0.4238	-0.8476	109.47
experiment[90]	-	-	0.991	-	-	105.5

(a) Structural parameters [2]

MODEL	MOLAR VOLUME [ $\text{cm}^3$ ]	NUMBER DENSITY	DIELECTRIC CONSTANT	DIPOLE MOMENT [D]	VAPOR PRESSURE
SPC			65 [185]	2.274[2]	
SPC/E			71 [3][36]	2.351[2]	
experiment	18.0685 [1006]		78.4	2.95	3.165 kPa (25 C) [808];

(b) Calculated physical properties. All the data is at 25 °C and 1 atm.

Table 2.1: Parameters for SPC and SPC/E water

### 2.2.5 Flexible and polarizable models

Flexible models give extra degrees of freedom in vibration and internal rotation. The interaction potential can contain several terms, typically about 5 kind of force: the direct interactions (figure ), in addition to the indirect interactions (LJ and Coulomb).

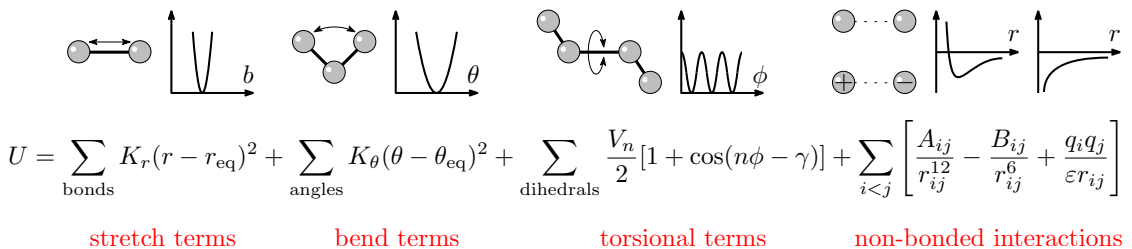


Figure 2.6: Direct interactions

The flexible model can deal with non-rigidity of solvent, and it partially polarized owing to the vibration freedom. **(Interaction site model can also deal with non-rigidity of solvent?)**

A rigid model can be polarized by amusing a modifiable charge distribution. **(What else to be added?)**

Complex models require expensive computing cost, but still can have large fluctuations due to use of small system size. There is a compromise between the choice of model and the choice of system size. For this reason, rigid model is now the most popular. On

the other hand, computing technology has largely developed comparing to the theories themselves, which allows more and more precise models to be used in computation.

## 2.3 MODEL OF SOLUTE

The model of solute also gives an influence to the energy and structure of solvation. The compromise to have a better model of solvent or solute is debatable, and it varies according to the application. For example, we never use a quantum solvent model in the case of an implicit solute, since this would not be profitable even if the solute is of simple geometry (wall). On the other hand, Most of QM calculations in apolar solvents (toluene, etc.) use implicit SCRF model, or even without solvent correction, and this has been proven to work well. In the case of molecular solutes, we generally require the solute to have at least a model at the same scale of description (figure 2.7).

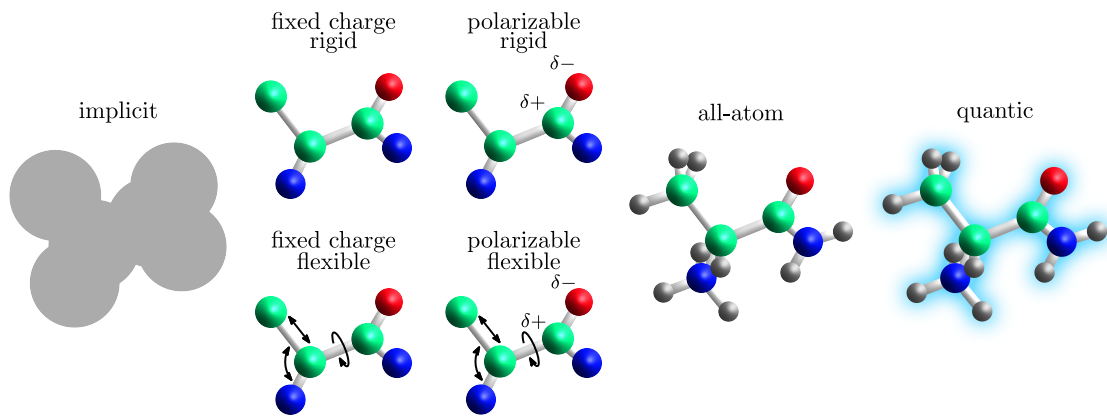


Figure 2.7: Hierarchy of models

In this thesis, we use also rigid model to describe solute to be coherent with IET, which cannot treat the solvent and solute in different scale of description. Polarizable, flexible model of solute, and coupling with QM will be described in perspective.

In a word, the choice of the model of system is a compromise between the required precision according to application, and the computing cost that the research can afford.



# 3

## STATISTICAL MECHANICS OF CLASSICAL FLUIDS

---

The link between statistical mechanics and thermodynamics

From pair distribution functions and interaction potential, we can derive information about solvent equilibrium state.

equilibrium statistical mechanics of classical fluids.  
one component bulk fluids. thermodynamic state point is specified by  $\rho$  and temperature  $T$ .

As the theory of liquid was firstly built for atom-like spherical particles, the deduction of the theory departs from an atom-like spherical particles model.

### 3.1 HAMILTONIAN OF A MICRO-STATE

effective Hamiltonian, i.e. the theorist constructs a model fluid.

In classical mechanics, the instantaneous state (phase point) of an  $N$ -particle solvent system is specified by  $3N$  coordinates  $\mathbf{r}^N \equiv \mathbf{r}_1, \dots, \mathbf{r}_N$  and  $3N$  momenta  $\mathbf{p}^N \equiv \mathbf{p}_1, \dots, \mathbf{p}_N$ . The Hamiltonian of the system is

$$H_N(\mathbf{r}^N, \mathbf{p}^N) = K_N(\mathbf{p}^N) + V_N(\mathbf{r}^N) + V_N^{\text{ext}}(\mathbf{r}^N) \quad (3.1)$$

where

$$K_N(\mathbf{p}^N) = \sum_{i=1}^N \frac{\mathbf{p}_i^2}{2m} \text{ is the kinetic energy}$$

$$V_N(\mathbf{r}^N) = \sum_{i < j}^N u(|\mathbf{r}_i - \mathbf{r}_j|) + 3 \text{ body} + \dots \text{ is the interatomic potential energy } \mathcal{U}(\mathbf{r}^N), \text{ One then has a pair}$$

$$V_N^{\text{ext}}(\mathbf{r}^N) = \sum_{i=1}^N V_{\text{ext}}(\mathbf{r}_i) \text{ is the potential energy arising from the interaction of the particles with the exterr}$$

The distribution of phase points of systems in **the ensemble** is described by a phase space probability density  $f^{[N]}(\mathbf{r}^N, \mathbf{p}^N; t)$ , such that

$$\int f^{[N]}(\mathbf{r}^N, \mathbf{p}^N; t) d\mathbf{r}^N d\mathbf{p}^N = 1 \quad (3.2)$$

for all  $t$ .

subset of particles of size  $n$ , reduced phase space distribution function

$$f^{[n]}(\mathbf{r}^n, \mathbf{p}^n; t) = \frac{N!}{(N-n)!} \int f^{[N]}(\mathbf{r}^N, \mathbf{p}^N; t) d\mathbf{r}^{N-n} d\mathbf{p}^{N-n} = 1 \quad (3.3)$$

where  $\mathbf{r}^n \equiv \mathbf{r}_1, \dots, \mathbf{r}_n$  and  $\mathbf{r}^{N-n} \equiv \mathbf{r}_{n+1}, \dots, \mathbf{r}_N$ . the probability of finding a subset of  $n$  particles in the reduced phase space element.... the factor is the number of ways one can choose a subset of size  $n$ .

The Liouville theorem shows that the probability density is independent of time.

The Bogoliubov–Born–Green–Kirkwood–Yvon hierarchy express  $f^{(n)}$  in terms of  $f^{(n+1)}$ , approximation closure

## 3.2 TIME AVERAGES AND ENSEMBLE AVERAGES / PARTITION FUNCTIONS AND THERMODYNAMICS

The classical canonical partition function for a one component fluid is given by,

$$Z_N(\beta, V) = \frac{h^{-dN}}{N!} \int d\mathbf{r}^N d\mathbf{p}^N e^{-\beta H_N} \quad (3.4)$$

$d$  is the dimensionality and  $V$  is the volume of the system. We can integrate over the momenta to obtain

$$Z_N(\beta, V) = \Lambda^{-dN} Q_N \quad (3.5)$$

$$Q_N = \frac{1}{N!} \int d\mathbf{r}^N e^{-\beta \mathcal{U}(\mathbf{r}_1, \dots, \mathbf{r}_n)} \quad (3.6)$$

is the configurational partition function. Note that the potential energy  $\mathcal{U}(\mathbf{r}_1, \dots, \mathbf{r}_n)$  may still include an external field contribution.

The Helmholtz free energy is simply

$$F_N(\beta, V) = -\beta^{-1} \ln Z_N$$

which leads to entropy

$$S = \left( \frac{\partial F_N}{\partial T} \right)_V$$

pressure

$$p = \left( \frac{\partial F_N}{\partial V} \right)_T$$

for bulk fluid

For an ideal (non-interacting) gas, where  $\Phi \rightarrow 0$ , in  $d = 3$ ???

$$\beta F_N = \ln(N! \Lambda^{3N} V^{-N}) = N \ln(\Lambda^3 \rho) - N$$

Sterling equation... number density  $\rho = N/V$  (a uniform ideal classical gas.)

Th grand function We consider open systems with fixed temperature  $T$  and chemical potential  $\mu$ . The partition function for the grand canonical ensemble is

$$\Xi(\beta???, \mu, T) = \sum_{N=0}^{\infty} \frac{e^{\beta \mu N}}{h^{3N} N!} \iint d\mathbf{r}^N d\mathbf{p}^N e^{-\beta H_N(\mathbf{r}^N, \mathbf{p}^N)} = \sum_{N=0}^{\infty} \frac{1}{N!} \int d\mathbf{r}^N e^{-\beta V_N(\mathbf{r}^N)} \left( \prod_{i=1}^N \frac{e^{\beta u(\mathbf{r}_i)}}{\Lambda^{3N}} \right) \quad (3.7)$$

with  $\Lambda = (2\pi \hbar^2/m)^{\frac{1}{2}}$  and  $u(\mathbf{r}) = \mu - V_{\text{ext}}(\mathbf{r})$ .

The equilibrium density of probability

$$f(\mathbf{r}^N, \mathbf{p}^N; N) = \frac{1}{h^{3N} N! \Xi} e^{-\beta [H_N(\mathbf{r}^N, \mathbf{p}^N) - \mu N]}$$

and the grand potential

$$\Omega = -\beta^{-1} \ln \Xi(\beta???, \mu, T)$$

which for the case of a uniform fluid, reduces to  $\Omega = -pV$ .

$$\begin{aligned} \Omega[u] &= \beta^{-1} \left\langle \ln \left( h^{3N} N! f(\mathbf{r}^N, \mathbf{p}^N; N) \right) + K_N(\mathbf{p}^N) + V_N(\mathbf{r}^N) - \sum_{i=0}^N u(\mathbf{r}_i) \right\rangle \\ u(\mathbf{r}_i) &= \int \delta(\mathbf{r} - \mathbf{r}_i) u(\mathbf{r}) d\mathbf{r} \end{aligned}$$

$$\rho(\mathbf{r}) = \left\langle \sum_{i=1}^N \delta(\mathbf{r} - \mathbf{r}_i) \right\rangle$$

$$\Omega[u] = \beta^{-1} \left\langle \ln \left( h^{3N} N! f(\mathbf{r}^N, \mathbf{p}^N; N) \right) + K_N(\mathbf{p}^N) + V_N(\mathbf{r}^N) \right\rangle - \int \rho(\mathbf{r}) u(\mathbf{r}) d\mathbf{r}$$

free energy of Helmholtz

$$\Omega[u] = F + \mu \langle N \rangle = F + \mu \int \rho(\mathbf{r})$$

### 3.3 DISTRIBUTION FUNCTIONS

the direct correlation function hierarchy:

$$\begin{aligned} c^{(1)}(\mathbf{r}) &= -\frac{\delta(\beta \mathcal{F}_{\text{exc}}[\rho])}{\delta \rho(\mathbf{r})} \\ c^{(2)}(\mathbf{r}_1, \mathbf{r}_2) &= \frac{\delta c^{(1)}(\mathbf{r}_1)}{\delta \rho(\mathbf{r}_2)} = -\frac{\delta^2(\beta \mathcal{F}_{\text{exc}}[\rho])}{\delta \rho(\mathbf{r}_1) \delta \rho(\mathbf{r}_2)} = c^{(2)}(\mathbf{r}_2, \mathbf{r}_1) \\ c^{(n)}(\mathbf{r}_1, \dots, \mathbf{r}_n) &= \frac{\delta c^{(n-1)}(\mathbf{r}_1, \dots, \mathbf{r}_{n-1})}{\delta \rho(\mathbf{r}_n)} \end{aligned}$$

for bulk solvent

$\mathcal{F}_{\text{exc}}[\rho]$  is the excess (over ideal) **Helmholtz free energy** functional arising from the interactions.



# 4

## INTEGRAL EQUATION THEORY

---

density-density pair correlation function  $\langle v(\mathbf{r})v(\mathbf{r}') \rangle \equiv \rho(\mathbf{r}, \mathbf{r}')$ , when the fluid is uniform, the quantity can be expressed by a function of only the distance between the two places, such that  $\rho(\mathbf{r}, \mathbf{r}') \rightarrow \rho(|\mathbf{r} - \mathbf{r}'|)$ [24]

### 4.1 ORNSTEIN-ZERNIKE EQUATION

The Ornstein-Zernike () equation for simple (atomic) liquids

$$h(\mathbf{r}, \mathbf{r}') = c(\mathbf{r}, \mathbf{r}') + \int_V c(\mathbf{r}, \mathbf{r}'') \rho(\mathbf{r}'') h(\mathbf{r}'', \mathbf{r}') d\mathbf{r}'' \quad (4.1)$$

The potential energy of the liquid system

$$U'_N(\mathbf{r}_1, \dots, \mathbf{r}_N) = \sum_{i=1}^N \varphi(\mathbf{r}_i) + U_N(\mathbf{r}_1, \dots, \mathbf{r}_N) \quad (4.2)$$

where  $\varphi(\mathbf{r}_i)$  is the interaction potential of  $i$ -th molecule of the system with an external field, and  $U_N(\mathbf{r}_1, \dots, \mathbf{r}_N)$  is the intermolecular potential energy. the local activity  $z(\mathbf{r}) = z \exp[-\beta\varphi(\mathbf{r})]$ , where  $z = \exp[\mu/k_B T]$ ,  $\beta = 1/k_B T$ ,  $\mu$  is the chemical potential, and  $k_B$  is the Boltzmann constant.

The grand canonical partition function

$$\Xi = \sum_N \frac{1}{N!} \int \dots \int \prod_i^N z(\mathbf{r}_i) \exp(-\beta U_N) d\mathbf{r}_1 \dots d\mathbf{r}_N \quad (4.3)$$

single particle and pair correlation functions of density

$$\rho(\mathbf{r}) = \frac{z(\mathbf{r})}{\Xi} \frac{\delta \Xi}{\delta z(\mathbf{r})} \quad (4.4)$$

$$\rho^{(2)}(\mathbf{r}, \mathbf{r}') = \frac{z(\mathbf{r})z(\mathbf{r}')}{\Xi} \frac{\delta^2 \Xi}{\delta z(\mathbf{r}) \delta z(\mathbf{r}')} \quad (4.5)$$

with the aid of the mathematical theorem concerning the functional derivative

$$\frac{\delta z(\mathbf{r})}{\delta z(\mathbf{r}')} = \delta(\mathbf{r} - \mathbf{r}') \quad (4.6)$$

the relation between

$$\frac{\delta \rho(\mathbf{r})}{\delta \ln z(\mathbf{r}')} = \rho^{(2)}(\mathbf{r}, \mathbf{r}') - \rho(\mathbf{r})\rho(\mathbf{r}') + \delta(\mathbf{r} - \mathbf{r}')\rho(\mathbf{r})$$

we define the direct correlation function

$$\frac{\delta \ln z(\mathbf{r})}{\delta \rho(\mathbf{r}')} = \frac{\delta(\mathbf{r} - \mathbf{r}')}{\rho(\mathbf{r}')} - c(\mathbf{r} - \mathbf{r}')$$

inserting eq... into the chain-rule theorem of functional derivatives

$$\int \frac{\delta \rho(\mathbf{r})}{\delta \ln z(\mathbf{r}'')} \frac{\delta \ln z(\mathbf{r}'')}{\delta \rho(\mathbf{r}')} d\mathbf{r}'' = \delta(\mathbf{r} - \mathbf{r}')$$

one obtains the Ornstein-Zernike equation.

## 4.2 CLOSURE

The general relation to close the OZ equation

$$g(\mathbf{r}, \mathbf{r}') = \exp [-\beta u(\mathbf{r}, \mathbf{r}') + t(\mathbf{r}, \mathbf{r}') + b(\mathbf{r}, \mathbf{r}')] \quad (4.7)$$

$b(\mathbf{r}, \mathbf{r}')$  is the bridge function  
hypernetted-chain (HNC) approximation

$$g(\mathbf{r}, \mathbf{r}') = \exp [-\beta u(\mathbf{r}, \mathbf{r}') + t(\mathbf{r}, \mathbf{r}')] \quad (4.8)$$

suitable ...

Percus-Yevick (PY) approximation

$$g(\mathbf{r}, \mathbf{r}') = \exp [-\beta u(\mathbf{r}, \mathbf{r}')] [1 + t(\mathbf{r}, \mathbf{r}')] \quad (4.9)$$

suitable...

Another type of closure, used for

$$u(r) = \begin{cases} \infty & (r \leq \sigma) \\ w(r) & (r > \sigma) \end{cases}$$

in the mean-spherical approximation (MSA)

$$h(r) = -1, r \leq \sigma$$

$$c(r) = -\beta w(r), r > \sigma$$

## 4.3 RISM AND 3D-RISM

## 4.4 MOLECULAR SOLVENT

Fries and Patey, Blum

## 4.5 BULK PROPERTIES AND BRIDGE FUNCTION

Luc

# 5

## MOLECULAR DENSITY FUNCTIONAL THEORY

---

Classical density functional theory (cDFT) provides a framework for determining thermodynamic properties and correlation functions over a wide variety of inhomogeneous (model) fluids beginning from a microscopic basis, i.e. the Hamiltonian describing interactions between particles. DFT is based on the principle that the grand potential of a specified inhomogeneous fluid is a functional of the average one-body density,

$$\rho(r) = \left\langle \sum_{i=1}^N \delta(\mathbf{r} - \mathbf{r}_i) \right\rangle$$

where  $\mathbf{r}_i$  is the position coordinate of particle  $i$ .

This article describes all the fundamental theories behind different Molecular Density Functional Theory (MDFT) algorithms involved in this thesis to evaluate excess free energy functional  $\mathcal{F}_{\text{exc}}$  under HRF approximation.

### 5.1 EQUILIBRIUM CLASSICAL DFT

The key idea is that  $\mathcal{F}[\rho]$  is a unique functional of  $\rho(\mathbf{r})$ ; its form does not depend on the external potential  $V(\mathbf{r})$ . !!!

variation principle: par minimization

In molecular density functional theory (MDFT), the grand potential density functional corresponding to an inhomogeneous fluid density  $\rho(\mathbf{r}, \Omega)$  is given by

$$\Theta[\rho(\mathbf{r}, \Omega)] = \Theta[\rho_0] + \mathcal{F}[\rho(\mathbf{r}, \Omega)] \quad (5.1)$$

Where  $\Theta[\rho_0]$  is the correspondent reference bulk fluid grand potential. And  $\rho$  is the fluid density function variable of 3 to 6 dimensions, including 3 coordinations for the position part, and 0 to 3 for the angular part. For instance, in an isotropic fluid:

$$\rho(\mathbf{r}, \Omega) = \begin{cases} n(\mathbf{r}) & \text{if atomic, } \Omega \equiv 1 \\ n(\mathbf{r})/4\pi & \text{if linear, } \Omega \equiv (\theta, \phi) \\ n(\mathbf{r})/8\pi^2 & \text{if non-linear, } \Omega \equiv (\theta, \phi, \psi) \end{cases} \quad (5.2)$$

Here the  $4\pi$  and  $8\pi^2$  is the normalization factor who equals to  $\int d\Omega$ . The 6D definition of the latest case in eq. 5.2 of  $\rho(\mathbf{r}, \Omega)$  is needed for arbitrary solvents, which results the most complex form of the functional.

According to the variation principle (c.f. Evans), the equilibrium density can be found by minimizing the free energy functional  $\mathcal{F}[\rho]$  regarding to  $\rho(\mathbf{r}, \Omega)$ :

$$\frac{\delta \mathcal{F}[\rho]}{\delta \rho(\mathbf{r}, \Omega)}|_{\rho=\rho_0} = 0 \quad (5.3)$$

And this functional is defined as a sum of functional contributions:

$$\mathcal{F}[\rho] = \mathcal{F}_{\text{id}}[\rho] + \mathcal{F}_{\text{ext}}[\rho] + \mathcal{F}_{\text{exc}}[\rho] \quad (5.4)$$

The ideal term  $\mathcal{F}_{id}[\rho]$  is deduced from the particle interaction-free condition:

$$\mathcal{F}_{id}[\rho] = \beta^{-1} \int d\mathbf{r}d\Omega \left[ \ln \left( \frac{\mathbf{a}(\mathbf{r}, \Omega)}{\mathbf{a}_0} \right) - \rho(\mathbf{r}, \Omega) + \rho_0 \right] \quad (5.5)$$

Where  $\beta = (K_B T)^{-1}$  and  $\rho_0$  is the reference bulk density of pure solvent.

The external potential term calculates the contribution of solute external potential  $V_{ext}$ :

$$\mathcal{F}_{ext}[\rho] = \int d\mathbf{r}d\Omega V_{ext}(\mathbf{r}, \Omega) \rho(\mathbf{r}, \Omega) \quad (5.6)$$

$$V_{ext}(\mathbf{r}, \Omega) = \sum_{j \in \text{solvent}} \left\{ q_j V_q(\mathbf{r}_j) + \sum_{i \in \text{solute}} 4\epsilon_{ij} \left[ \left( \frac{\sigma_{ij}}{r_{ij}} \right)^{12} - \left( \frac{\sigma_{ij}}{r_{ij}} \right)^6 \right] \right\} \quad (5.7)$$

Where  $V_{ext}$  is pre-calculated and stored as a 6-dimension double precision (8 bytes per real value) table. It contains the contribution of Lennard-Jones interaction and electrostatic potential.

This two terms  $\mathcal{F}_{id}[\rho]$  and  $\mathcal{F}_{ext}[\rho]$  are physically exact.

The excess term  $\mathcal{F}_{exc}[\rho]$  depends on the exact correlation function, which is a priori unknown:

$$C(\mathbf{r}_1, \mathbf{r}_2, \Omega_1, \Omega_2; \rho) \equiv \frac{\beta \delta^2 \mathcal{F}_{exc}[\rho]}{\delta \rho(\mathbf{r}_1, \Omega_1) \delta \rho(\mathbf{r}_2, \Omega_2)} \quad (5.8)$$

The ideal term  $\mathcal{F}_{id}[\rho]$  is deduced from the condition that the interaction potential of particles  $\Phi = 0$

$$Z_N(\beta, V) = \frac{\lambda^{-3N}}{N!} \int_V d\mathbf{r}^N e^{-\beta\Phi} = \frac{\lambda^{-3N}}{N!} V^N$$

$$F_N(\beta, V) = -\beta^{-1} \log Z_N = \beta^{-1} \log (N! \lambda^{3N} V^{-N}) = \beta^{-1} (N \log \lambda^3 \rho - N)$$

(also available for the inhomogeneous case.) Since we define

$$\mathcal{F}_{id}[\rho] = \int d\mathbf{X} f_{id}[\rho(\mathbf{X})]$$

We have

$$f_{id}[\rho(\mathbf{X})] = \beta^{-1} \Delta \rho (\log \lambda^3 \Delta \rho - 1)$$

and

$$\mathcal{F}_{id}[\rho] = \beta^{-1} \int d\mathbf{X}_1 [\rho(\mathbf{X}_1) \log (\frac{\rho(\mathbf{X}_1)}{\rho_0}) - \rho(\mathbf{X}_1) + \rho_0]$$

The external potential term

$$\mathcal{F}_{ext}[\rho] = \int d\mathbf{X}_1 V_{ext}(\mathbf{X}_1) \rho(\mathbf{X}_1)$$

Where  $V_{ext}$  is given by table.

The exact (in an approximation that C does not depend on  $\rho$ ) form of the excess term  $\mathcal{F}_{exc}$  is

$$\mathcal{F}_{exc}[\rho] = \beta^{-1} \int d\mathbf{X}_1 d\mathbf{X}_2 \Delta \rho(\mathbf{X}_1) \Delta \rho(\mathbf{X}_2) C(\mathbf{X}_1, \mathbf{X}_2; \rho)$$

where  $C(\mathbf{X}_1, \mathbf{X}_2; \rho)$  is the correlation function, a priori unknown, the definition of which is:

$$C(\mathbf{X}_1, \mathbf{X}_2; \rho) = \frac{\beta \delta^2 \mathcal{F}_{exc}[\rho]}{\delta \rho(\mathbf{r}_1) \delta \rho(\mathbf{r}_2)}$$

Figure 5.1: Flowchart of code MDFT

The code MDFT is built for minimizing the free energy functional  $\mathcal{F}[\rho]$  by minimizer L-BFGS (ref). Its main structure is shown in fig.

The minimizer requires the functional and its gradient as input, and at each iteration produces a new fluid density  $\rho(\mathbf{r}, \Omega)$  closer to the equilibrium density. The objective for **branch hesper** is to calculate the excess term  $\mathcal{F}_{\text{exc}}[\rho]$  of the functional in eq.??, as well as its gradient:

$$\gamma(\mathbf{r}_1, \Omega) = \frac{\delta \mathcal{F}_{\text{exc}}}{\delta \rho} = -\beta^{-1} \int d\mathbf{r}_2 d\Omega_2 \Delta \rho(\mathbf{r}_2, \Omega_2) c^{(2)}(\mathbf{r}_{12}, \Omega_1, \Omega_2) \quad (5.9)$$

## 5.2 EXTERNAL FREE ENERGY

The direct evaluation of the Coulomb sum for  $N$  particles is

$$U_C = \sum_{i < j} a \frac{q_i q_j}{\|\mathbf{r}_i - \mathbf{r}_j\|}, \quad (5.10)$$

where  $a$  is a constant that gives  $U_C$  the dimension of an energy, and  $q_i, \mathbf{r}_i$  are the charge and position of particle  $i$ . The computation of equation 5.10 is demanding because it requires a large number of distances  $r_{ij} \equiv \|\mathbf{r}_i - \mathbf{r}_j\|$  to be computed. In our case, we have  $\text{nfft}_1 \times \text{nfft}_2 \times \text{nfft}_3 \times N_\Omega \times N_\psi \times N_{qv}$ , where  $N_{qv}$  is the number of point charges of the solvent molecule, to be computed per point charge of the solute. This is typically  $10^9$  distances for MDFT.

L'énergie électrostatique s'écrit

$$\mathcal{F}_q = \frac{1}{2} \iiint \frac{\rho_c^{\text{soluté}}(\mathbf{r}') \rho_c^{\text{solvant}}(\mathbf{r}, \Omega)}{4\pi\epsilon_0 \|\mathbf{r} - \mathbf{r}'\|} d\mathbf{r} d\mathbf{r}' d\Omega \quad (5.11)$$

$$= \frac{1}{2} \frac{1}{4\pi\epsilon_0} \iiint \frac{\rho_c^{\text{soluté}}(\mathbf{r}')}{\|\mathbf{r} - \mathbf{r}'\|} [\rho^{\text{solvant}} * \sigma](\mathbf{r}, \Omega) d\mathbf{r} d\mathbf{r}' d\Omega \quad (5.12)$$

$$= \frac{1}{2} \frac{1}{4\pi\epsilon_0} \iint [\rho_c^{\text{soluté}} * \|\mathbf{r}\|^{-1}](\mathbf{r}, \Omega) [\rho^{\text{solvant}} * \sigma](\mathbf{r}, \Omega) d\mathbf{r} d\Omega \quad (5.13)$$

$$= \quad (5.14)$$

On définit une densité de charge d'une molécule  $\sigma(\mathbf{r}, \Omega)$ :

$$\sigma(\mathbf{r}, \Omega) = \sum_{m=1}^{\text{sites du solvant}} q_m \delta(\mathbf{r} - \mathbf{s}_m(\Omega)). \quad (5.15)$$

$\mathbf{s}_m(\Omega)$  désigne la position du  $m^{\text{ième}}$  site de la molécule de solvant quand elle a l'orientation  $\Omega$ .

## 5.3 EXCESS FREE ENERGY

In the molecular density functional theory (MDFT), the excess free energy functional  $\mathcal{F}_{\text{exc}}$  can be developed via Taylor expansion

$$\mathcal{F}_{\text{exc}}[\rho] \equiv \mathcal{F}_{\text{exc}}[\rho_0] + \int d\mathbf{X}_1 \frac{\delta \mathcal{F}_{\text{exc}}[\rho]}{\delta \rho(\mathbf{X}_1)} \Delta \rho(\mathbf{X}_1) + \frac{1}{2} \int d\mathbf{X}_1 d\mathbf{X}_2 \frac{\delta^2 \mathcal{F}_{\text{exc}}[\rho]}{\delta \rho(\mathbf{X}_1) \delta \rho(\mathbf{X}_2)} \Delta \rho(\mathbf{X}_1) \Delta \rho(\mathbf{X}_2) + \mathcal{O}(\Delta \rho^3) \quad (5.16)$$

where  $\mathbf{X} \equiv (\mathbf{r}, \Omega)$ ,  $\beta^{-1} = k_B T$ ,  $\Delta \rho = \rho - \rho_0$ , and  $\rho(\mathbf{X})$  the single-particle density of the fluid.

### 5.3.1 Homogenous Reference Fluid Approximation

In the molecular density functional theory (MDFT), the excess free energy functional  $\mathcal{F}_{\text{exc}}$  can be developed via Taylor expansion

$$\mathcal{F}_{\text{exc}} [\rho] \equiv \mathcal{F}_{\text{exc}} [\rho_0] + \int d\mathbf{X}_1 \frac{\delta \mathcal{F}_{\text{exc}} [\rho]}{\delta \rho(\mathbf{X}_1)} \Delta\rho(\mathbf{X}_1) + \frac{1}{2} \int d\mathbf{X}_1 d\mathbf{X}_2 \frac{\delta^2 \mathcal{F}_{\text{exc}} [\rho]}{\delta \rho(\mathbf{X}_1) \delta \rho(\mathbf{X}_2)} \Delta\rho(\mathbf{X}_1) \Delta\rho(\mathbf{X}_2) + \mathcal{O}(\Delta\rho^3) \quad (5.17)$$

where  $\mathbf{X} \equiv (\mathbf{r}, \Omega)$ ,  $\beta^{-1} = k_B T$ ,  $\Delta\rho = \rho - \rho_0$ , and  $\rho(\mathbf{X})$  the single-particle density of the fluid.

According to the variation principle, the first derivative in eq. (5.17) is zero

$$\left. \frac{\delta \mathcal{F}_{\text{exc}} [\rho]}{\delta \rho(\mathbf{X}_1)} \right|_{\rho=\rho_{\text{eq}}} = 0 \quad (5.18)$$

And  $\mathcal{F}_{\text{exc}} [\rho_0]$  can be compensated by the grand potential of bulk fluid (to be detailed), we can then focus on only  $\mathcal{O}(\Delta\rho^2)$  and higher order terms.

As  $\mathcal{F}_{\text{exc}}$  is a generating functional of  $c^{(n)}(\mathbf{X}^n)$ , the direct correlations functions (DCF) [22], for example

$$c^{(2)}(\mathbf{X}_1, \mathbf{X}_2) = -\beta \frac{\delta^2 \mathcal{F}_{\text{exc}} [\rho]}{\delta \rho(\mathbf{X}_1) \delta \rho(\mathbf{X}_2)} \quad (5.19)$$

eq. (5.17) can be rewritten as

$$\begin{aligned} \mathcal{F}_{\text{exc}} [\rho] &= -\frac{\beta^{-1}}{2} \int d\mathbf{X}_1 d\mathbf{X}_2 c^{(2)}(\mathbf{X}_1, \mathbf{X}_2) \Delta\rho(\mathbf{X}_1) \Delta\rho(\mathbf{X}_2) + \mathcal{O}(\Delta\rho^3) \\ &\simeq -\frac{\beta^{-1}}{2} \int d\mathbf{X}_1 d\mathbf{X}_2 c_0^{(2)}(\mathbf{X}_1, \mathbf{X}_2) \Delta\rho(\mathbf{X}_1) \Delta\rho(\mathbf{X}_2) \end{aligned} \quad (5.20)$$

If we take further approximation, to assume that

$$c^{(2)}(\mathbf{X}_1, \mathbf{X}_2) \simeq c_0^{(2)}(\mathbf{X}_1, \mathbf{X}_2) \quad (5.21)$$

where  $c_0^{(2)}(\mathbf{X}_1, \mathbf{X}_2)$  is the DCF of the bulk fluid, it's called the homogenous reference fluid (HRF) approximation.

### 5.3.2 nn\\_cs

We define  $r = \|\mathbf{r} - \mathbf{r}'\|$ , and  $\Delta n(\mathbf{r}) = n(\mathbf{r}) - n_0$ , and  $n_0$  the density (given in dft.in) of the homogeneous fluid of reference, e.g., 0.0332891 molecule per  $\text{\AA}^3$  for water.

We also define  $n(\mathbf{r}) = \int \rho(\mathbf{r}, \Omega) d\Omega$ . We have

$$F_{\text{exc}} = -\frac{1}{2} k_B T \iint \Delta n(\mathbf{r}) \Delta n(\mathbf{r}') c(r) d\mathbf{r} d\mathbf{r}', \quad (5.22)$$

Now, we consider the convolution in the right-hand side of the equation,  $\gamma \equiv (\Delta n * c)$ , which can be computed much more efficiently than in  $O(N^2)$  by Fast Fourier Transform in  $O(N \log N)$ .

Inputs:

- $\rho(\mathbf{r}, \Omega)$
- $c_s(k)$ , with  $k \equiv \|\mathbf{k}\|$
- functions to Fast Fourier Transform (FFT) and inverse Fast Fourier Transform ( $\text{FFT}^{-1}$ )

- $n_0$ , the density of the homogeneous fluid of reference
- $T$  the temperature in Kelvin
- $k_B$  the Boltzmann constant.

### 5.3.3 polarisation

$$\mathcal{F}_{exc} = -\frac{k_B T}{2} \iiint_{\mathcal{R}^3} \int_{\theta=0}^{\pi} \int_{\phi=0}^{2\pi} \int_{\psi=0}^{2\pi} \Delta\rho(\mathbf{r}_1, \boldsymbol{\Omega}_1) c^{(2)}(\mathbf{r}_1, \mathbf{r}_2, \boldsymbol{\Omega}_1, \boldsymbol{\Omega}_2) \Delta\rho(\mathbf{r}_2, \boldsymbol{\Omega}_2) d\mathbf{r}_1 d\mathbf{r}_2 d\boldsymbol{\Omega}_1 d\boldsymbol{\Omega}_2 \quad (5.23)$$

where  $\rho = n / (8\pi^2)$  and we define

$$\mathbf{P}(\mathbf{r}) = \int \mathbf{p}\rho(\mathbf{r}, \boldsymbol{\Omega}) d\boldsymbol{\Omega} \quad (5.24)$$

with  $\mathbf{p} = p\boldsymbol{\Omega}$  the dipolar moment of a water molecule.

## 5.4 OZ EQUATION IN MDFT AND IEM FORMALISM

The wall-particle OZ equiation

...

Ornstein-Zernike (OZ) equation is a fundamental equation to the theory of liquids, which defines  $c^{(2)}(\mathbf{X}_1, \mathbf{X}_2)$ . Its most common form is shown here [22]:

$$h^{(2)}(\mathbf{X}_1, \mathbf{X}_2) = c^{(2)}(\mathbf{X}_1, \mathbf{X}_2) + \int c^{(2)}(\mathbf{X}_1, \mathbf{X}_3)\rho(\mathbf{X}_3)h^{(2)}(\mathbf{X}_3, \mathbf{X}_2)d\mathbf{X}_3 \quad (5.25)$$

where  $h^{(2)}(\mathbf{X}_1, \mathbf{X}_2)$  is the pair correlation function (PCF). When the fluid is homogenous, eq. (5.25) becomes:

$$h^{(2)}(\mathbf{X}_1, \mathbf{X}_2) = c^{(2)}(\mathbf{X}_1, \mathbf{X}_2) + \rho_0 \int c^{(2)}(\mathbf{X}_1, \mathbf{X}_3)h^{(2)}(\mathbf{X}_3, \mathbf{X}_2)d\mathbf{X}_3 \quad (5.26)$$

which gives

$$\gamma(\mathbf{X}_1, \mathbf{X}_2) = h^{(2)}(\mathbf{X}_1, \mathbf{X}_2) - c^{(2)}(\mathbf{X}_1, \mathbf{X}_2) = \rho_0 \int c^{(2)}(\mathbf{X}_1, \mathbf{X}_3)h^{(2)}(\mathbf{X}_3, \mathbf{X}_2)d\mathbf{X}_3 \quad (5.27)$$

If we take  $\mathbf{X}_2$  as the origin in the laboratory coordinate system, eq. (5.27) becomes:

$$\gamma(\mathbf{X}_1) = \int c^{(2)}(\mathbf{X}_1, \mathbf{X}_3)\Delta\rho(\mathbf{X}_3)d\mathbf{X}_3 \quad (5.28)$$

which coincides with the gradient of  $\mathcal{F}_{exc}[\rho]$  in eq. (??).

It can be further proven that the homogenous reference fluid (HRF) approximation of molecular density functional theory (MDFT) is mathematically equivalent to the hypernetted chain (HNC) approximation to integral equations method (IEM) if the fluid is homogenous. (To be detailed.)

## 5.5 CODE MDFT

The code MDFT is the implementation of MDFT theory. It reads the force field (pair potential)  $u(\mathbf{r}, \boldsymbol{\Omega})$  of solute and solvent as input, as well as necessary parameters like the temperature  $T$ , number density of solvent  $n_0$ , etc. It minimizes the functional [ref] and gives the equilibrium density  $\rho(\mathbf{r}, \boldsymbol{\Omega})$ , then computes output properties. The main structure of the code is shown in figure 5.2.

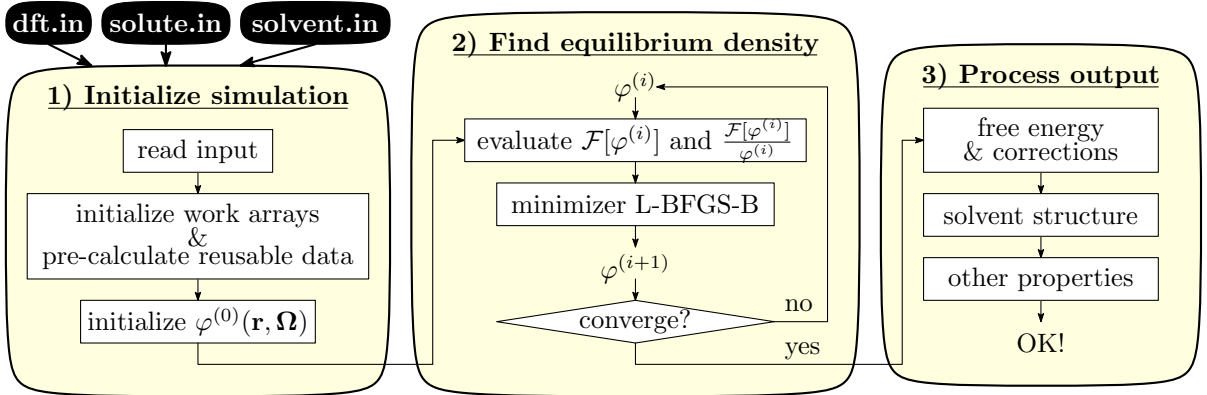


Figure 5.2: Main structure of code MDFT

### 5.5.1 Supercell discretization

$L_x \times L_y \times L_z$  Å<sup>3</sup> space is discretized on a regular grid of nfft<sub>1</sub> × nfft<sub>2</sub> × nfft<sub>3</sub> nodes. Angular grid is discretized with Lebedev (L) or Gauss-Legendre (GL) quadrature for  $\Omega \equiv \{\theta, \phi\}, \theta \in [0, \pi], \phi \in [0, 2\pi]$ , and regular quadrature for  $\psi \in [0, \pi]$ .

TRANSLATE\_SOLUTE\_TO\_CENTER = {T,F}

This translates your solute to the center of the supercell: all solute coordinates are moved by {Lx/2., Ly/2., Lz/2.}, with {Lx,Ly,Lz} the length of the supercell.

The solute center is at  $\left(\frac{L_x}{2}, \frac{L_y}{2}, \frac{L_z}{2}\right)$  of the box, characterized by  $\mathbf{r}_T$ . Internal coordinates of solute  $\mathbf{r}_M$ , solute coordinates in the box  $\mathbf{r} = \mathbf{r}_M + \mathbf{r}_T$ .

### 5.5.2 Minimizer L-BFGS-B

The minimizer adopted by MDFT is the L-BFGS-B [5, 62] package version 3.0 written in Fortran 77, implementing the limited-memory Broyden-Fletcher-Goldfarb-Shanno (BFGS) algorithm with constraints of the form  $l \leq x \leq u$  to the variable  $x$ . During the evaluation of the initial code which use L-BFGS, the constraint function is not used.

The functional  $F[x_i]$  and the gradient of functional  $\nabla F[x_i] = \frac{\delta F}{\delta x}(x_i)$  are required by L-BFGS to minimize the functional. It saves the variables  $x_i$  and gradient of the past  $m$  iterations, which is a memory eater.

The functional in MDFT to be minimized is eq. (ref), and its gradient is

$$\frac{\delta F[\rho]}{\delta \rho(\mathbf{r}, \Omega)} = \beta^{-1} \ln \left( \frac{\rho(\mathbf{r}, \Omega)}{\rho_0} \right) + V_{\text{ext}}(\mathbf{r}, \Omega) + V_{\text{exc}}(\mathbf{r}, \Omega) \quad (5.29)$$

where  $\rho_0$  is the angular density of bulk solvent  $\rho_0 = n_0 / (8\pi^2)$

### 5.5.3 Treatment to avoid unphysical density

During minimization, the density variable  $\rho(\mathbf{r}, \Omega)$  can have unphysical negative numbers, which also cause the divergence of the minimization. To avoid this phenomenon, a normalized  $\varphi(\mathbf{r}, \Omega)$  is used as the variable during the minimization in place of  $\rho(\mathbf{r}, \Omega)$ , so that

$$\rho(\mathbf{r}, \Omega) = \rho_0 \varphi^2(\mathbf{r}, \Omega) \quad (5.30)$$

According to the definition (5.30), we see

$$\frac{\delta\rho(\mathbf{r}, \boldsymbol{\Omega})}{\delta\varphi} = 2\rho_0\varphi(\mathbf{r}, \boldsymbol{\Omega}) \quad (5.31)$$

Therefore the gradient to feed the L-BFGS minimizer (but in the code there is additional  $\mathbf{drd}\boldsymbol{\Omega}$  ??? for all the three parts)

$$\frac{\delta\mathcal{F}}{\delta\varphi} = \frac{\delta\mathcal{F}}{\delta\rho} \cdot \frac{\delta\rho}{\delta\varphi} = 2\rho_0\varphi(\mathbf{r}, \boldsymbol{\Omega}) \cdot [\beta^{-1} \ln \varphi^2 + V_{\text{ext}} + V_{\text{exc}}] \quad (5.32)$$

#### 5.5.4 Evaluation of $V_{\text{ext}}$

In eq. (ref) we define the external potential  $V_{\text{ext}}$  as the gradient of external free energy functional due to the solute, of unity []. When the solute is a molecule with force field, it contains two components:

$$V_{\text{ext}}(\mathbf{r}, \boldsymbol{\Omega}) = V_{\text{LJ}}(\mathbf{r}) + V_{\text{coul}}(\mathbf{r}, \boldsymbol{\Omega}) \quad (5.33)$$

The Lennard-Jones potential is given by

$$V_{\text{LJ}}(\mathbf{r}) = \sum_u \sum_v 4\epsilon_{uv} \left[ \left( \frac{\sigma_{uv}}{r_{uv}} \right)^{12} - \left( \frac{\sigma_{uv}}{r_{uv}} \right)^6 \right] \quad (5.34)$$

where  $u$  stands for solute, and  $v$  stands for solvent,  $\epsilon_{uv} = \sqrt{\epsilon_u \epsilon_v}$  and  $\sigma_{uv} = (\sigma_u + \sigma_v)$  are the geometric and arithmetic average Lennard-Jones parameters between solute and solvent, according to the Lorentz-Berthelot mixing rules.  $r_{ij}$  is the norm of relative site-site vector

$$\mathbf{r}_{uv} = \mathbf{r} + \mathbf{R}(\boldsymbol{\Omega})\mathbf{s}_v - \mathbf{r}_u \quad (5.35)$$

where  $\mathbf{r}_u$  and  $\mathbf{s}_j$  are the coordinates of solute/solvent molecules in the molecular frame, and  $\mathbf{R}(\boldsymbol{\Omega})$  is the rotation matrix of the Euler angles  $\boldsymbol{\Omega}$ .

In cases where the solvent site wears only one LJ centre, eq. (5.35) reduces to

$$\mathbf{r}_{uv} = \mathbf{r} - \mathbf{r}_u \quad (5.36)$$

which is actually what we use in the code as the solvent is SPC/E water.

...

The Coulomb interaction is calculated by solving the Poisson equation [40].

The charge density of the solute is projected onto a space grid,

$$\rho_q(\mathbf{r}) = \sum_u q_{ijk} \quad (5.37)$$

where  $q_{ijk}$  is the charge on the space grid distributed by its nearby point charge as shown in figure 5.3a.

$$V_{\text{coul}}(\mathbf{r}, \boldsymbol{\Omega}) = \sum_v q_v V_q(\mathbf{r}_u) \quad (5.38)$$

Poisson solver

Field

$$\mathbf{E}(\mathbf{r}) = -\vec{\nabla} V_q(\mathbf{r}) \quad (5.39)$$

where  $V_q(\mathbf{r})$  is ... of unity ...

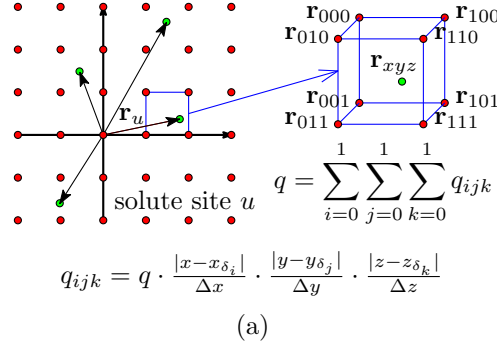


Figure 5.3: Charge density projected onto grids. (a) Solute. (b) Solvent.

Local expression of Gauss's theorem

$$\nabla \cdot E(\mathbf{r}) = \frac{\rho_q(\mathbf{r})}{\varepsilon_0} \quad (5.40)$$

therefore

$$\nabla^2 V_q(\mathbf{r}) = -\frac{\rho_q(\mathbf{r})}{\varepsilon_0} \quad (5.41)$$

$$\hat{V}_q(\mathbf{k}) = \frac{\hat{\rho}_q(\mathbf{k})}{\varepsilon_0 k^2} \quad (5.42)$$

where  $\hat{V}_q(\mathbf{k})$  is the Fourier transform of  $V_q(\mathbf{r})$ .

The Fourier transform, since the Laplacian is a linear operator:

$$\nabla^2 f(\mathbf{r}) = \nabla^2 \int d\mathbf{k} \hat{f}(k) e^{2\pi i \mathbf{r} \cdot \mathbf{k}} \quad (5.43)$$

$$= \int d\mathbf{k} \hat{f}(k) \nabla^2 e^{2\pi i \mathbf{r} \cdot \mathbf{k}} \quad (5.44)$$

$$= \int d\mathbf{k} (-4\pi^2 |\mathbf{k}|^2) \hat{f}(k) e^{2\pi i \mathbf{r} \cdot \mathbf{k}} \quad (5.45)$$

$$\mathcal{F} [\nabla^2 V_q(\mathbf{r})] = -4\pi^2 |\mathbf{k}|^2 \hat{V}_q(\mathbf{k}) \quad (5.46)$$

For Fourier series  $-4\pi^2 |\mathbf{k}|^2$  is the eigenvalue of laplacian:

$$\mathcal{F} [\nabla^2 V_q(\mathbf{r})] = \mathcal{F} \left[ -\frac{\rho_q(\mathbf{r})}{\varepsilon_0} \right] = (i\mathbf{k})^2 \hat{V}_q(\mathbf{k}) = -4\pi \hat{\rho}_q(\mathbf{k}) \quad (5.47)$$

$$\hat{V}_{\text{Poisson}}(\mathbf{k}) = \frac{4\pi \hat{\rho}_q(\mathbf{k})}{k^2} \quad (5.48)$$

### 5.5.5 Evaluation of $V_{\text{exc}}$

$V_{\text{exc}}$  is ... of unity []

Diople

We define  $r = \|\mathbf{r} - \mathbf{r}'\|$ , and  $\Delta n(\mathbf{r}) = n(\mathbf{r}) - n_0$ , and  $n_0$  the density of the bulk solvent, e.g., 0.0332891 molecule per  $\text{\AA}^3$  for water.

We also define  $n(\mathbf{r}) = \int \rho(\mathbf{r}, \Omega) d\Omega$ . We have

$$F_{\text{exc}} = -\frac{1}{2} k_B T \iint \Delta n(\mathbf{r}) \Delta n(\mathbf{r}') c(r) d\mathbf{r} d\mathbf{r}', \quad (5.49)$$

Now, we consider the convolution in the right-hand side of the equation,  $\gamma \equiv (\Delta n * c)$ , that can be computed much efficiently than in  $O(N^2)$  by fast Fourier transform in  $O(N \log N)$ .

$$\mathbf{P}(\mathbf{r}) = \int \mathbf{p}\rho(\mathbf{r}, \Omega) d\Omega \quad (5.50)$$

with  $\mathbf{p} = p\Omega$  the dipolar moment of a water molecule.

HRF approximation [61]

Work by Zhao et al.



# 6

## MOLECULAR DYNAMICS & MONTE CARLO SIMULATIONS

---

As reference method [Allen and Tildesley] [Frenkel and Smit]

The data we used in this thesis issue from MD and MC simulations are in two aspects:

- (1) The DCF of bulk water produced by the work of Zhao et al. [ref] and Belloni et al. [ref].
- (2) The **RDF!** (**RDF!**) of ions and molecules. The first two topics give a brief review of the principle of MD and MC, the last two detail the generation of data for the first two.

### 6.1 MOLECULAR DYNAMICS

#### 6.1.1 *Principle*

#### 6.1.2 *Determination of free energy: umbrella sampling*

### 6.2 MONTE CARLO METHOD

### 6.3 DIRECT CORRELATION FUNCTION OF WATER

described the direct correlation functions (DCF) used during the thesis, including different sources and forms, as well as their comparison.

#### 6.3.1 *Dipole DCF from molecular dynamics simulation*

#### 6.3.2 *Extraction of DCF from bulk Monte Carlo simulation*

This DCF set is calculated by Belloni *et al.* [50] and is presented here briefly for the purpose of clarification. First rotational invariant of the Fourier transform of the total correlation function  $h$

example:

$$\hat{c}^{000}(k) = \frac{\hat{h}^{000}(k)}{1 + n_0 \hat{h}^{000}(k)}$$

$g$  accumulated, solve the inverse OZ equation to find  $c$

norm of wave vector  $\|\mathbf{q}\| = \{i \cdot \Delta_q \mid 0 \leq i \leq n, i \in \mathbb{Z}\}$ , beginning from the 10th line, where  $\Delta_q$  is the minimum difference between two norm  $q$ .

#### 6.3.3 *Conventions*

whereas I take the notation of Wertheim and Hansen, or in k-space

$$\begin{aligned}
\Phi^{000} &= 1 \\
\Phi^{011} &= \hat{\mathbf{k}} \cdot \boldsymbol{\Omega}_1 \\
\Phi^{101} &= \hat{\mathbf{k}} \cdot \boldsymbol{\Omega}_2 \\
\Phi^{110} &= \boldsymbol{\Omega}_1 \cdot \boldsymbol{\Omega}_2 \\
\Phi^{112} &= 3(\hat{\mathbf{k}} \cdot \boldsymbol{\Omega}_1)(\hat{\mathbf{k}} \cdot \boldsymbol{\Omega}_2) - \boldsymbol{\Omega}_1 \cdot \boldsymbol{\Omega}_2
\end{aligned} \tag{6.1}$$

Different rotational invariant projections from Luc's c. Luc defines (according to Blum)

$$\begin{aligned}
\Phi^{000} &= 1 \\
\Phi^{011} &= i\mathbf{k} \cdot \boldsymbol{\Omega}_1 = i \cos \theta_1 \\
\Phi^{101} &= i\mathbf{k} \cdot \boldsymbol{\Omega}_2 = i \cos \theta_2 \\
\Phi^{110} &= -\sqrt{3}\boldsymbol{\Omega}_1 \cdot \boldsymbol{\Omega}_2 = -\sqrt{3}(\sin \theta_1 \sin \theta_2 \cos \phi_{12} + \cos \theta_1 \cos \theta_2) \\
\Phi^{112} &= \sqrt{\frac{3}{10}} [3(\mathbf{k} \cdot \boldsymbol{\Omega}_1)(\mathbf{k} \cdot \boldsymbol{\Omega}_2) - \boldsymbol{\Omega}_1 \cdot \boldsymbol{\Omega}_2] = \sqrt{\frac{3}{10}} (2 \cos \theta_1 \cos \theta_2 - \sin \theta_1 \sin \theta_2 \cos \phi_{12})
\end{aligned} \tag{6.2}$$

#### 6.3.4 Comparison with non-coupling dipole DCF in MDFT ( $n_{\max} = 1$ )

$$c_s^{000}, c_{\Delta}^{110}, c_d^{112}$$

#### 6.3.5 Comparison with respect to $n_{\max}$

first rotational invariants  $m_{\max} = 1$  (4 independent projections  $c_s^{000}, c_{\Delta}^{110}, c_d^{112}$  and  $c_{+}^{011} = -c_{-}^{101}$ ).

#### 6.3.6 Transform between ck\_angular and projections

$$\hat{c}_q(\cos \theta_1, \cos \theta_2, \phi, \psi_1, \psi_2)$$

columns:  $\cos \theta_1, \cos \theta_2, \psi_1, \psi_2, \phi = \phi_1 - \phi_2, \operatorname{Re}(\hat{c}), \operatorname{Im}(\hat{c})$ ; with  $(n_{\theta} + 1)n_{\theta}n_{\phi}n_{\psi}^2/4$  items as only  $\cos \theta_1 + \cos \theta_2 > 0$  and  $\phi \in [0, \pi]$  is stocked, where  $n_{(\text{angle})}$  is the number of angles for each dimension.

## 6.4 UMBRELLA SAMPLING

## Chapter II

# THEORY: HRF APPROXIMATION, FOR MOLECULAR SOLVENT

This chapter presents a complete theory of the  $\mathcal{F}_{\text{exc}}$  evaluation under HRF approximation:

$$\mathcal{F}_{\text{exc}} = -\frac{\beta^{-1}}{2} \int d\mathbf{r}_1 d\mathbf{r}_2 d\Omega_1 d\Omega_2 \Delta\rho(\mathbf{r}_1, \Omega_1) \Delta\rho(\mathbf{r}_2, \Omega_2) c(r_{12}, \Omega_1, \Omega_2)$$

which is based on previous work of Zhao et al. [61], where the HRF approximation has been applied to linear molecules ( $\Omega \equiv (\Theta, \Phi)$ ). In this thesis, the method is generated to molecular solvent, using 3 Euler angles, i. e.  $\Omega \equiv (\Theta, \Phi, \Psi)$ , where the computing cost of the original algorithm is no longer reasonable. Further approximation is therefore made, where the density variable  $\rho(\mathbf{r}, \Omega)$  is expended on generalized spherical harmonics. Theoretically, this approximation gives little loss of accuracy, but makes a great advantage in computing time and memory requirement. The prove is shown in the implementation part.

Section 7 describes the FFT treatment for the spatial convolution in the gradient  $\gamma$  of the excess functional  $\mathcal{F}_{\text{exc}}$ , which reduces the algorithm complexity from  $O(N^2)$  to  $O(N \log_2 N)$ . A DCF directly issue of Monte Carlo simulation and solution HNC is used, in both intermolecular and projection form. To use the intermolecular form, the matrix which does the transform from laboratory to intermolecular coordinates system is generalized to molecular case compared to previous work, then interpolation of zero and first order is involved. To use the projection form, DCF is reconstructed with all projections. For order of projections  $n_{\text{max}} = 1$ , the formula of each projections are written explicitly.

Section 8 presents the treatment of angular convolution. As IEM and MDFT have mathematical equivalence, an algorithm inspired by the work of Fries [14] and Blum [3, 4] for IEM is built for MDFT. In this algorithm, the density variable  $\rho(\mathbf{r}, \Omega)$  is expended on generalized spherical harmonics, then rotated onto intermolecular frame. It is shown that in this form, the OZ equation is largely simplified.

The solvent properties involved in this thesis are presented in the next two chapters. Section 9 presents some thermodynamic quantities, including the solvation free energy and its corrections, ... and section 10 gives some forms of structure that can be preformed, such as the radical distribution function, radical polarization functions, rotational invariants expansion, etc.



## REDUCTION OF SPATIAL CONVOLUTION BY FFT

---

As presented in section 5, to complete the minimization process of MDFT, we need to evaluate the excess functional as well as its gradient:

$$\mathcal{F}_{\text{exc}} = -\frac{\beta^{-1}}{2} \int d\mathbf{r}_1 d\mathbf{r}_2 d\Omega_1 d\Omega_2 \Delta\rho(\mathbf{r}_1, \Omega_1) \Delta\rho(\mathbf{r}_2, \Omega_2) c(\mathbf{r}_{12}, \Omega_1, \Omega_2) \quad (7.1)$$

$$\gamma(\mathbf{r}_1, \Omega_1) = -\beta^{-1} \int d\mathbf{r}_2 d\Omega_2 \Delta\rho(\mathbf{r}_2, \Omega_2) c(\mathbf{r}_{12}, \Omega_1, \Omega_2) \quad (7.2)$$

To evaluate the gradient  $\gamma$  for each  $(\mathbf{r}, \Omega)$ ,  $N \equiv N_r N_\Omega$  function evaluations (FE) are required, the total number of FE is thus  $N^2 = O(N^2)$ , which, with typically  $N_r = 64^3$  and  $N_\Omega = 50 \sim 100$ , is far too costly for current computing technology. For this reason, Fourier transform is used to treat the spatial convolution in eq. (7.2).

A convolution

$$h(x_1) \equiv f(x_2) \otimes g(x_2) \equiv \int_a^b f(x_2) g(x_1 - x_2) dx_2 \quad (7.3)$$

has the property that

$$\mathfrak{F}[h(x_1)] = \mathfrak{F}[f(x_2)] \mathfrak{F}[g(x_2)] \quad (7.4)$$

$\mathfrak{F}$  being the Fourier transform (FT) operation (*Attention d'avoir bien défini les FFT 3D avant*). As  $\mathbf{r}_{12} = \mathbf{r}_1 - \mathbf{r}_2$ , eq. (7.2) is a 3D convolution, which leads to

$$\hat{\gamma}(\mathbf{k}, \Omega_1) = -\beta^{-1} \int d\Omega_2 \Delta\hat{\rho}(\mathbf{k}, \Omega_2) \hat{c}(\mathbf{k}, \Omega_1, \Omega_2) \quad (7.5)$$

Thus the integral  $\int d\mathbf{r}_2$  in eq. (7.2) is transformed into a simple product in eq. (7.5). To get  $\hat{\gamma}(\mathbf{k}, \Omega_1)$  with given  $\Delta\hat{\rho}(\mathbf{k}, \Omega_2)$ , only  $N_r N_\Omega^2$  FE are needed. To this computational cost should be added the transform from  $\Delta\rho(\mathbf{r}, \Omega)$  to  $\Delta\hat{\rho}(\mathbf{k}, \Omega)$  and the backward transform from  $\hat{\gamma}(\mathbf{k}, \Omega)$  to  $\gamma(\mathbf{r}, \Omega)$  which are both of order  $N_\Omega \cdot O(N_r \log_2 N_r)$ , due to the properties of Fast Fourier Transforms (FFT). The total number of FE is thus reduced from quadratic complexity  $O(N_r^2 N_\Omega^2)$  to  $N_r N_\Omega^2 + 2N_\Omega \cdot O(N_r \log_2 N_r) = O(N_r \log_2 N_r N_\Omega^2)$ . As the total number of spatial grid  $N_r$  is of magnitude  $10^5 \sim 10^6$ , this procedure, which is mathematically equivalent to the direct evaluation (7.2), gives a great advantage in terms of computational efficiency (figure A.1 in section 1).

Once  $\gamma(\mathbf{r}, \Omega)$  is obtained by inverse Fourier transform of  $\hat{\gamma}(\mathbf{k}, \Omega)$ , the excess functional can be calculated as:

$$\mathcal{F}_{\text{exc}}[\rho(\mathbf{r}, \Omega)] = \frac{1}{2} \int d\mathbf{r} d\Omega \Delta\rho(\mathbf{r}, \Omega) \gamma(\mathbf{r}, \Omega) \quad (7.6)$$

It should be pointed out that the direct correlation function (DCF),  $\hat{c}(\mathbf{k}, \Omega_1, \Omega_2)$ , used as an input data in eq. (7.5) is very memory-costly. For instance, with a normal setting with  $64^3$  spatial grid and a Lebedev quadrature of order 2 (14 angles for  $\Theta$  and  $\Phi$ ), and 3  $\Psi$ -angles, even if the DCF is stocked in simple precision, it takes  $64^3 \times 42^2 \times 4$  bytes = 1.76GB, and for a Lebedev quadrature of order 5 and correspondingly 5  $\Psi$ -angles, it takes  $64^3 \times 250^2 \times 4$  bytes = 65.5GB. As a normal PC has only 4 to 16 GB of RAM, it can cause a memory leak. Therefore, two strategies are developed to reduce the storage of the DCF.

## 7.1 USING INTERMOLECULAR DCF

(In the previous work, the interpolation has been done with  $\Omega \equiv (\Theta, \Phi)$ . Here, we discuss the case of full 3 Euler angles  $\Omega \equiv (\Theta, \Phi, \Psi)$ . : To be put somewhere else.)

The first strategy aims to work in the so-called intermolecular frame described in fig. 7.1 for which, in  $\mathbf{r}$ -space, the  $z$  axis is oriented along the vector  $\mathbf{r}_{12} = \mathbf{r}_2 - \mathbf{r}_1$ , or in  $\mathbf{k}$ -space is oriented along the vector  $\mathbf{k}$ . In the latter case, an orientation  $\Omega \equiv (\Theta, \Phi, \Psi)$  in laboratory frame become  $\omega \equiv (\theta, \phi, \psi)$  in intermolecular frame.

To store the DCF in the intermolecular coordinates system, it can be defined as  $\hat{c}(k, \omega_1, \omega_2)$ , where  $(\omega_1, \omega_2) \equiv (\cos \theta_1, \cos \theta_2, \phi, \psi_1, \psi_2)$  and  $k$  is always oriented along the  $z$  axis (figure 7.1) such that only 6 variables are needed instead of 9 for  $\hat{c}(\mathbf{k}, \Omega_1, \Omega_2)$ , and the storage is considerably reduced. The transform from  $\hat{c}(k, \omega_1, \omega_2)$  to  $\hat{c}(\mathbf{k}, \Omega_1, \Omega_2)$  relies on the correspondence  $\omega(\mathbf{k}, \Omega) \equiv (\cos \theta, \phi, \psi)$ , which can be pre-calculated as a table of data.

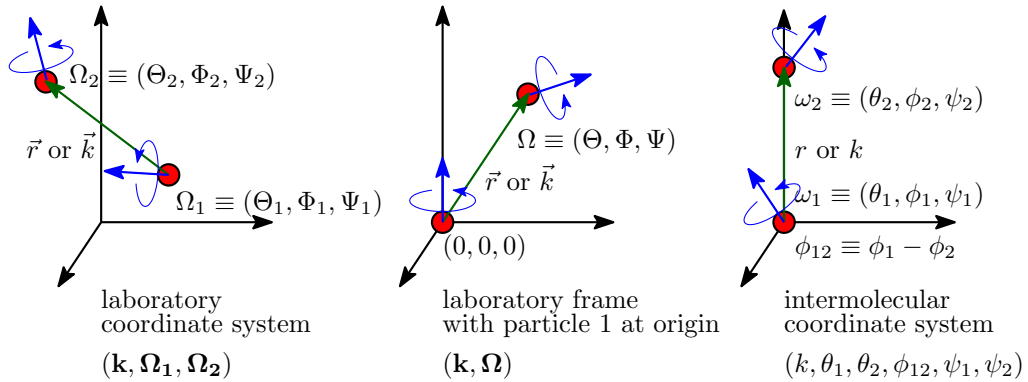


Figure 7.1: Molecules 1 and 2 in different coordinate systems

Finding  $\omega$  from  $\Omega$  amounts to defining the correspondence between the rotation matrices of the two coordinate systems.

The rotation matrix  $\hat{\mathbf{R}}_\Omega$  rotates the solvent molecule from  $\mathbf{I}$  to its orientation  $\hat{\mathbf{R}}_\Omega$ :

$$\hat{\mathbf{R}}_\Omega \mathbf{I} = \hat{\mathbf{R}}_\Omega \quad (7.7)$$

It can be expressed by 3 rotation operations  $\hat{\mathbf{R}}_\Phi$ ,  $\hat{\mathbf{R}}_\Theta$ , and  $\hat{\mathbf{R}}_\Psi$  which rotate along  $z - y - z$  axes (the same convention as defined in Messiah and Gray-Gubbins):

$$\begin{aligned} \hat{\mathbf{R}}_\Omega &= \begin{bmatrix} R_{xx} & R_{xy} & R_{xz} \\ R_{yx} & R_{yy} & R_{yz} \\ R_{zx} & R_{zy} & R_{zz} \end{bmatrix} \\ &= \begin{bmatrix} \cos \Phi & -\sin \Phi & 0 \\ \sin \Phi & \cos \Phi & 0 \\ 0 & 0 & 1 \end{bmatrix} \begin{bmatrix} \cos \Theta & 0 & \sin \Theta \\ 0 & 1 & 0 \\ -\sin \Theta & 0 & \cos \Theta \end{bmatrix} \begin{bmatrix} \cos \Psi & -\sin \Psi & 0 \\ \sin \Psi & \cos \Psi & 0 \\ 0 & 0 & 1 \end{bmatrix} \\ &= \begin{bmatrix} \cos \Phi \cos \Theta \cos \Psi - \sin \Phi \sin \Psi & -\cos \Phi \cos \Theta \sin \Psi - \sin \Phi \cos \Psi & \cos \Phi \sin \Theta \\ \sin \Phi \cos \Theta \cos \Psi + \cos \Phi \sin \Psi & -\sin \Phi \cos \Theta \sin \Psi + \cos \Phi \cos \Psi & \sin \Phi \sin \Theta \\ -\sin \Theta \cos \Psi & \sin \Theta \sin \Psi & \cos \Theta \end{bmatrix} \end{aligned} \quad (7.8)$$

As shown in fig. 7.2, the rotation matrix for transforming the DCF from the intermolecular coordinates to laboratory coordinates  $\hat{\mathbf{R}}_\omega$  can be written as:

$$\hat{\mathbf{R}}_\omega = \hat{\mathbf{R}}_k^{-1} \hat{\mathbf{R}}_\Omega \quad (7.9)$$

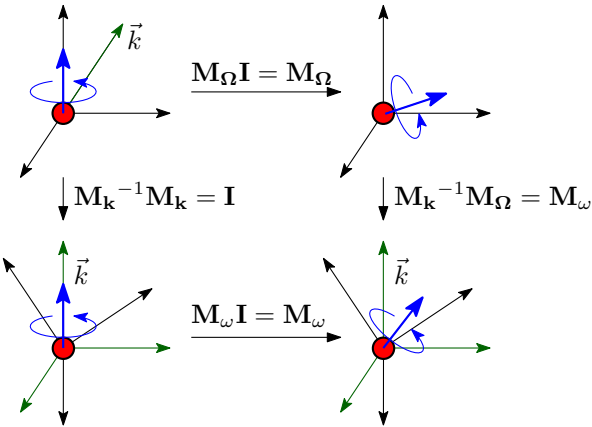


Figure 7.2: Rotation matrices

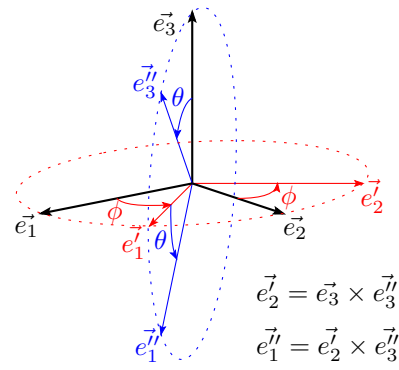


Figure 7.3: Rotation to k-frame

with the rotation matrix related to  $\mathbf{k}$  vector:

$$\hat{\mathbf{R}}_k^{-1} = \begin{bmatrix} \cos \theta_k \cos \phi_k & \cos \theta_k \sin \phi_k & -\sin \theta_k \\ -\sin \phi_k & \cos \phi_k & 0 \\ \sin \theta_k \cos \phi_k & \sin \theta_k \sin \phi_k & \cos \theta_k \end{bmatrix} \quad (7.10)$$

Here we fix  $\psi_k = 0$ . As  $\theta_k$  and  $\phi_k$  are calculated from Cartesian coordinates ( $k_x, k_y, k_z$ ), in the extreme cases that we cannot define  $\theta_k$  (for  $\|\mathbf{k}\| = 0$ ) and  $\phi_k$  (for  $k_x^2 + k_y^2 = 0$ ), we can arbitrarily fix those angles to zero.

A faster way to find the rotation matrix of  $\mathbf{k}$ , avoiding the evaluation of trigonometric functions, is shown in figure 7.3, where the matrix can be calculated by the cross products of basis vectors from  $z$  axis and  $\mathbf{k}$  vector ( $\mathbf{k} = \mathbf{e}_3''$ ):

$$\begin{bmatrix} \mathbf{e}_1'' & \mathbf{e}_2' & \mathbf{e}_3'' \end{bmatrix} = \begin{bmatrix} \mathbf{e}_1 & \mathbf{e}_2 & \mathbf{e}_3 \end{bmatrix} \hat{\mathbf{R}}_k = \hat{\mathbf{R}}_k \quad (7.11)$$

The two ways to calculate  $\mathbf{k}$  differ only in the case of  $\hat{\mathbf{k}} = [0 \ 0 \ -1]^T$ , where one is the inverse of the other. This is due to the different definitions of  $\phi_k$  (0 or  $\pi$  when  $\vec{k}_z$  superposes with  $\vec{k}_z$ ) in the two cases. Tests have shown that it has no influence on the final result of the excess functional evaluation.

Therefore, the elements of  $\hat{\mathbf{R}}_\omega$  can be calculated according to eq. (7.9):

$$\begin{aligned} \hat{\mathbf{R}}_\omega &= \begin{bmatrix} u_x & v_x & w_x \\ u_y & v_y & w_y \\ u_z & v_z & w_z \end{bmatrix} \\ &= \begin{bmatrix} \cos \phi \cos \theta \cos \psi - \sin \phi \sin \psi & -\cos \phi \cos \theta \sin \psi - \sin \phi \cos \psi & \cos \phi \sin \theta \\ \sin \phi \cos \theta \cos \psi + \cos \phi \sin \psi & -\sin \phi \cos \theta \sin \psi + \cos \phi \cos \psi & \sin \phi \sin \theta \\ -\sin \theta \cos \psi & \sin \theta \sin \psi & \cos \theta \end{bmatrix} \end{aligned} \quad (7.12)$$

The angles  $\omega$  are thus found as:

$$\begin{aligned} \cos \theta &= w_z \\ \phi &= \arccos(w_x / (w_x^2 + w_y^2)^{\frac{1}{2}}) \\ \psi &= \arccos(-u_z / (u_z^2 + v_z^2)^{\frac{1}{2}}) \end{aligned} \quad (7.13)$$

The resulting angles are between normal intervals,  $\cos \theta \in [-1, 1]$ ,  $\phi \in [0, 2\pi]$ . As water possesses  $C_{2v}$  symmetry, we take  $\psi \in [0, \pi]$ .

(Expliquer ici -à nouveau- pourquoi tu as besoin de faire des interpolations: grille plus fine pour om dans  $c(k, \text{om\_1}, \text{om\_2})$  et pour chaque  $(k, \Omega)$  on doit trouver le om corerspondant.)

The interpolation of these found angles to the intermolecular grid can be done with different orders: zeroth order interpolation, which directly takes the nearest point, or linear interpolation.

### 7.1.1 Zero-order interpolation of DCF

At this order, for each possible value of  $\mathbf{k}$  and  $\boldsymbol{\Omega}$ , the corresponding  $\cos \theta$  and  $\psi$  which relate to only one solvent molecule are stored as an index (single precision integer), which gives the nearest angle in a pre-defined table:

$$\begin{aligned} i_{\cos \theta} &= \lfloor (\cos \theta + 1)(n_{\cos \theta}/2) \rfloor + 1 \\ i_\psi &= \text{mod}(\lfloor \psi(n_\psi/\pi) \rfloor, n_\psi) + 1 \end{aligned} \quad (7.14)$$

where  $\lfloor f \rfloor$  is the floor function. For the angle  $\phi$  which relate to two solvent molecules, the operation  $\phi = \phi_1 - \phi_2$  introduces a double error when integer indices are used, as shown in figure 7.4.

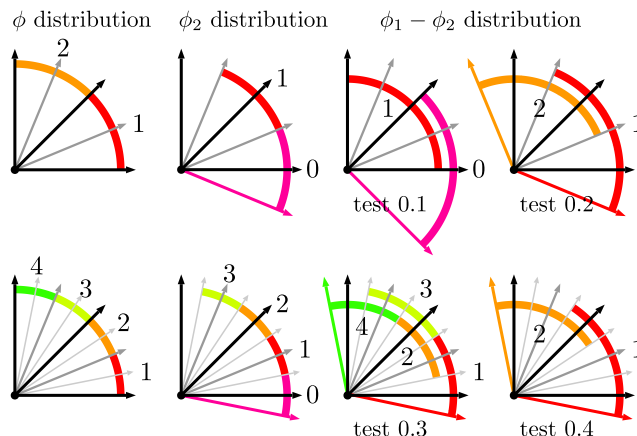


Figure 7.4:  $\phi_1 - \phi_2$  distribution: Test 0.1 is the direct subtraction of  $\phi$  established in the same way with  $\theta$  and  $\psi$ , as shown in the top first schema. Test 0.2 tabulates  $\phi_2$  by taking the nearest point in another manner, as shown in the second schema. In test 0.3-0.4, all  $\phi$  or only  $\phi_2$  is doubled.

In the actual implementation, as an integer takes 4 bytes and a real takes 8 bytes, there is no profit to tabulate  $\phi$  in integer two times, thus  $\phi$  is stored directly in real.

### 7.1.2 Linear interpolation of DCF

At this order,  $\omega(\mathbf{k}, \boldsymbol{\Omega})$  is stored in double precision. All angles are stored in real type, and the corresponding DCF is calculated as

$$c(\omega) = w_0 c(\omega_0) + w_1 c(\omega_1) \quad (7.15)$$

where  $w_0 = \frac{\omega_1 - \omega}{\omega_1 - \omega_0}$  and  $w_1 = \frac{\omega - \omega_0}{\omega_1 - \omega_0}$ . Here  $\omega$  is one of the 5 dimensions in  $\tilde{\omega}(\mathbf{k}, \boldsymbol{\Omega}_1, \boldsymbol{\Omega}_2) \equiv (\cos \theta_1, \cos \theta_2, \phi, \psi_1, \psi_2)$ ,  $\omega_0$  and  $\omega_1$  are the 2 nearest value points, while other variables

are fixed. If we express the weight for each dimension as  $w_{n_i}^i$  where  $i = 1, 2, 3, 4, 5$  is the  $i$ th variable, the total equation with 5 variables is:

$$c(\tilde{\omega}) = \left[ \sum_{n_1=0}^1 \sum_{n_2=0}^1 \sum_{n_3=0}^1 \sum_{n_4=0}^1 \sum_{n_5=0}^1 \left( \prod_i^5 w_{n_i}^i c(\tilde{\omega}_{n_1, n_2, n_3, n_4, n_5}) \right) \right] \quad (7.16)$$

These two equations are available for both interpolation and extrapolation, where the latter applies, e.g., for  $\cos \theta_1$  and  $\cos \theta_2$ .

An error evaluation of these two strategies of interpolation is shown in appendix F. Results demonstrate that the linear interpolation scheme is absolutely essential. On the other hand, as seen in eq. (7.16), it is computationally much more expensive than the simple histogram scheme as it requires  $2^5 = 32$  times of operations.

## 7.2 DIRECT CALCULATION OF DCF FROM ROTATIONAL INVARIANT PROJECTIONS

Another strategy to calculate  $\hat{c}(\mathbf{k}, \Omega_1, \Omega_2)$  is to use the DCF expressed in terms of rotational invariant projections, which takes far less memory than in the intermolecular form thanks to their angular independence and symmetric properties.

### 7.2.1 Using projections in form of $\hat{c}_{\mu\nu}^{mn}(k)$

As described by Blum [3, 4],  $\hat{c}(\mathbf{k}, \Omega_1, \Omega_2)$  can be expanded as

$$\hat{c}(\mathbf{k}, \Omega_1, \Omega_2) = \sum_{mn\mu\nu} \hat{c}_{\mu\nu}^{mn}(k) \Phi_{\mu\nu}^{mn}(\hat{\mathbf{k}}, \Omega_1, \Omega_2) \quad (7.17)$$

where  $\Phi_{\mu\nu}^{mn}(\hat{\mathbf{k}}, \Omega_1, \Omega_2)$  is the rotational invariant that depends on both the spatial and angular coordinates of the two particles (detailed in appendix C).

For projections of order  $n_{\max} = 1$ , the DCF can be expressed in very simple form. Only 4 projections  $\hat{c}^{mn}(k)$  are independent:  $\hat{c}_S \equiv \hat{c}^{000}$ ,  $\hat{c}_\Delta \equiv \hat{c}^{110}$ ,  $\hat{c}_D \equiv \hat{c}^{112}$  and  $\hat{c}_+ \equiv \hat{c}^{011} = -\hat{c}^{101}$ , with the corresponding rotational invariants expressed below both in laboratory and intermolecular frames (il faut définir ici OM\_1 et OM\_2 comme des vecteurs d'orientation !)

$$\begin{aligned} \Phi^{000} &= 1 \\ \Phi^{011} &= i\mathbf{k} \cdot \Omega_1 = i \cos \theta_1 \\ \Phi^{101} &= i\mathbf{k} \cdot \Omega_2 = i \cos \theta_2 \\ \Phi^{110} &= -\sqrt{3}\Omega_1 \cdot \Omega_2 = -\sqrt{3}(\sin \theta_1 \sin \theta_2 \cos \phi_{12} + \cos \theta_1 \cos \theta_2) \\ \Phi^{112} &= \sqrt{\frac{3}{10}} [3(\mathbf{k} \cdot \Omega_1)(\mathbf{k} \cdot \Omega_2) - \Omega_1 \cdot \Omega_2] \\ &= \sqrt{\frac{3}{10}} (2 \cos \theta_1 \cos \theta_2 - \sin \theta_1 \sin \theta_2 \cos \phi_{12}) \end{aligned} \quad (7.18)$$

To express the DCF at higher orders, the number of FE needed for  $\Phi_{\mu\nu}^{mn}(\hat{\mathbf{k}}, \Omega_1, \Omega_2)$  becomes huge and the DCF should be calculated in intermolecular frame as indicated above.

### 7.2.2 Using projections in form of $\hat{c}_{\mu\nu,\chi}^{mn}(k)$

Compared to the expression of  $\Phi_{\mu\nu}^{ml}(\hat{\mathbf{k}}, \Omega_1, \Omega_2)$  in laboratory frame (eq. (C.2) in appendix C), its intermolecular form has far fewer terms (eq. (C.18) in appendix C), such that

$$\hat{c}(k, \omega_1, \omega_2) = \frac{1}{2l+1} \sum_{mn\mu\nu\chi} \hat{c}_{\mu\nu,\chi}^{mn}(k) r_{\chi\mu}^m(\theta_1) r_{-\chi\nu}^n(\theta_2) e^{-i\chi(\phi_{12}\equiv\phi_1-\phi_2)} e^{-i\mu\psi_1} e^{-i\nu\psi_2} \quad (7.19)$$

where  $r$  is the generalized Legendre polynomial,  $m, n \leq n_{\max}$ ,  $|\mu| \leq m$ ,  $|\nu| \leq n$ , and  $\chi \in [-\min(m, n), \min(m, n)]$ .

$r_{\chi\mu}^m(\theta)$ ,  $e^{-i\chi\phi}(\phi)$  and  $e^{-i\mu\psi}(\psi)$  can be separately pre-tabulated for each given  $\mathbf{k}$ , to avoid double evaluation of each term.

E.q. (7.19) replaces the interpolation of eq. (7.16) by an exact formula and it requires the projections  $\hat{c}_{\mu\nu,\chi}^{mn}(k)$  to be stored in memory rather than the full angular representation  $\hat{c}(k, \omega_1, \omega_2)$ . It also requires the passage from orientations in laboratory frame to orientations in intermolecular frame, i.e. use of the formulas (7.13) for each  $\mathbf{k}$  vector.

# 8

## ANGULAR CONVOLUTION, A BETTER ALGORITHM

---

In section 7, the spatial convolution is treated by FFT thanks to the transitional invariance that leads to  $\mathbf{r}_{12} = \mathbf{r}_1 - \mathbf{r}_2$ . However, as the angular grid is not homogeneous, the relative coordinates of two angles cannot be simply represented  $\Omega_{12} = \Omega_1 - \Omega_2$ , therefore we cannot take advantage of the convolution property shown in eq. (7.3-7.4). On the other hand, these two-particle quantities also have rotational invariance. As proposed by Blum [3, 4] and used by Fries and Patey [14], a rotational invariant expansion technique reduces the molecular Ornstein-Zernike (MOZ) equation into smaller irreducible matrix equations. As there is a mathematical equivalence between IEM and MDFT (section 5), where eq. (7.5) can be regarded as the molecular OZ equation, this formalism can also be applied to MDFT.

### 8.1 ANGULAR CONVOLUTION USING BLUM'S REDUCTION

To build a relation between the irreducible form of the molecular OZ equation deduced by Blum (detailed in section 4)

$$\hat{\gamma}_{\lambda\mu,\chi}^{lm}(k) = \sum_{n=0}^{n_{\max}} \sum_{\nu=-n}^n (-)^{\chi+\nu} \Delta \hat{\rho}_{\lambda\nu,\chi}^{ln}(k) \hat{c}_{\mu\nu,\chi}^{mn}(k) \quad (8.1)$$

and the MDFT, a generalized spherical harmonic transform (GSHT) treatment is proposed by Luc Belloni, developing the functional gradient  $\hat{\gamma}$  and the density  $\hat{\rho}$  in eq. (7.5) on Wigner generalized spherical harmonics (GSH):

$$\hat{\gamma}(\mathbf{k}, \Omega_1) = \sum_{m\mu'\mu} f_m \hat{\gamma}_{\mu'\mu}^m(\mathbf{k}) R_{\mu'\mu}^m(\Omega_1) \quad (8.2)$$

$$\Delta \hat{\rho}(\mathbf{k}, \Omega_2) = \sum_{n\nu'\nu} f_n \Delta \hat{\rho}_{\nu'\nu}^n(\mathbf{k}) R_{\nu'\nu}^n(\Omega_2) \quad (8.3)$$

where  $0 \leq m \leq m_{\max}$ ,  $|\mu'|, |\mu| < m$  and  $|\nu'|, |\nu| < n$ .  $f_m = (2m+1)^{\frac{1}{2}}$  is the normalization factor (according to Luc's definition).

The DCF can also be expanded on rotational invariants [4], with the normalization factors derived according to Luc's definition:

$$\hat{c}(k, \Omega_1, \Omega_2) = \sum_{mnl\mu\nu} f_m f_n \hat{c}_{\mu\nu}^{mnl}(k) \sum_{\mu'\nu'\lambda'} \begin{pmatrix} m & n & l \\ \mu' & \nu' & \lambda' \end{pmatrix} R_{\mu'\mu}^m(\Omega_1) R_{\nu'\nu}^n(\Omega_2) R_{\lambda'0}^l(\hat{\mathbf{k}}) \quad (8.4)$$

As GSH possess orthogonality eq. (E.21) and symmetry eq. (E.15), eq. (7.5) can be rewritten by (8.2, 8.3, 8.4), which gives

$$\hat{\gamma}_{\mu'\mu}^m(\mathbf{k}) = \sum_{nl\nu} \hat{c}_{\mu\nu}^{mnl}(k) \sum_{\nu'\lambda'} (-)^{\nu'+\nu} \Delta \hat{\rho}_{\nu'\nu}^n(\mathbf{k}) \begin{pmatrix} m & n & l \\ \mu' & \nu' & \lambda' \end{pmatrix} R_{\lambda'0}^l(\hat{\mathbf{k}}) \quad (8.5)$$

thus the OZ equation is expanded on GSHs and rotational invariants.

Here the projections  $F_{\mu\nu,\chi}^{mn}$  is defined as eq. (appendix) with symmetries eq. (appendix). It's mathematically identical with [ref] but using  $R_{\mu'\mu}^m = D_{\mu'\mu}^{m*}$ .

Note that eq. (8.5) is reducible. Blum's  $\chi$ -transform defines[3]

$$\hat{c}_{\mu\nu,\chi}^{mn}(k) = \sum_l \begin{pmatrix} m & n & l \\ \chi & -\chi & 0 \end{pmatrix} \hat{c}_{\mu\nu}^{mnl}(k) \quad (8.6)$$

$\hat{c}_{\mu\nu,\chi}^{mn}(k)$  is exactly the invariant in eq. (8.1).

$$\hat{c}_{\mu\nu}^{mnl}(k) = (2l+1) \sum_{\chi} \begin{pmatrix} m & n & l \\ \chi & -\chi & 0 \end{pmatrix} \hat{c}_{\mu\nu,\chi}^{mn}(k) \quad (8.7)$$

Invariants of form  $F_{\mu\nu,\chi}^{mn}(k)$  have a very simple relation with their combined function  $F(k, \omega_1, \omega_2)$  in the intermolecular coordinate system (eq. (C.26, C.27)). In MDFT formalism, the projections of  $\hat{\gamma}$  and  $\hat{\rho}$  in local frame ( $\omega_i = \hat{k}\Omega_i$ ) are

$$\hat{\gamma}'(\mathbf{k}, \omega_1) = \sum_{m\chi\mu} f_m \hat{\gamma}_{\chi\mu}^m(\mathbf{k}) R_{\chi\mu}^m(\omega_1) \quad (8.8)$$

$$\Delta\hat{\rho}'(\mathbf{k}, \omega_2) = \sum_{n\chi\nu} f_n \Delta\hat{\rho}_{\chi\nu}^n(\mathbf{k}) R_{\chi\nu}^n(\omega_2) \quad (8.9)$$

and with the rotation formula of GSH (eq. (E.23)), we have

$$\hat{\gamma}_{\chi\mu}^m(\mathbf{k}) = \sum_{\mu'} \hat{\gamma}_{\mu'\mu}^m(\mathbf{k}) R_{\mu'\chi}^m(\hat{\mathbf{k}}) \quad (8.10)$$

$$\Delta\hat{\rho}_{\nu'\nu}^n(\mathbf{k}) = \sum_{\chi} \Delta\hat{\rho}_{\chi\nu}^n(\mathbf{k}) R_{\nu'\chi}^{n*}(\hat{\mathbf{k}}) = \sum_{\chi} \Delta\hat{\rho}_{\chi\nu}^n(\mathbf{k}) (-)^{\chi+\nu'} R_{\nu'\chi}^n(\hat{\mathbf{k}}) \quad (8.11)$$

Using eq. (8.10), (8.5), eq. (8.11), eq. (8.7) and GSH products relation eq. (E.24) and 3j-symbol orthogonality eq. (E.7), we deduce that:

$$\hat{\gamma}_{\chi\mu}^m(\mathbf{k}) = \sum_{n\nu} (-)^{\chi+\nu} \hat{c}_{\mu\nu,\chi}^{mn}(k) \Delta\hat{\rho}_{\chi\nu}^n(\mathbf{k}) \quad (8.12)$$

Eq. (8.12) is mathematically identical to eq. (8.1), as (to be verified with patient...)

$$\hat{\gamma}_{\chi\mu}^m(\mathbf{k}) = \sum_{l\lambda} \hat{\gamma}_{\lambda\mu,\chi}^{lm*}(k) R_{\chi\lambda}^l(\hat{\mathbf{k}}) \quad (8.13)$$

$$\hat{\rho}_{\chi\nu}^n(\mathbf{k}) = \sum_{l\lambda} \Delta\hat{\rho}_{\lambda\nu,\chi}^{ln*}(k) R_{\chi\lambda}^l(\hat{\mathbf{k}}) \quad (8.14)$$

And in this way, the integral of the angular part in eq. (7.5) is reduced to a sum of a few terms.

Table 8.1 shows some parameters linking to computing cost of different algorithms. It shows that the expansion on GSH (eq. (8.5)) projections does not give an enormous reduction of FE compared to its 6D function form (eq. (7.5)); but after the Blum's  $\chi$ -transform, the OZ function is largely reduced. As the spatial convolution takes advantage of the transitional invariance  $r_{12}$ , the  $\chi$ -transform in fact makes use of the rotational invariance.

## 8.2 FAST GENERALIZED SPHERICAL HARMONIC TRANSFORM

In the angular convolution algorithm above, the OZ equation is reduced to a few function evaluations by taking advantage of the orthogonality and symmetries of rotation invariants. It's analogous to the treatment of the convolution with FFT for spatial grids, in which the **generalized spherical harmonics transform** (GSHT) is used as an alternative of FFT for inhomogeneous grids, and it *a priori* should be fast.

$m_{\max}$	0	1	2	3	4	5
$N_{\Theta}$	1	2	3	4	5	6
$N_{\text{ang}}$ (Gauss-Legendre)	1 (1)	18 (6)	75 (45)	196 (84)	405 (225)	726 (330)
$N_{\text{ang}}$ (Lebedev $\times \psi$ )	1 (1)	18 (6)	70 (42)	182 (78)	342 (190)	550 (250)
$N_{\text{proj}}$	1 (1)	10 (4)	35 (19)	84 (40)	165 (85)	286 (140)
FE for eq. (7.5)	1 (1)	324 (36)	5625 (2025)	38416 (7056)	164025 (50625)	527076 (108900)
FE for eq. (8.5)	1 (1)	262 (6)	4787 (483)	36588 (1932)	175989 (13157)	633490 (36882)
FE for eq. (8.12)	1 (1)	34 (6)	259 (75)	1092 (252)	3333 (877)	8294 (2002)

Table 8.1: Number of FE needed by OZ equation of different form for arbitrary solvent (outside the parentheses) and solvent possessing  $C_{2v}$  symmetry (inside the parentheses)

The FGHST provides a forward-backward transform between a general angular function  $F(\boldsymbol{\Omega}) \equiv F(\cos \Theta, \Phi, \Psi)$  and its projections  $F_{\mu' \mu}^m$  ( $|\mu'|, |\mu| \leq m$ )

$$F_{\mu' \mu}^m = \frac{f_m}{8\pi^2} \int d\boldsymbol{\Omega} F(\boldsymbol{\Omega}) R_{\mu' \mu}^{m*}(\boldsymbol{\Omega}) \quad (\text{forward}) \quad (8.15)$$

$$F(\boldsymbol{\Omega}) = \sum_{m, \mu', \mu} f_m F_{\mu' \mu}^m R_{\mu' \mu}^m(\boldsymbol{\Omega}) \quad (\text{backward}) \quad (8.16)$$

where  $f_m = (2m+1)^{\frac{1}{2}} = \|R_{\mu' \mu}^m\|^{-1}$  is the normalization factor, and  $R_{\mu' \mu}^m(\boldsymbol{\Omega})$  is the Wigner generalized spherical harmonics (Appendix [Ref]) being defined as

$$R_{\mu' \mu}^m(\boldsymbol{\Omega}) = r_{\mu' \mu}^m(\Theta) e^{-i(\mu' \Phi + \mu \Psi)} \quad (8.17)$$

which form a complete orthogonal set.

### 8.2.1 Equivalence of order in angular quadratures and projections

Suppose that  $F(\boldsymbol{\Omega})$  is a polynomial of both  $\cos \Theta$ ,  $\cos \Phi$  and  $\cos \Psi$  of order  $n$ , ( $n+1$  polynomial terms). To expand completely this function as shown in equation (8.16), at least  $n_{\max} = n$  is needed. Then to evaluate exactly the integration in equation (8.15), at least  $n+1$  for  $\cos \Theta$  (Gauss-Legendre grid),  $2n+1$  for  $\Phi$  (equal-spaced grid),  $2n+1$  for  $\Psi$  (equal-spaced grid) points of angular grid are needed (c. f. appendix B). In the case of water which possesses a  $C_2$  symmetry  $F(\Psi + \pi) = F(\Psi)$ , only projections of even  $\mu$  are nonzero:

$$F_\mu = \int d\Psi F(\Psi) e^{i\mu\Psi} = \int d(\Psi + \pi) F(\Psi + \pi) e^{i\mu(\Psi+\pi)} = e^{i\mu\pi} \int d\Psi F(\Psi) e^{i\mu\Psi} = e^{i\mu\pi} F_\mu \quad (8.18)$$

$$F_\mu = \begin{cases} 0 & \mu = 2n+1, n \in \mathbb{Z} \\ F_\mu & \mu = 2n, n \in \mathbb{Z} \end{cases} \quad (8.19)$$

Therefore the function

$$F(\Psi) = \sum_\mu F_\mu e^{-i\mu\Psi} \quad (8.20)$$

can be rewritten as

$$F(\Psi_2/2 \equiv \Psi) = \sum_{\mu_2 \equiv \mu/2} F_{2\mu_2} e^{-i\mu_2\Psi_2} \quad (8.21)$$

As  $|\mu_2| \leq n/2$ ,  $F(\Psi_2/2 \equiv \Psi)$  is a polynomial of  $\cos \Psi_2$  of order  $\text{floor}(n/2) \equiv \lfloor n/2 \rfloor$ , in the forward transform

$$F_{2\mu_2 \equiv \mu} = \int d\Psi F(\Psi) e^{i\mu\Psi} = \frac{1}{2} \int d\Psi_2 F(\Psi_2/2 \equiv \Psi) e^{i\mu_2\Psi_2} \quad (8.22)$$

the total degree  $\cos \Psi_2$  polynomial in the integrand is  $2 \lfloor n/2 \rfloor$ , then  $2 \lfloor n/2 \rfloor + 1$  points of  $\Psi_2$  (or  $\Psi$ ) are needed.

For further implementation, it is interesting to distinguish the order of quadrature  $m_{\max}$  and the order of projection  $n_{\max}$ .

### 8.2.2 Integration of $\Phi, \Psi$ using FFT

$$\begin{aligned} F_{\mu'\mu}^m &= \frac{f_m}{8\pi^2} \sum_{i=0}^{m_{\max}} \sum_{j=0}^{2m_{\max}} \sum_{k=0}^{2\lfloor m_{\max}/s \rfloor} w_i F(\Theta_i \Phi_j \Psi_k) R_{\mu'\mu}^{m*}(\Theta_i \Phi_j \Psi_k) \quad (\text{forward}) \\ F(\Omega) &= \sum_{m=0}^{n_{\max}} \sum_{\mu'=-m}^m \sum_{\mu=-m}^m f_m F_{\mu'\mu}^m R_{\mu'\mu}^m(\Omega) \quad (\text{backward}) \end{aligned}$$

To integrate eq. (8.15) in a direct way,  $(m_{\max} + 1)(2m_{\max} + 1)(2 \lfloor m_{\max}/s \rfloor + 1) = N_\Theta N_{\Phi\Psi} = N_{FE}$  function evaluations (FE) are needed for each  $F_{\mu'\mu}^m$  ( $s = 1$  or  $2$  according to the symmetry  $C_s$  of solvent), an overall  $O(N_{FE}^2)$  process is needed and *vice versa*. A faster algorithm proposed by Numerical Recipes [49] suggests reducing this cost to  $O(N_\Theta^2 N_{\Phi\Psi} \ln N_{\Phi\Psi} \simeq N_{FE}^{4/3})$  by Fast Fourier Transform.

Following this idea, eq. (8.15) can be rewritten as:

$$F_{\mu'\mu}^m = \frac{f_m}{8\pi^2} \int d\Theta r_{\mu'\mu}^m(\Theta) F_{\mu'\mu}(\Theta) \simeq \frac{f_m}{8\pi^2} \sum_{i=1}^{m_{\max}+1} w_i r_{\mu'\mu}^m(\Theta_i) F_{\mu'\mu}(\Theta_i) \quad (8.23)$$

where  $w_i$  is the Gauss-Legendre quadrature weight with  $m_{\max} + 1$  points ( $\sum w_i = 2$ ), and  $F_{\mu'\mu}(\Theta_i)$  the  $\Phi, \Psi$  integration part with trapezoid (or Gauss-Chebyshev) quadrature

$$\begin{aligned} F_{\mu'\mu}(\Theta) &= \sum_{k'=0}^{2m_{\max}} \sum_{k=0}^{2\lfloor m_{\max}/s \rfloor} F(\Phi_{k'}, \Psi_k, \Theta) e^{i(\mu'\Phi_{k'} + \mu\Psi_k)} \\ &= \sum_{k'=0}^{2m_{\max}} \sum_{k=0}^{2\lfloor m_{\max}/s \rfloor} F(\Phi_{k'}, \Psi_k, \Theta) e^{2\pi i \mu' k' / (2m_{\max} + 1)} e^{2\pi i \mu k / (2 \lfloor m_{\max}/s \rfloor + 1)} \end{aligned} \quad (8.24)$$

which shares the same formula with an FFT-2D process.

Similarly, the backward process (8.16) can be rewritten as:

$$\begin{aligned} F(\Theta, \Phi, \Psi) &= \sum_{m=0}^{n_{\max}} \sum_{\mu'=-m}^m \sum_{\mu=-m}^m f_m F_{\mu'\mu}^m R_{\mu'\mu}^m(\Omega) \\ &= \sum_{\mu'=-n_{\max}}^{n_{\max}} \sum_{\mu=-n_{\max}}^{n_{\max}} \sum_{m=\max(|\mu'|, |\mu|)}^{n_{\max}} f_m F_{\mu'\mu}^m R_{\mu'\mu}^m(\Omega) \\ &= \sum_{\mu'=-n_{\max}}^{n_{\max}} \sum_{\mu=-n_{\max}}^{n_{\max}} F_{\mu'\mu}(\Theta) e^{-i(\mu'\Phi + \mu\Psi)} \end{aligned} \quad (8.25)$$

with

$$F_{\mu'\mu}(\Theta) = \sum_{m=\max(|\mu'|, |\mu|)}^{n_{\max}} f_m F_{\mu'\mu}^m R_{\mu'\mu}^m(\Theta) \quad (8.26)$$

The FFTW3 library [15] is used for implementation, which performs discrete Fourier Transform (DFT) as defined here:

$$Y_k = \sum_{j=0}^{n-1} X_j e^{-2\pi i j k / n} \quad (\text{forward}) \quad (8.27)$$

$$X_j = \sum_{k=0}^{n-1} Y_k e^{2\pi i j k / n} \quad (\text{backward}) \quad (8.28)$$

Note that after a forward-backward Fourier transform, the original function is multiplied by a normalization factor  $N_k$ , which is the total number of nodes  $k$ .

For real input function  $Y_k$  ( $k = 0, \dots, n-1$ ), FFTW3 only outputs elements  $k = 0, \dots, \lfloor n/2 \rfloor$  ( $\lfloor n/2 \rfloor + 1$  complex numbers of  $X_j$  are stocked), with the “Hermitian” symmetry

$$Y_k = Y_{n-k}^* \quad (8.29)$$

used to regenerate elements of  $k > \lfloor n/2 \rfloor$ . The resulting  $X_j$  issue from the corresponding backward transform is purely real. As the angular function  $F(\Omega)$  is real, and the GSHs possess symmetry [19, 44] of

$$\begin{aligned} r_{-\mu', -\mu}^m(\Theta) &= (-1)^{\mu' + \mu} r_{\mu' \mu}^m(\Theta) \\ R_{-\mu', -\mu}^m(\Omega) &= (-1)^{\mu' + \mu} R_{\mu' \mu}^{m*}(\Omega) \end{aligned} \quad (8.30)$$

the symmetry relation between the projections are

$$F_{-\mu', -\mu}^m = (-1)^{\mu' + \mu} F_{\mu' \mu}^{m*} \quad (8.31)$$

Therefore only the projections of  $\mu \geq 0$  need to be stocked, which can be calculated with only these FFTW3 output elements. The full process of FFTW3-2D real to real transform is illustrated in figure 8.1.

<b>dim 1</b>		in_forward / out_backward (real)	in_backward / out_forward (complex)
array index		1 2 3 ... $m'+1$ $m'+2$ ... $2m'$ $2m'+1$	1 2 3 ... $m'+1$
real index		0 1 2 ... $m'$ $m'+1$ ... $2m'-1$ $2m'$	0 1 2 ... $m'$
$k \leftrightarrow \mu$		1 2 3 ... $m'+1$ $m'+2$ ... $2m'$ $2m'+1$	0 1 2 ... $m'$
<b>dim 2</b>		in_forward / out_backward (complex)	in_backward / out_forward (complex)
array index		1 2 3 ... $m+1$ $m+2$ ... $2m$ $2m+1$	1 2 3 ... $m+1$ $m+2$ ... $2m$ $2m+1$
real index		0 1 2 ... $m$ $m+1$ ... $2m-1$ $2m$	0 1 2 ... $m$ $m+1$ ... $2m-1$ $2m$
$k' \leftrightarrow \mu'$		1 2 3 ... $m+1$ $m+2$ ... $2m$ $2m+1$	0 1 2 ... $m$ $-m$ $-m+1$ ... $-1$

Figure 8.1: Indices arrangement in a complete forward-backward process of FFT-2D. The DFT of dim 1 ( $\Psi_k$  to  $\mu$ ) and dim 2 ( $\Phi_{k'}$  to  $\mu'$ ) are done sequentially and *vice versa*. Array index is the one used by Fortran array, real index is the one shown in eq. (8.27) and (8.28),  $k$  and  $k'$  indices shown in the left as well as  $\mu$  and  $\mu'$  in the right are those in eq. (8.24) and (8.25). Here  $m = m_{\max}$  and  $m' = \lfloor m_{\max} / s \rfloor$ .

As the output array of FFTW3 is periodic,

$$e^{2\pi i \mu k / n} = e^{2\pi i (\mu - n) k / n} e^{2\pi i k} = e^{2\pi i (\mu - n) k / n} \quad (8.32)$$

the indices  $\mu = m_{\max} + 1, \dots, 2m_{\max}$  actually correspond to  $\mu = -m_{\max}, \dots, -1$ . Note that eq. (8.24) and (8.25) do not possess the periodicity of eq. (8.32), only in the domain of definition of  $\mu'$  and  $\mu$  some intermediary functions share the same formula with FFT.

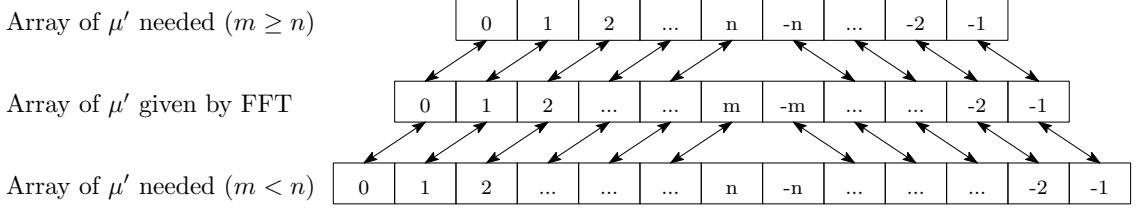


Figure 8.2: mmax to nmax

Moreover, from eq. (8.24), (8.26) and (8.31), we can verify that

$$F_{\mu'\mu}(\Theta) = F_{-\mu',-\mu}^*(\Theta) \quad (8.33)$$

The latter is used in the code because according to the definition in eq. (8.27) and (8.28),  $F_{-\mu',-\mu}(\Theta)$  is calculated instead of  $F_{\mu'\mu}(\Theta)$ .

### 8.3 OPERATIONAL ALGORITHM

As described above, the whole process of  $\gamma$  and  $\mathcal{F}_{\text{exc}}$  functional evaluation is as shown below:

Firstly, the solvent density variable  $\Delta\rho(\mathbf{r}, \Omega)$  is expanded on generalized spherical harmonics

$$\Delta\rho_{\mu'\mu}^m(\mathbf{r}) = \frac{f_m}{8\pi^2} \int d\Omega \Delta\rho(\mathbf{r}, \Omega) R_{\mu'\mu}^{m*}(\Omega) \quad (8.34)$$

Then the Fourier transform of these projections is computed:

$$\hat{\Delta\rho}_{\mu'\mu}^m(\mathbf{k}) = \int d\mathbf{r} \Delta\rho_{\mu'\mu}^m(\mathbf{r}) e^{-i\mathbf{r}\cdot\mathbf{k}} \quad (8.35)$$

Afterwards the projections in k-frame are then rotated into the local coordinate system along the unit vector  $\hat{\mathbf{k}}$

$$\hat{\Delta\rho}_{\chi\mu}^m(\mathbf{k}) = \sum_{\mu'} \hat{\Delta\rho}_{\mu'\mu}^m(\mathbf{k}) R_{\mu'\chi}^m(\hat{\mathbf{k}}) \quad (8.36)$$

where the evaluation of rotation matrix elements by recurrence is detailed [in appendix](#).

Next, computing the OZ equation with Blum's reduction:

$$\hat{\gamma}_{\chi\mu}^m(\mathbf{k}) = \sum_{n,\nu} (-1)^{\chi+\nu} \hat{c}_{\mu\nu,\chi}^{mn}(\mathbf{k}) \hat{\Delta\rho}_{\chi\nu}^n(\mathbf{k}) \quad (8.37)$$

The  $\gamma$  projections are then transformed back to global coordinates system:

$$\hat{\gamma}_{\mu'\mu}^m(\mathbf{k}) = \sum_{\chi} \hat{\gamma}_{\chi\mu}^m(\mathbf{k}) R_{\mu'\chi}^{m*}(\hat{\mathbf{k}}) \quad (8.38)$$

From here the inverse Fourier transform of these projections is:

$$\gamma_{\mu'\mu}^m(\mathbf{r}) = \int d\mathbf{k} \hat{\gamma}_{\mu'\mu}^m(\mathbf{k}) e^{i\mathbf{r}\cdot\mathbf{k}} \quad (8.39)$$

Then the function in angular frame can thus be rebuilt

$$\gamma(\mathbf{r}, \Omega) = \sum_{m,\mu',\mu} f_m \gamma_{\mu'\mu}^m(\mathbf{r}) R_{\mu'\mu}^m(\Omega) \quad (8.40)$$

Finally, the functional  $\mathcal{F}_{\text{exc}}$  is computed by

$$\mathcal{F}_{\text{exc}} = \frac{1}{2} \int d\mathbf{r} d\Omega \Delta\rho(\mathbf{r}, \Omega) \gamma(\mathbf{r}, \Omega) \quad (8.41)$$

### 8.3.1 Reduction by symmetry

A further reduction of computing cost can be made by performing approximately only half of the operations, thanks to the symmetric relations between the projections.

In eq. (8.34),  $\Delta\rho(\mathbf{r}, \Omega)$  is real. Thanks to the property of GSH (eq. (appendix)),

$$R_{\mu'\mu}^m(\Omega) = (-)^{\mu'+\mu} R_{-\mu'-\mu}^{m*}(\Omega)$$

we find

$$\Delta\hat{\rho}_{\mu'\mu}^m(\mathbf{r}) = (-)^{\mu'+\mu} \Delta\hat{\rho}_{-\mu',-\mu}^{m*}(\mathbf{r}) \quad (8.42)$$

therefore only  $\mu' > 0$  or  $\mu > 0$  is needed to generate all information.

When  $\Delta\hat{\rho}_{\mu'\mu}^m(\mathbf{r})$  is transformed into  $k$ -space, replacing eq. (8.35) with eq. (8.42) gives

$$\Delta\hat{\rho}_{\mu'\mu}^m(\mathbf{k}) = (-)^{\mu'+\mu} \Delta\hat{\rho}_{-\mu',-\mu}^{m*}(-\mathbf{k}) \quad (8.43)$$

Thus only the projections of  $\mu' > 0$ ,  $\mu > 0$  or  $\mathbf{k}$  where one of the dimensions  $k_i > 0$  are independent.

The rotation to local frame is governed by the relation (prove?):

$$R_{\mu'\chi}^m(\hat{\mathbf{k}}) = (-)^m R_{\mu',-\chi}^m(-\hat{\mathbf{k}}) = (-)^{m+\mu'+\chi} R_{-\mu',\chi}^m(-\hat{\mathbf{k}}) \quad (8.44)$$

which gives

$$\Delta\hat{\rho}_{\chi\mu}^m(\mathbf{k}) = (-)^{m+\mu+\chi} \Delta\hat{\rho}_{\chi,-\mu}^{m*}(-\mathbf{k}) \quad (8.45)$$

Thanks to the symmetry (eq. (appendix))

$$\hat{c}_{\mu\nu,\chi}^{mn}(k) = (-)^{m+n+\mu+\nu} \hat{c}_{\underline{\mu}\underline{\nu},\chi}^{mn*}(k) \quad (8.46)$$

$$\hat{c}_{\mu\nu,\chi}^{mn}(k) = (-)^{m+n} \hat{c}_{\nu\mu,\chi}^{nm}(k) \quad (8.47)$$

$$\hat{c}_{\mu\nu,\chi}^{mn}(k) = \hat{c}_{\underline{\mu}\underline{\nu},\chi}^{mn}(k) = (-)^{m+n} \hat{c}_{\mu\nu,\chi}^{mn*}(k) \quad (8.48)$$

$\hat{\gamma}_{\chi\mu}^m(\mathbf{k})$  possesses the same symmetry. Thus the OZ equation can be reduced by a factor of two.

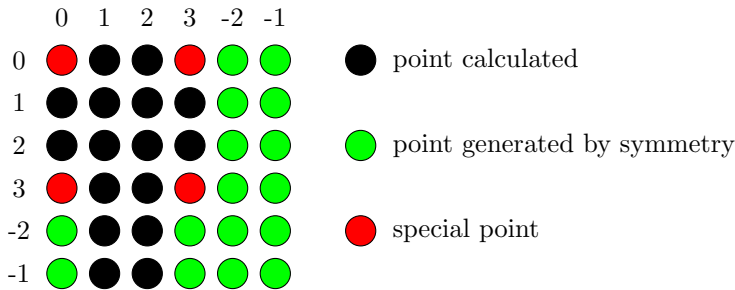


Figure 8.3: Distribution of points to be calculated according to symmetry in a 2D plan

### 8.3.2 Commutativity between operations

As mentioned in the operational algorithm, three types of operations are being done before and after the OZ equation. They are

1. Fast Fourier Transform for 3-dimensional spatial grid (FFT3D): implemented by package FFTW3 [15], mathematically leading to no accuracy lost.

2. Fast generalized spherical harmonics transform (FGSHT): has real or complex input, is exact if  $F(\Omega)$  is a polynomial of  $\cos \Theta$ ,  $\cos \Phi$  and  $\cos \Psi$  of order at most  $m_{\max}$ .
3. Rotation between laboratory coordinate system and local system linked to vector  $\mathbf{k}$  (RotS): can be done for both function and projections. It introduces a minus error in accuracy at origin and border of the box, which will be discussed in the next chapter.

Their commutativity is shown in figure 8.4.

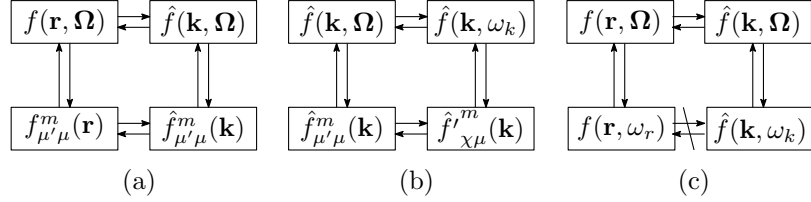


Figure 8.4: Commutativity of operations. (a) FFT3D and FGSHT; (b) RotS and FGSHT; (c) FFT3D and RotS

### 8.3.2.1 FFT3D and FGSHT

The FFT3D

$$f(\mathbf{r}) = \int \hat{f}(\mathbf{k}) e^{i\mathbf{k}\cdot\mathbf{r}}$$

$$\hat{f}(\mathbf{k}) = \int f(\mathbf{r}) e^{-i\mathbf{k}\cdot\mathbf{r}}$$

does not depend on the angular part of the function, and

$$f(\Omega) = \sum_{m\mu'\mu} f_m f_{\mu'\mu}^m R_{\mu'\mu}^m(\Omega)$$

$$f_{\mu'\mu}^m = \int f(\Omega) R_{\mu'\mu}^m(\Omega)$$

does not depend on the spatial part of the function. The two operations are commutative.

### 8.3.2.2 FGSHT and coordinate rotation

Function  $\hat{f}'$  intermolecular frame can be deduced from the function  $\hat{f}$  in laboratory frame

$$\hat{f}(\mathbf{k}, \Omega) = \hat{f}'(\mathbf{k}, \omega_k)$$

where the two can both be expanded on GSH

$$\hat{f}(\mathbf{k}, \Omega) = \sum_{m\mu'\mu} f_m \hat{f}_{\mu'\mu}^m(\mathbf{k}) R_{\mu'\mu}^m(\Omega)$$

$$\hat{f}'(\mathbf{k}, \omega_k) = \sum_{m\chi\mu} f_m \hat{f}'_{\chi\mu}^m(\mathbf{k}) R_{\chi\mu}^m(\omega_k)$$

And the relations between projections are simple

$$f'_{\chi\mu}^m(\mathbf{k}) = \sum_{\mu'} R_{\mu'\chi}^m(\hat{\mathbf{k}}) f_{\mu'\mu}^m(\mathbf{k})$$

$$f_{\mu'\mu}^m(\mathbf{k}) = \sum_{\chi} R_{\mu'\chi}^{m*}(\hat{\mathbf{k}}) f'_{\chi\mu}^m(\mathbf{k})$$

Thus the two operations are commutative.

### 8.3.2.3 Coordinate rotation and FFT3D

The rotation from  $f(\mathbf{r}, \Omega)$  to  $f(\mathbf{r}, \omega)$  depends on the vector  $\mathbf{r}$ , of which the information is totally lost after FFT3D. The rotation from  $f(\mathbf{k}, \Omega)$  to  $f(\mathbf{k}, \omega)$  can only depend on the vector  $\mathbf{k}$ , they are not the same rotation, therefore non-commutative.



# 9

## FREE ENERGY AND RELATED THERMODYNAMIC QUANTITIES

---

The solvation free energy is the most important property that we seek; as shown in previous sections, it can be calculated by the minimization of free energy functional  $\mathcal{F}[\rho]$ . Here is a discussion about some corrections needed for charged solutes and some related thermodynamic quantities that can be obtained directly from the solvation free energy.

The solvation properties often involve the three-dimensional microscopic structure of the solvent around the dissolved molecule, as well as thermodynamic quantities such as the enthalpy, entropy, and free energy of solvation. [ref gubbins] pKa [ref]

The solvation properties can be determined if the two principle properties, free energy and structure, are accurately calculated. In this thesis, we focus on these two aspects.

### 9.1 FREE ENERGY CORRECTION FOR SINGLE IONS

In the calculation of external potential as well as the total solvation free energy, the use of different conventions can lead to a charge-independent offset, which introduces error for charged solutes [27, 34, 35]. This offset is mainly caused by two sources: (1) resulting from the use of a finite system size; in our case, is a system with cubic periodic boundary conditions, which presents artificial interactions between the ion and its own periodic copies, as well as between the solvent and the periodic copies of the ion (Type-B in [35]); (2) resulting from the choice of convention for summing up the contributions of solvent charges to the electrostatic potential in the sample system (Type-C in [35]).

#### 9.1.1 Correction of type B

Type B correction should be added for systems with finite size or periodic boundary conditions, accounting for the error in the solvent polarization

$$\Delta G_B = \frac{1}{8\pi\epsilon_0} (1 - \epsilon^{-1}) \frac{q^2}{L} \left[ \xi + \frac{4\pi}{3} \left( \frac{R_I}{L} \right)^2 - \frac{16\pi}{45} \left( \frac{R_I}{L} \right)^5 \right] \quad (9.1)$$

where

$\epsilon_0$  is the vacuum permittivity;

$\epsilon$  is the solvent permittivity (dielectric constant);

$q$  is the solute charge;

$L$  is the box length;

$R_I$  is the ionic radius;

$\xi$  is the energy per particle in a simple cubic lattice,  $\xi \simeq -2.837297$  [45].

Another way to evaluate this error is to make a numerical extrapolation of the inverse of the box size ( $1/L$ ); it is more accurate, but demands much more calculation.

As  $R_I$  is significantly smaller than the size of the computational box, i. e.  $R_I \ll L$ , its quadratic as well as higher order of  $(R_I/L)$  is considered negligible, thus eq. (9.1) becomes

$$\Delta G_B = \frac{\xi}{8\pi\epsilon_0} (1 - \epsilon^{-1}) \frac{q^2}{L} \quad (9.2)$$

It links to Born correction.

### 9.1.2 Correction of type C

Type-C corrections are needed when the systems to be compared use different electrostatic summation schemes: on the basis of point charges within entire solvent molecules (M scheme) or on the basis of individual point charges (P scheme), shown in figure 9.1 (c) and (d), which brings a fixed free energy difference at the boundary.

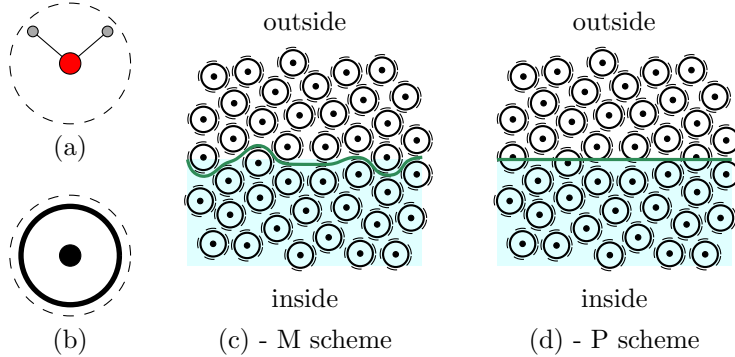


Figure 9.1: IQ model and summation scheme. (a) The solvent molecule. (b) The equivalent isotropic quadrupole (IQ) fluid model. (c) In the M scheme, one evaluates the Coulombic potential generated by the solvent charges belonging to all molecules within the boundary. (d) In the P scheme, one evaluates the Coulombic potential generated by all solvent charges within the boundary.

It can be deduced analytically by considering the solvent as a **canonical ensemble** under the orientational disorder limit (ODL) [34], which becomes an isotropic quadrupole (IQ) fluid, whose solvent molecule (figure 9.1 (b)) possesses the same quadrupole trace  $\gamma$

$$\gamma = \text{tr}(\mathcal{Q}) = \mathcal{Q}_{xx} + \mathcal{Q}_{yy} + \mathcal{Q}_{zz} \quad (9.3)$$

$\gamma$  is elsewhere referred to as the spheropole moment [41, 55], which is the spherical component of the quadrupole moment, and is invariant with respect to rotations.

where the quadrupole moment of the solvent molecule can be calculated by its definition [51]

$$\mathcal{Q}_{ij} = \int_V r_i r_j \rho(\mathbf{r}) dv = \sum_{\alpha=1}^N q^{(\alpha)} r_i^{(\alpha)} r_j^{(\alpha)} \quad (9.4)$$

It can be shown that the charge density of the solvent located within the boundary of the sample system vanishes everywhere, except at the boundary in the M scheme, which results in a uniform normal surface polarization. The correction needed for **M scheme** is

$$\Delta G_C = -q \left( 1 - \frac{4\pi R_I^3}{3L^3} \right) \Delta \Phi_{\text{ODL}} \quad (9.5)$$

where  $\Delta \Phi_{\text{ODL}} = (6\epsilon_0)^{-1} \eta \gamma$ ,  $\eta$  being the solvent number density.

In the same way, when we consider  $R_I \ll L$ , eq. (9.5) becomes

$$\Delta G_C = -(6\epsilon_0)^{-1} \eta \gamma q \quad (9.6)$$

## 9.2 SOME RELATED THERMODYNAMIC QUANTITIES

"expansion work" term PV

Thermodynamic quantities such as the internal energy, pressure, compressibility and heat capacity are obtained as derivatives of the classical partition function. [Evans poly]  
 Structure and Thermodynamic Properties of Bulk Liquids  
 pressure is (virial pressure equation)

$$p = \rho k_B T - \frac{\rho^2}{2} \int d\mathbf{r} g(r) \frac{r}{3} \frac{du(r)}{dr} \quad (9.7)$$

the The Gibbs free energy G is simply [Evans 1979]

$$G = \mu \int d\mathbf{r} \rho(\mathbf{r})$$

### 9.2.1 Solubility

### 9.2.2 Pressure

enthalpy, entropy [3] pH



# 10

## SOLVATION STRUCTURE

---

In MDFT, all the information about solvation structure can be deduced from the solvent density  $\rho(\mathbf{r}, \Omega)$ . This section presents some examples of structure which are used in later chapters.

### 10.1 RADIAL DISTRIBUTION FUNCTION AND SITE-SITE DISTRIBUTION FUNCTION

Radial distribution function (**RDF!**) and site-site distribution function

It should be the same with

### 10.2 RADIAL POLARIZATION FUNCTIONS

It should be the same with

### 10.3 ROTATIONAL INVARIANT EXPANSION

appendix C

### 10.4 REBUILT OF DENSITY IN A CERTAIN ORIENTATION

appendix C

#### 10.4.1 Radical distribution function of numeric density

Content.

#### 10.4.2 Radical distribution function of polarization

$$F(\mathbf{r}, \Omega) = \sum_{nl\nu} F_{0\nu}^{0nl}(r) \Phi_{0\nu}^{0nl}(\mathbf{r}, \Omega)$$

conversely

$$F_{0\nu}^{0nl}(r) = \int d\hat{\mathbf{r}} d\Omega F(\mathbf{r}, \Omega) \Phi_{0\nu}^{0nl*}(\mathbf{r}, \Omega) / \int d\hat{\mathbf{r}} d\Omega \left\| \Phi_{0\nu}^{0nl}(\mathbf{r}, \Omega) \right\|^2$$

with

$$\Phi_{0\nu}^{0nl}(\mathbf{r}, \Omega) = f_n \sum_{\nu'} \begin{pmatrix} 0 & n & l \\ 0 & \nu' & -\nu' \end{pmatrix} R_{\nu'\nu}^n(\Omega) R_{-\nu',0}^l(\hat{\mathbf{r}})$$

in particular

$$\begin{aligned}\Phi_{00}^{011}(\mathbf{r}, \boldsymbol{\Omega}) &= \sqrt{3} \begin{pmatrix} 0 & 1 & 1 \\ 0 & 0 & 0 \end{pmatrix} R_{00}^1(\boldsymbol{\Omega}) R_{00}^1(\hat{\mathbf{r}}) \\ &+ \sqrt{3} \begin{pmatrix} 0 & 1 & 1 \\ 0 & 1 & -1 \end{pmatrix} R_{10}^1(\boldsymbol{\Omega}) R_{-10}^1(\hat{\mathbf{r}}) \\ &+ \sqrt{3} \begin{pmatrix} 0 & 1 & 1 \\ 0 & -1 & 1 \end{pmatrix} R_{-10}^1(\boldsymbol{\Omega}) R_{10}^1(\hat{\mathbf{r}})\end{aligned}$$

or

$$\begin{aligned}\Phi_{00}^{011}(\mathbf{r}, \boldsymbol{\Omega}) &= -3R_{00}^1(\boldsymbol{\Omega}) R_{00}^1(\hat{\mathbf{r}}) \\ &+ 3R_{10}^1(\boldsymbol{\Omega}) R_{-10}^1(\hat{\mathbf{r}}) \\ &+ 3R_{-10}^1(\boldsymbol{\Omega}) R_{10}^1(\hat{\mathbf{r}})\end{aligned}$$

noting

$$R_{00}^1(\boldsymbol{\Omega}) = \cos \theta$$

$$R_{10}^1(\boldsymbol{\Omega}) = -\frac{1}{\sqrt{2}} \sin \theta e^{-i\phi}$$

one finds

$$\begin{aligned}\Phi_{00}^{011}(\mathbf{r}, \boldsymbol{\Omega}) &= -3R_{00}^1(\boldsymbol{\Omega}) R_{00}^1(\hat{\mathbf{r}}) \\ &+ 3R_{10}^1(\boldsymbol{\Omega}) R_{-10}^1(\hat{\mathbf{r}}) \\ &+ 3R_{-10}^1(\boldsymbol{\Omega}) R_{10}^1(\hat{\mathbf{r}}) \\ &= -3\boldsymbol{\Omega} \cdot \hat{\mathbf{r}}\end{aligned}$$

such that

$$\begin{aligned}F_{00}^{011}(r) &= -\frac{1}{3} \int \\ &= P(\mathbf{r}) \cdot \hat{\mathbf{r}}\end{aligned}$$

proportionality coefficient to be determined precisely... One thus gets the radial projection of the polarization.

Content.

## Chapter III

# IMPLEMENTATION

The code MDFT developed in this thesis is based on the branch master of Git project MDFT (<https://github.com/maxlevesque/MDFT/>), version [Fri Jun 20 19:05:52 2014 +0200]. All the implementations are run on **POINCARE** machines of IDRIS, which involved two kinds of machines:

**poincare[001-092]:** 2 processors Sandy Bridge E5-2670 (2.60GHz, 8 cores per processor, being 16 cores per node); 32 GB of memory per node.

**poincarebig[01-02]:** 4 processors AMD Opteron 6282 (2.60GHz, 16 cores per processor, being 64 cores per node); 128 GB of memory per node.

The former is used for regular calculation, whose memory hierarchy is shown in figure 10.1. The later is only used in the evaluation of accuracy, in case of memory leak in the former.

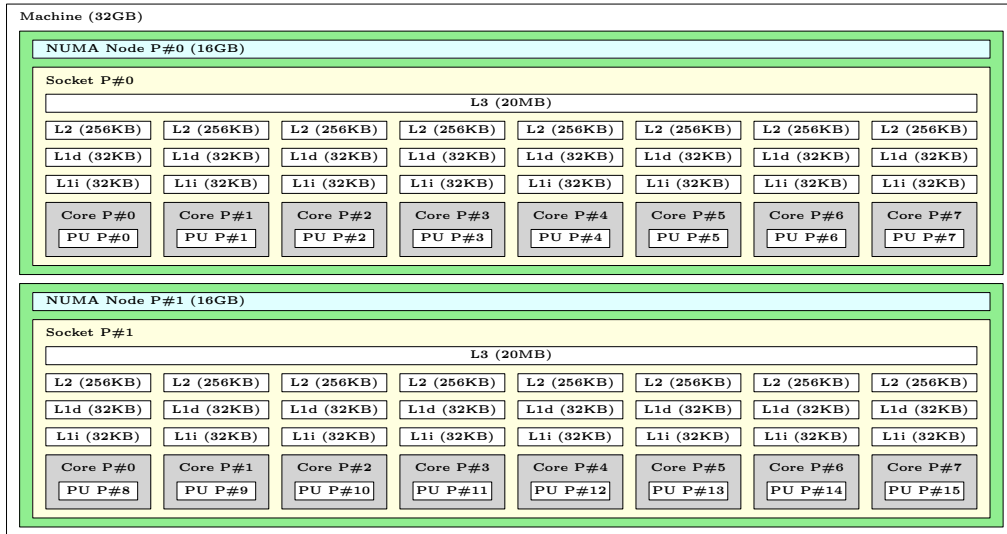


Figure 10.1: Structure of a POINCARE node

Section 11,

Section 12 discussion on precision,

Section 13 computing performance and memory limits,

Section 14 OpenMP, MPI giving the possibility to go beyond the memory limit. Due to the complexity of minimizer L-BFGS, this process is only added on the part of  $\mathcal{F}_{\text{exc}}$  evaluation. Tests of performance stability with respect to both threads and nodes are made.



## ALGORITHMS AND BRANCHES

According to the commutativity of operations (see §8.3.2), the only possible algorithms to evaluate  $\gamma(\mathbf{r}, \Omega)$  from  $\Delta\rho(\mathbf{r}, \Omega)$  are shown in the figure 11.1.

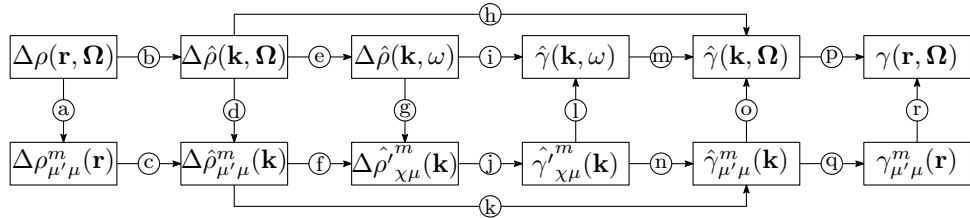


Figure 11.1: Possible algorithms for  $\gamma$  evaluation

Several branches are built to test and compare between algorithms, which are shown below in table 11.1 and will be detailed in the following context.

METHOD	SUB-METHOD	DESCRIPTION	THEORY
reference	dipole	calculate $n(r)$ and $P(r)$ separately	§5 [ref]
naive	standard	use $c_{\mu\nu,\chi}^{mn}(k)$ as input DCF	§7.2.2
	zero-order	use $\hat{c}(k, \omega_1, \omega_2)$ and take the nearest point	§7.1.1
	interpolation	use $\hat{c}(k, \omega_1, \omega_2)$ with linear interpolation	§7.1.2
	dipole	use $c_S, c_\Delta, c_D$ issue from [ref]	§7.2.1
	nmax1	use $c_S, c_\Delta, c_D, c_\pm$ issue from [ref]	§7.2.1
convolution	standard	algorithm with symmetry reduction	§8.3.1
	asymm	algorithm without symmetry reduction	§8.3.1
	pure-angular	inverse FFT and FGSHT	§11

These branches should give numerically the same result in certain conditions, that will be discussed in later sections.

Table 11.1: Branch option in MDFT

### 11.1 BRANCHES "NAIVE"

Branches **naive** are the algorithms mentioned in section 7, which go through the path

$$(b) \rightarrow (h) \rightarrow (p)$$

in figure 11.1, calculating directly  $\hat{\gamma}(\mathbf{k}, \Omega)$  from  $\Delta\rho(\mathbf{k}, \Omega)$ . The difference between branches is the way to calculate  $\hat{c}(\mathbf{k}, \Omega_1, \Omega_2)$ . Branch **naive\_standard** use  $c_{\mu\nu,\chi}^{mn}(k)$  as input DCF. Branch **naive\_zero-order** and **naive\_interpolation** using  $\hat{c}(k, \omega_1, \omega_2)$  with zero-order and linear interpolation, where the former is rejected in the implementation due to a lack of precision (appendix F).

The discussion of the accuracy to transform c projection to c table is given in section ...

As one is constant other has a  $O(N^3)$  dependence on  $n_{\max}$ , the discussion between the computing performance and memory usage with respect to  $n_{\max}$  and it will be given in section ...

## 11.2 BRANCHES "CONVOLUTION"

Branches **convolution\_asymm** and **convolution\_standard** are operational algorithms of angular convolution show in section 8, which go through the path

$$(a) \rightarrow (c) \rightarrow (f) \rightarrow (j) \rightarrow (n) \rightarrow (q) \rightarrow (r)$$

Branches **convolution\_asymm** uses the original operational algorithm (§8.3) without symmetry reduction (§8.3.1), and **convolution\_standard** without it.

Branch **convolution\_pure\_angular** goes through the path

$$(b) \rightarrow (d) \rightarrow (f) \rightarrow (j) \rightarrow (n) \rightarrow (o) \rightarrow (p)$$

which inverse the first and last two steps of the two algorithms mentioned above.

mathematically

a discussion the comparison of computing speed in in section ...

## 11.3 TESTING BRANCHES FOR NMAX=1

Branches **naive\_dipole**, **naive\_nmax1** pass by  $(b) \rightarrow (h) \rightarrow (p)$  , using DCF separately in reference [ref] and [ref], whose slight difference is shown in §6.3.4. Branch **reference\_dipole** use DCF in [ref], which is the original method in MDFT to calculate  $\mathcal{F}_{\text{exc}}$  via multipole expansion. In addition with branch **convolution\_standard**, which can also use the two DCF mentioned above, a test of validation can be performed (§), which should at any case exactly numerically the same if the same DCF is used.

## 11.4 OTHER PATHS

There will also be a discussion of other paths, such as those passes by  $(i)$  and  $(k)$ , of their accuracy (§), and of the computing cost (§).

# 12

## NUMERICAL AND PHYSICAL ACCURACY

---

This chapter gives a systematic comparison between algorithms for the evaluation of  $\gamma$  in terms of accuracy. The different methods should lead to mathematical equivalent results. The comparison for a series of CH4 with IEM and MD is done as validation of method.

### 12.1 GENERALIZED SPHERICAL HARMONICS TRANSFORM

#### 12.1.1 FFT

FFT3D is implemented by package FFTW3 [15] with discrete Fourier transform (DFT) defined as:

$$Y_k = \sum_{j=0}^{n-1} X_j e^{-2\pi i j k / n} \quad (\text{forward}) \quad (12.1)$$

$$X_j = \sum_{k=0}^{n-1} Y_k e^{2\pi i j k / n} \quad (\text{backward}) \quad (12.2)$$

Mathematically, these transforms lead to no accuracy lost. It should be noticed that after a forward-backward Fourier transform, the original function is multiplied by a normalization factor  $N_k$ , which is the total number of nodes  $k$ . The numerical tests for selected functions  $f(x) \in [-5, 5]$  (100 values) are shown in table 12.1.

$f(x)$	1	$x^3$	$e^x$	random number
$E_a^{\max}$	0	$2.84 \cdot 10^{-14}$	$3.32 \cdot 10^{-14}$	$1.80 \cdot 10^{-16}$

Table 12.1: Maximum absolute error introduced by a forward-backward (real-complex-real) DFT1D process on a 100-value double precision array using FFTW3 package

We can see that the errors are about machine precision.

The algorithmic complicity of FFT is about  $\mathcal{O}(N_k \ln N_k)$  [49], and the computing time will be discussed in later sessions.

mmax/nmax

#### 12.1.2 $m_{\max}$ and $n_{\max}$ of projections

The numerical error tests of a forward-backward GSHT process with different order  $m_{\max}$  ( $m$  in table) of GSH and order  $n$  of quadrature is shown in table 12.2.

It is shown that

It should be noticed that the tested functions are theoretically the same if the order of quadrature / GSH is sufficient. The real case of  $\rho$  is in later session.

#### 12.1.3 From $\rho$ to $\gamma$

Unphysical rho after transform, Gamma more smooth, Orientation

$m \setminus n$	0	1	2	3	4	$m \setminus n$	0	1	2	3	4
0						0					
1						1					
2						2					
3						3					
4						4					

(a)  $f(\Omega) = 1$

$m \setminus n$	0	1	2	3	4	$m \setminus n$	0	1	2	3	4
0						0					
1						1					
2						2					
3						3					
4						4					

(b)  $f(\Omega) = \cos 3\Theta$

$m \setminus n$	0	1	2	3	4	$m \setminus n$	0	1	2	3	4
0						0					
1						1					
2						2					
3						3					
4						4					

(c)  $f(\Omega) = \cos 3\Phi$

$m \setminus n$	0	1	2	3	4	$m \setminus n$	0	1	2	3	4
0						0					
1						1					
2						2					
3						3					
4						4					

(d)  $f(\Omega) = \cos \frac{3}{2}\Psi$

Table 12.2: Logarithm of maximum absolute error  $\lg(E_a^{\max})$  introduced by a forward-backward GSHT process.

## 12.2 COMPARISON BETWEEN BRANCHES

### 12.2.1 Error evaluation in $\hat{c}(\mathbf{k}, \Omega_1, \Omega_2)$ calculation

In appendix F, we compared the error introduced by the interpolation strategy of  $\hat{c}(\mathbf{k}, \Omega_1, \Omega_2)$  calculation from the intermolecular  $\hat{c}(k, \omega_1, \omega_2)$ . Here, we want to compare the error introduced by **naive\_interpolation** and **naive\_standard** concerned both  $\hat{c}(\mathbf{k}, \Omega_1, \Omega_2)$  and the free energy and structure issued from a single-k calculation.

As shown in table ,

### 12.2.2 A single k-kernel

As shown in figure 12.1, four paths are presented to be tested, (1) (2) (3) (4)

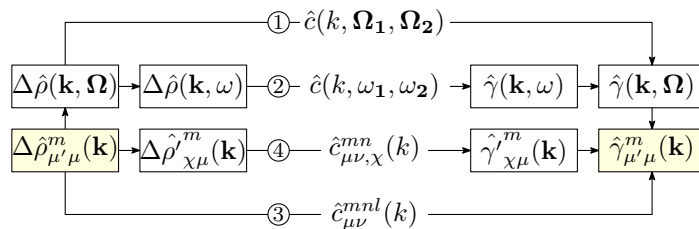


Figure 12.1: Schema of a k-kernel test

The result of error in energy for the result  $\hat{\gamma}_{\mu'\mu}^m(\mathbf{k})$  with certain  $\mathbf{k}$  is presented in table. As shown, there is no accuracy lost for different paths in both 4 cases of  $\mathbf{k}$ . This means, the

final result of energy and structure is independent to the choice of path inside a k-kernel, if  $\Delta\hat{\rho}(\mathbf{k}, \Omega)$  is a polynomial of ... as discussed in §12.1.

$\mathbf{k}$	$E_2^{\max}$	$E_3^{\max}$	$E_4^{\max}$
(2, 3, 5)			
(4, 0, 1)			
(0, 0, 0)			
(0, 0, 1)			

Table 12.3: Maximum absolute error introduced by paths (1) ... (4) shown figure 12.1, using an input  $\Delta\hat{\rho}_{\mu'\mu}^m(\mathbf{k})$  issue of MDFT minimization.  $\mathbf{k}$  is of unity [ $\text{\AA}^{-3}$ ]. For special case  $\mathbf{k} = (0, 0, 0)$ , ...  $E_i^{\max}$  is the absolute difference between path (1) and path ( $i$ ).

### 12.2.3 $k$ -border effect

	<code>convolution_standard</code>	<code>convolution_asymm</code>	<code>convolution_pure-angular</code>
$E_{\gamma}^{\max}(64)$			
$\mathcal{F}_{\text{exc}}(64)$			
$E_{\gamma}^{\max}(65)$			
$\mathcal{F}_{\text{exc}}(65)$			

Table 12.4: Maximum absolute error introduced by different branches in calculated  $\gamma(\mathbf{r}, \Omega)$  and the difference in  $\mathcal{F}_{\text{exc}}$  from a given  $\Delta\hat{\rho}_{\mu'\mu}^m(\mathbf{r})$  compared to `naive_standard` before border correction for a  $64^3$  and  $65^3$  spatial grid,  $n_{\max} = 5$ .

standard, asymm and pure-angular different because...

In MDFT, the symmetry

$$\Delta\hat{\rho}_{\chi\mu}^m(\mathbf{k}) = (-)^{m+\mu+\chi}\Delta\hat{\rho}_{\chi,-\mu}^{m*}(-\mathbf{k}) \quad (12.3)$$

is generated by two symmetries

$$\Delta\hat{\rho}_{\mu'\mu}^m(\mathbf{k}) = (-)^{\mu'+\mu}\Delta\hat{\rho}_{-\mu',-\mu}^{m*}(-\mathbf{k}) \quad (12.4)$$

$$R_{\mu'\chi}^m(\hat{\mathbf{k}}) = (-)^{m+\mu'+\chi}R_{-\mu',\chi}^m(-\hat{\mathbf{k}}) \quad (12.5)$$

For the points “at border”, it’s to say that after the FFT where the point having  $\pm k_i = k_i^{\max}$ ,  $i = 1, 2, 3$ , for example for  $k_1$ ,

$$\Delta\hat{\rho}_{\mu'\mu}^m(\pm k_1, k_2, k_3) = \Delta\hat{\rho}_{\mu'\mu}^m(k_1^{\max}, k_2, k_3)$$

is naturally put in the same array by FFT for the grids having even number.

But

$$R_{-\mu',\chi}^m(-\hat{\mathbf{k}} \equiv (-k_1, -k_2, -k_3)) \neq R_{\mu',\chi}^m(k_1^{\max}, -k_2, -k_3)$$

Thus the symmetries (12.5) and (12.3) are not respected for these points

In the backward process, if we make sense of all the  $\gamma_{\mu'\mu}^m(\mathbf{k})$ , as

For example, for a grid 1D, the FFT having 6 points gives the values for indices 0, 1, 2, 3, -2, -1, and the FFT having 7 points gives the values for 0, 1, 2, 3, -3, -2, -1.

$$\gamma_{\mu'\mu}^m(-\hat{k} \equiv (-k_1, -k_2, -k_3)) \neq \gamma_{\mu'\mu}^m(k_1^{\max}, -k_2, -k_3)$$

the symmetry

$$\gamma_{\mu'\mu}^m(\mathbf{k}) = (-)^{\mu'+\mu} \gamma_{-\mu',-\mu}^{m*}(-\mathbf{k}) \quad (12.6)$$

is not respected totally, and this imposes that  $\gamma_{\mu'\mu}^m(\mathbf{r})$  have a imaginary part. In the version FFTW3, we keep only the part of none-negative  $\mathbf{k}$  or none-negative, supposing that the part we omit respects the symmetry.

0	1	...	$k-1$	$k$	$-k+1$	...	-1
				-k			

Figure 12.2: k-border effet

convolution_standard	convolution_asymm	convolution_pure-angular
$E_\gamma^{\max}(65)$		
$\mathcal{F}_{\text{exc}}(65)$		

Table 12.5: Maximum absolute error introduced by different branches after border correction

the mysterious error between **naive\_standard** and the **convolution** branches cannot explained, this implied that there is probably a bug in **naive\_standard**.

## 12.3 INTRINSIC VARIATION OF FREE ENERGY

Before study of free energy dependence on angular algorithms, we are interested in the grid dependance, with can have an influence in the follow tests.

### 12.3.1 Spatial grid: length and resolution

### 12.3.2 Angular grid: effect of psi

## 12.4 SERIES OF CHARGED LJ CENTRE

charged CH<sub>4</sub> centre

here we use 298K according to habitude instead of 303K recommended in reference [ref].

### 12.4.1 Box length dependance and charge dependance of free energy

As discussed in section 9, for single ions, two types of corrections need to be added on the free energy, which depend on the box length and and charge of the ion. To verify these dependence, we implement a systematic calculation from charge shown in figure

Figure 12.3: structure of gamma in rotational invariants

charge	sigma []	epsilon []	x [Å]	y [Å]	z [Å]	temperature [K]	number density of solvent
-1.0 to 1.0	3.73	1.23	0	0	0	298	0.0332891

Table 12.6: Parameters of charged Lenard-Jones centre (modified from CH<sub>4</sub>)

Figure 12.4: free energy (without correction) of charged CH<sub>4</sub> centre (-1.0 to 1.0) with respect to the box length

Continuum model correction at boundary

It satisfies the Born model.

memory leak can cause divergence.

#### 12.4.2 Comparison with IET

Old data in appendix G, which use 2m phi. It gives quite similar result, which shows the insensibility of grid.

#### 12.4.3 Comparison with DM

## 12.5 PREMIER CONCLUSION

Capable to produce the same result with IEM, but have more ability to calculate 3D molecules which is not suitable for spherical coordinates.

Figure 12.5: Parabolic charge dependence of free energy of CH<sub>4</sub> centre series

Figure 12.6: Linear dependence of charge in the comparison to IET. Old algorithm / new algorithm, without correction

Figure 12.7: Comparison to IET. Old algorithm / new algorithm, with P-scheme correction

## COMPUTING PERFORMANCE OF SEQUENTIAL CODE

---

This section evaluates the computing performance of the code without parallelization. Our goal is to show that the new algorithm of angular convolution is faster than the old naive one, and the huge amount of simulation has shown that it is absolutely the case. But a raw result, where the implementation goes for an indefinite number of iterations during minimization, cannot give a proper and systematic performance evolution. This gives the propose of this section.

As discussed in appendix A, two main factors give influence to the performance of a sequential code: the algorithm complexity, and the memory delay. To study the algorithm complexity, testing with respect to parameters is done to some simple but important components. The result can match the theoretical algorithm complexity, or completely different due to the overhead of function calling or the inhomogeneity of memory access. Etude of this small parts permits a further understanding of the entire code.

### 13.1 FFT

The **FFT!** play a great role in the implementation, which is used by the spatial convolution and the FGSHT process. As shown in figure 13.1a, the dependance on  $O(N \log_2 N)$  doesn't totally exist, due to the algorithm of FFT [ref dft]. To compare between the algorithms involved in this thesis, we are not really interested in computing performance with respect to the number of spatial grid, but the **FFT!** used in FGSHT process (figure 13.1b).

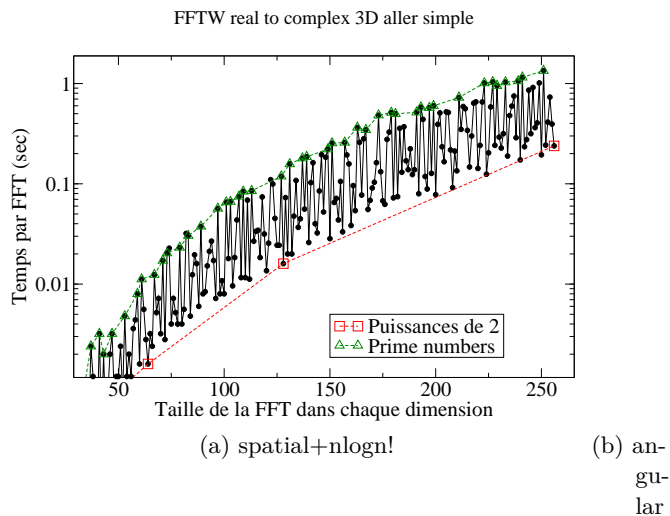


Figure 13.1: timing FFT

## 13.2 FGSHT

### 13.2.1 Computing time of GSHT and FGSHT

To serve as an alternative of FFT for angular grid, the algorithmic complicity of GSHT should be at least less than  $O(N_\Omega^2)$ , where  $N_\Omega$  is the total number of Euler angles. But to integrate eq. (??) in a direct way,  $(n+1)(2n+1)(2\lfloor n/s \rfloor + 1) = N_\Theta N_{\Phi\Psi} = N_\Omega$  function evaluations (FE) are needed for each  $F_{\mu'\mu}^m$  ( $s = 1$  or  $2$  according to the symmetry of axe  $C_s$ ), an overall  $O(N_\Omega^2)$  process is needed and *vice versa*. A faster algorithm proposed by Numerical Recipes [49] suggests reducing this cost to  $O(N_\Theta^2 N_{\Phi\Psi} \ln N_{\Phi\Psi} \simeq N_\Omega^{4/3})$  by FFT. The implementation is detailed in appendix ???. The computing time of GSHT and FGSHT are shown in figure 13.2, for the case that  $\Psi$  possesses no symmetry.

It is shown that the computing cost reduced by FFT is about ... times of the original cost, which is agreed with the prediction. ?

Figure 13.2: Computing time of GSHT and FGSHT (per 1000 times)

### 13.2.2 Performance with respect to $m_{\max}$

### 13.2.3 Performance with respect to $n_{\max}$

psi treatment for mmax/nmax different

## 13.3 K-KERNEL

### 13.3.1 Comparison between paths

Timing paths in figure 12.1

### 13.3.2 $m_{\max}$ and $n_{\max}$ dependance of OZ equation

Theoretical listed in table 8.1.

with respect to nmax

## 13.4 ENTIRE ITERATION OF $\mathcal{F}_{\text{exc}}$ EVALUATION

### 13.4.1 Comparison between “naive\_standard” and “convolution\_pure-angular”

Figure 13.3

difference after FFT.

verified the conclusion of k-kernel test.

### 13.4.2 Comparison between “convolution\_standard” and “convolution\_asymm”

Figure 13.4

The symmetries, ideally the time should be reduced by two, but as shown in §, convolution\_standard need more “decoration”.

### 13.4.3 Comparison between “convolution\_standard” and “convolution\_pure\_angular”

Figure 13.5

#### The inversion of FFT and FGSHT

we can see the other part is almost identical, but the implementation of FFT takes different time. Because in convolution\_standard the number of FE we need for FFT is the number of projections, and in convolution\_pure\_angular it is the number of angular grid nodes. As there is less projections than angular nodes, convolution\_standard reasonably takes less time.

## 13.5

### GLOBAL VIEW OF THE SEQUENTIAL CODE PERFORMANCE

Computing time and memory limits

Hotspots and bottlenecks



# 14

## COMPUTING PERFORMANCE OF PARALLEL CODE

---

### 14.1 NODE-LEVEL PARALLELIZATION

OpenMP, scalability with respect to the number of thread

### 14.2 PARALLELIZATION ON SEVERAL NODES

MPI, scalability with respect to the number of node



## Chapter IV

# APPLICATIONS

Only a few applications are made due to the time limit of this thesis, concluding

Section [ref] to show the capability of MDFT to calculate ions and small molecules.

Section [ref] to show a qualitative influence of polar solvent on the reaction including metal-oxo centre.



# 15

## IONS AND SMALL MOLECULES COMPARED TO MD SIMULATION

---

### 15.0.1 *ions*

test solute

#	$q$	$\sigma$	$\varepsilon$	$r_x^M$	$r_y^M$	$r_z^M$	atom name

---

---

---

Table 15.1

[single ions P113]



# 16

## HYDROGEN TRANSFER REACTION OF Mn-Oxo: ROLE OF SOLVENT IN REACTION SIMULATION

---

### 16.1 REINVESTIGATION OF THE MANGANESE-OXO

This is the case we talked about in the introduction, which is the thesis of university , the motivation of this thesis



## Chapter V

# CONCLUSION AND PERSPECTIVES

The only one publication during this thesis



## CONCLUSION

---

Here is the publication during this thesis:



## PERSPECTIVES

---

Due to the difficulty of this thesis and my mental state, there are a lot of un finished work and theory. Here lists some to give un idea.

### 18.1 REDUCE MEMORY USE IN MDFT

As shown in chapter III, memory leak can cause divergence and other problem.

#### 18.1.1 *Pass to simple precision*

L-BFGS-B is in double precision

#### 18.1.2 *MPI of the L-BFGS-B minimizer*

As the code is a blackbox, in Fortran 77, it is difficult to parallelize it.

### 18.2 POLARISABLE SOLUTE

Vext variable

### 18.3 MDFT VIEWER

This thesis contains a part of visualization

Viewer is an important part of code developing, which provide beautiful visualization and easy analyzing helps to popularize the code. GaussViewer is a good example.

The popular language of visualization is c++, OpenDM, ...

### 18.4 CLASSICAL SCF METHOD

To be more compatible with Gaussian, [Jensen]

This is only an idea, the mathematical deduction is not fully verified.

### 18.5 OTHER BRANCHES OF DEVELOPMENT ABOUT MDFT

3-body, polarization,



Chapter VI

## APPENDIX



# A

## BASIC CONCEPTS ABOUT COMPUTING PERFORMANCE

---

In addition to the theory work, the performance of the code being developed is also an important aspect of this thesis. It is essential to have a fast and accurate method. To evaluate code in a strict and systematic way, some basic concepts of computing performance are listed here.

### a.1 ALGORITHM COMPLEXITY

Algorithm complexity is a crucial criteria for sequential code. A definition is given below.

Let  $f$  and  $g$  be two real (or even complex) functions defined over the natural numbers  $\mathbb{N}$ . We write

$$f = O(g) \quad (\text{A.1})$$

if there is a constant  $c > 0$  such that from certain number  $n > n_0$  we always have  $|f(n)| \leq c|g(n)|$ . The  $O$  is also named as the big-O notation [16], or order of growth. Figure A.1 shows the growth tendency of some frequent functions; from this we can conclude the following:

$$O(1) > O(\log_2 n) > O(n) > O(n \log_2 n) > O(n^2) > O(2^n) > O(n!) \quad (\text{A.2})$$

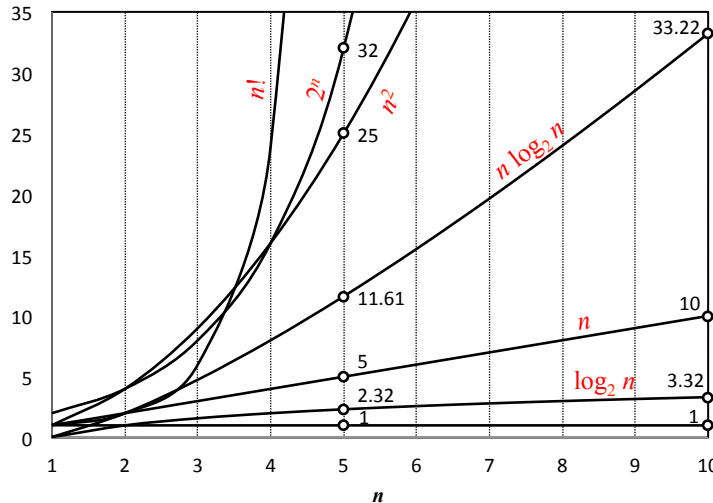


Figure A.1: Function growth

In this thesis, the big-O notation is used to measure algorithm complexity. Other notations can also be used for the same purpose, such as:

- $f = o(g)$  if  $f(n)/g(n) \rightarrow 0$ ,  $n \rightarrow \infty$
- The inverse of big-O notation  $f = \Omega(g)$  if  $g = O(f)$

- The notation  $f = \Theta(g)$  means that both  $f = O(g)$  and  $g = O(f)$  hold, and we can also say they are of the same order.

In a code we always search algorithms with a lower algorithm complexity. Ideally, the implementation of code matches the model and have the same growth tendency as its complexity, but in the practical case, overheads and memory delay can also limit the performance. (part to be modified to adapt implementation results)

## a.2 ROOFLINE MODEL AND MEMORY DELAY

The simplest model aiming to distinguish whether a piece of code is limited by the computing power (CPU) or the memory bandwidth (RAM to Caches) is the roofline model [60] for single loop:

$$P = \min(P_{\max}, I \cdot b_S) \quad (\text{A.3})$$

where

- $P$  is the applicable peak performance of a loop, assuming that data comes from the level 1 cache, of unity GFlop/s.
- $I$  is the computational intensity (“work” per byte transferred) over the slowest data path utilized, of unity Flop/Byte.
- $b_S$  is the applicable peak bandwidth of the slowest data path utilized, of unity GByte/s.

As shown in figure A.2, the overall performance is limited by both the peak performance and the memory bandwidth. The computational intensity  $I$  depends on the code, while the other two terms in eq. (A.3) depend on hardware. The optimal use of resources occurs at the intersection point.

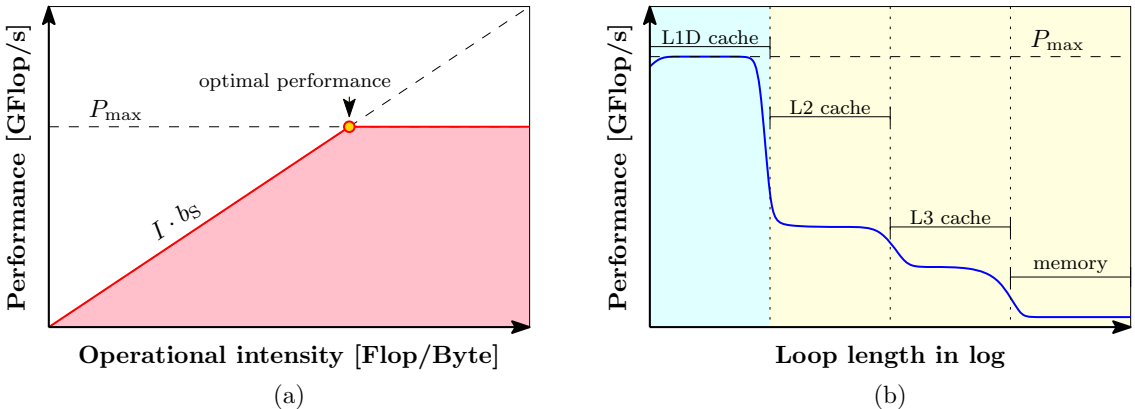


Figure A.2: The roofline model and performance pattern. (a) The roofline model. (b) Performance pattern of a simple loop with respect to the loop length in logarithm. The blue part is limited by operation execution, and the yellow part is limited by memory bottleneck.

The roofline model can give an idea of whether the diminuition of algorithm complexity is the most important optimization strategy, because it only counts the number of operations. In most cases, avoiding slow data paths is the key to performance optimization.

As shown in figure A.3, the memory hardware has hierarchical architectures. The fastest ones are the registers included in the microprocessor, which are used for temporary storage of data, instructions and addresses required by the arithmetic logic unit (ALU) and the

control unit (CU) in CPU during execution of a program. The lowest is normally the input/output (I/O) process. The reading strategy of data (contiguous or not), as well as the size and initialized location of arrays, both play pivotal roles in the overall computing performance.

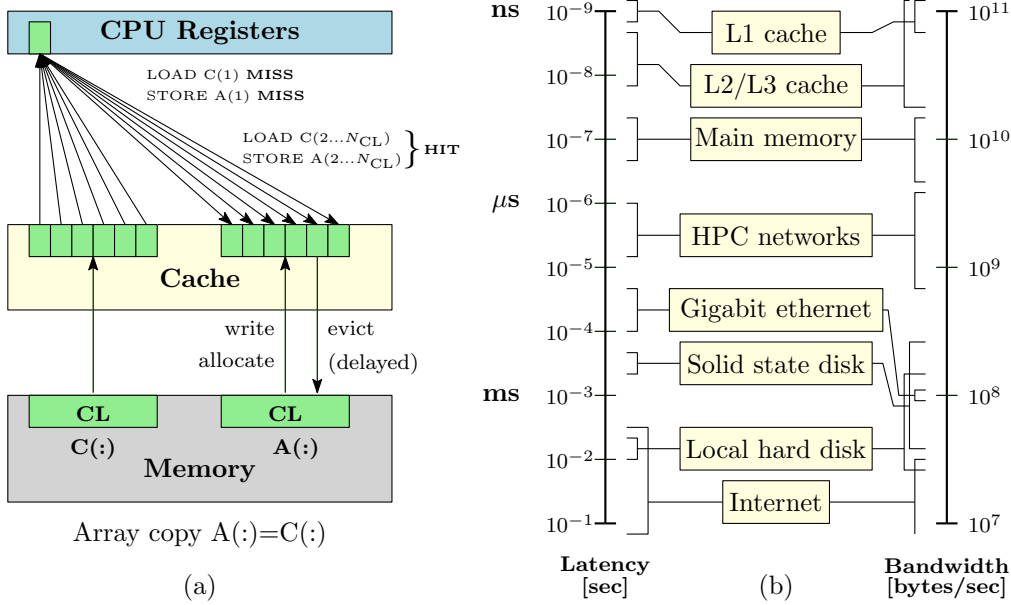


Figure A.3: Memory usage in hardware level [20]. (a) An example of array copy  $A(:)=C(:)$ . Caches are organized in cache lines (CL), only complete cache lines are transferred between memory hierarchy levels (except registers). HIT/MISS: Load or store instruction does/doesn't find the data in a cache level. (b) Computing latency and memory bandwidth vary by magnitude, from the fastest cache transfers to the lowest processes.

### a.3 SCALABILITY OF PARALLELIZED CODE

For parallelized code, scalability is the key issue. Highly scalable codes can take advantage of numerous nodes of HPC centers, so that single core performance no longer matters.

The speed-up is defined as:

$$S(N) = \frac{t(1)}{t(N)} \quad (\text{A.4})$$

And the relative efficiency

$$E(N) = \frac{S(N)}{N} = \frac{t(1)}{Nt(N)} \quad (\text{A.5})$$

$S(N) \sim N$  or  $E(N) \sim 100\%$  means the application scales. By contrast,  $S(N) < N/2$  or  $E(N) < 50\%$  means the application does not scale.

Amdahl's Law gives the theoretical speedup in latency of the execution of a task at fixed workload:

$$S(N) = \frac{1}{\alpha_s + \alpha_p/N} \quad (\text{A.6})$$

where  $\alpha_s$  is the serial fraction and  $\alpha_p$  the parallel fraction of the source code. Therefore the overall computing speed is limited by the unscalable part:

$$\lim_{N \rightarrow \infty} S(N) = \frac{1}{\alpha_s} \quad (\text{A.7})$$

making it the focus we wish to reduce.

## a.4 PROFILING AND TRACING TOOLKITS

There are several types of software and toolkits for performance evaluation. They comprise two categories: profiling and tracing. A trace is a collection of events or timestamps. A profile is a collection of timings. Profiling tools are usually more simple and rapid, but for subroutines that are called a large number of times, the overhead in time measurement is not negligible.

The tool used in this thesis is mainly VTune, where application execution is interrupted every  $\sim 100 \text{ ns}$  and information is stored (call stack, hardware counters, etc.). The execution time overhead is small. (To be detailed.)

# B

## EQUIVALENCE OF QUADRATURE-PROJECTION ORDER

---

### b.1 GAUSSIAN QUADRATURE

Theorem:

Let  $P_n(x)$  be a nonzero polynomial of degree  $n$ , and  $w(x)$  a positive weight function so that

$$\int_a^b x^k P_n(x) w(x) dx = 0, \quad (k = 0, \dots, n-1) \quad (\text{B.1})$$

If  $\{x_i\}$  ( $i = 1, \dots, n$ ) are the zeros of  $P_n(x)$ , then

$$\int_a^b f(x) w(x) dx \simeq \sum_{i=1}^n A_i f(x_i) \quad (\text{B.2})$$

with

$$A_i = \int_a^b l_{i-1}(x) w(x) dx \quad (\text{B.3})$$

is exact for all polynomials  $f(x)$  of degree at most  $2n - 1$ , where  $\{l_i\}$  are the usual Lagrange interpolating polynomials.

Proof:

Assume that  $f(x)$  is a polynomial of degree at most  $2n - 1$ . Using long division

$$f(x) = P_n(x)p(x) + r(x) \quad (\text{B.4})$$

$p(x)$  and  $r(x)$  are obtained as polynomials of degree at most  $n - 1$ .

By taking  $\{x_i\}$  as the zeros of  $P_n(x)$ , we can easily find  $f(x_i) = r(x_i)$ , ( $i = 1, \dots, n$ ), then

$$\begin{aligned} \int_a^b f(x) w(x) dx &= \int_a^b [P_n(x)p(x) + r(x)] w(x) dx \\ &\simeq \underbrace{\sum_{i=1}^n P_n(x_i)p(x_i)w_i}_{=0} + \sum_{i=1}^n A_i r(x_i) \end{aligned} \quad (\text{B.5})$$

is exact for  $r(x)$  of degree at most  $n - 1$  (c.f. Numerical Recipes [49] p.118), and thus exact for  $f(x)$  of degree at most  $2n - 1$ .

### b.2 ANGULAR INTEGRATION IN GSHT

To expand a function onto GSHs, as in eq. (8.15), quadrature is needed. Assume that  $F(\Omega)$  is a polynomial of  $\cos \Theta$ ,  $\cos \Phi$  and  $\cos \Psi$  of order  $n$ . As  $R_{\mu' \mu}^{m*}(\Omega)$  is also a polynomial

of order  $n$ , the total degree of integrand is  $2n$ . It should be noted that the surface area element is:

$$d\Omega = \sin \Theta d\Theta d\Phi d\Psi = d \cos \Theta d\Phi d\Psi \quad (\text{B.6})$$

For  $\cos \Theta$  integration, considering  $w(x) = 1$  and  $x = \cos \Theta$ , Gauss-Legendre quadrature should be used. Thus  $n + 1$  points on  $x$  should be taken, with  $\{x_i\}$  given by Legendre polynomials  $P_{n+1}(x)$ .

For  $\Phi$  and  $\Psi$  integration, taking  $w(x) = (1 - x^2)^{-\frac{1}{2}}$ , the abscissae are given by the  $N = n + 1$  roots of the Chebyshev polynomial of the first kind:

$$T_N(x) = \cos(N \cos x) \Rightarrow x_i = \cos \left[ \frac{(2i-1)\pi}{2N} \right], \quad i \in 1, \dots, N \quad (\text{B.7})$$

with weight  $w_i = \frac{\pi}{N}$ , it corresponds to points in  $\Phi \in [0, \pi]$  regularly distributed. However, for  $\Phi \in [0, 2\pi]$ , two times of function evaluation should be calculated:

$$\begin{aligned} & \int_{-1}^1 f(\cos \Phi) \frac{1}{\sqrt{1 - \cos^2 \Phi}} d \cos \Phi \\ &= \begin{cases} \int_{\pi}^0 f(\cos \Phi) d\Phi = - \int_0^{\pi} f(\cos(\Phi)) d\Phi & \Phi \in [0, \pi] \\ \int_{-\pi}^0 f(\cos(\Phi)) d(\Phi) = \int_0^{\pi} f(\cos(-\Phi')) d\Phi' & \Phi' \in [0, \pi] \end{cases} \end{aligned} \quad (\text{B.8})$$

so that

$$\int_0^{2\pi} f(\cos \Phi) d\Phi = \int_{-\pi}^{\pi} f(\cos \Phi) d\Phi = \int_0^{\pi} [f(\cos(-\Phi)) - f(\cos \Phi)] d\Phi \quad (\text{B.9})$$

It corresponds to  $2n + 2$  points in  $\Phi \in [0, 2\pi]$  regularly distributed. However, it's not the minimal number of points necessary to do the exact integration. Suppose that  $\Phi_2 \equiv \Phi/2$ ,

$$\int_0^{2\pi} f(\cos \Phi) d\Phi = \int_0^{\pi} f(\cos(2\Phi_2)) d\Phi_2 = \int_0^{\pi} [f(2 \cos^2 \Phi_2 - 1)] d\Phi_2 \quad (\text{B.10})$$

As  $f(2 \cos^2 \Phi_2 - 1)$  is a polynomial of  $\Phi$  of degree  $2n$ , it's a polynomial of  $\Phi_2$  of degree  $4n$ . Thus only  $2n + 1$  points are needed.

# C

## ROTATIONAL INVARIANT EXPANSION

---

If a function  $F(\mathbf{X}_1, \mathbf{X}_2)$ ,  $\mathbf{X}_i \equiv (\mathbf{r}_i, \boldsymbol{\Omega}_i)$  has transitional and rotational invariance [4], it can be expanded as

$$F(\mathbf{X}_1, \mathbf{X}_2) = \sum_{mnl\mu\nu} F_{\mu\nu}^{mnl}(\|\mathbf{r}_{12}\|) \Phi_{\mu\nu}^{mnl}(\boldsymbol{\Omega}_1, \boldsymbol{\Omega}_2, \hat{\mathbf{r}}_{12}) \quad (\text{C.1})$$

where  $\mathbf{r}_{12} \equiv \mathbf{r}_1 - \mathbf{r}_2$  according to the transitional invariance, and

$$\Phi_{\mu\nu}^{mnl}(\boldsymbol{\Omega}_1, \boldsymbol{\Omega}_2, \hat{\mathbf{r}}_{12}) = f^{mnl} \sum_{\mu'\nu'\lambda'} \begin{pmatrix} m & n & l \\ \mu' & \nu' & \lambda' \end{pmatrix} R_{\mu'\mu}^m(\boldsymbol{\Omega}_1) R_{\nu'\nu}^n(\boldsymbol{\Omega}_2) R_{\lambda'0}^l(\hat{\mathbf{r}}_{12}) \quad (\text{C.2})$$

where  $R_{\mu'\mu}^m$  is the Wigner generalized spherical harmonics or Wigner D-symbol defined in the same convention as Messiah [44] (different than Edmonds [11]).  $f^{mnl}$  can be any arbitrary non-zero constant [14]. Here we define  $f^{mnl} = f^m f^n = \sqrt{2m+1} \sqrt{2n+1}$  according to the definition of Belloni [1].

Two special cases are adopted in this thesis, these being the laboratory coordinate system with particle 1 at origin (fixed frame) and intermolecular coordinate system (local frame) shown in figure 7.1. Their formalism and symmetry properties are presented later.

### C.1 ORTHOGONALITY OF $\Phi$

The rotational invariant  $\Phi$  in eq. (C.2) is orthogonal, as proven below:

$$\begin{aligned} \langle \Phi | \Phi_2 \rangle &= \int d\boldsymbol{\Omega}_1 d\boldsymbol{\Omega}_2 d\hat{\mathbf{r}} \Phi_{\mu\nu}^{mnl}(\boldsymbol{\Omega}_1, \boldsymbol{\Omega}_2, \hat{\mathbf{r}}_{12}) \Phi_{\mu_2\nu_2}^{m_2 n_2 l_2 *}(\boldsymbol{\Omega}_1, \boldsymbol{\Omega}_2, \hat{\mathbf{r}}_{12}) \\ &= f^m f^n f^{m_2} f^{n_2} \sum_{\mu'\nu'\lambda'} \begin{pmatrix} m & n & l \\ \mu' & \nu' & \lambda' \end{pmatrix} \sum_{\mu'_2\nu'_2\lambda'_2} \begin{pmatrix} m_2 & n_2 & l_2 \\ \mu'_2 & \nu'_2 & \lambda'_2 \end{pmatrix} \\ &\quad \times \left\{ \int d\boldsymbol{\Omega}_1 R_{\mu'\mu}^m(\boldsymbol{\Omega}_1) R_{\mu'_2\mu_2}^{m_2 *}(\boldsymbol{\Omega}_1) \right. \\ &\quad \left[ \int d\boldsymbol{\Omega}_2 R_{\nu'\nu}^n(\boldsymbol{\Omega}_2) R_{\nu'_2\nu_2}^{n_2 *}(\boldsymbol{\Omega}_2) \left( \int d\hat{\mathbf{r}} R_{\lambda'0}^l(\hat{\mathbf{r}}_{12}) R_{\lambda'_20}^{l_2 *}(\hat{\mathbf{r}}_{12}) \right) \right] \} \\ &= f^m f^n f^{m_2} f^{n_2} \sum_{\mu'\nu'\lambda'} \begin{pmatrix} m & n & l \\ \mu' & \nu' & \lambda' \end{pmatrix} \sum_{\mu'_2\nu'_2\lambda'_2} \begin{pmatrix} m_2 & n_2 & l_2 \\ \mu'_2 & \nu'_2 & \lambda'_2 \end{pmatrix} \\ &\quad \times \delta_{m,m_2} \delta_{n,n_2} \delta_{l,l_2} \delta_{\mu,\mu_2} \delta_{\nu,\nu_2} \delta_{\mu',\mu'_2} \delta_{\nu',\nu'_2} \delta_{\lambda',\lambda'_2} \\ &= (2l+1)^{-1} \sum_{\mu'\nu'\lambda'} \begin{pmatrix} m & n & l \\ \mu' & \nu' & \lambda' \end{pmatrix} \begin{pmatrix} m & n & l \\ \mu' & \nu' & \lambda' \end{pmatrix} \quad (\text{C.3}) \end{aligned}$$

and using the orthogonality of 3j-symbol [11]

$$\sum_{l\lambda'} (2l+1) \begin{pmatrix} m & n & l \\ \mu'_1 & \nu'_1 & \lambda' \end{pmatrix} \begin{pmatrix} m & n & l \\ \mu'_2 & \nu'_2 & \lambda' \end{pmatrix} = \delta_{\mu'_1\mu'_2} \delta_{\nu'_1\nu'_2} \quad (\text{C.4})$$

$$\sum_{\mu' \nu'} \begin{pmatrix} m & n & l \\ \mu' & \nu' & \lambda' \end{pmatrix} \begin{pmatrix} m & n & l_2 \\ \mu' & \nu' & \lambda'_2 \end{pmatrix} = (2l+1)^{-1} \delta_{ll_2} \delta_{\lambda'_1 \lambda'_2} \quad (\text{C.5})$$

it gives

$$\langle \Phi | \Phi_2 \rangle = (2l+1)^{-1} \quad (\text{C.6})$$

## C.2 ROTATIONAL INVARIANCE OF $\Phi$

In any coordinate system, the value of  $\Phi_{\mu\nu}^{mn l}$  remains the same. Here is a partial demonstration with the fixed and local frame mentioned above, described in figure 7.1.

Let's use the definition in eq. (C.2):

$$\Phi_{\mu\nu}^{mn l}(\omega_1, \omega_2, 0) = f^{mn l} \sum_{\mu'' \nu'' \lambda''} \begin{pmatrix} m & n & l \\ \mu'' & \nu'' & \lambda'' \end{pmatrix} R_{\mu'' \mu}^m(\omega_1) R_{\nu'' \nu}^n(\omega_2) R_{\lambda'' 0}^l(0) \quad (\text{C.7})$$

$$\Phi_{\mu\nu}^{mn l}(0, \Omega, \hat{\mathbf{r}}) = f^{mn l} \sum_{\mu' \nu' \lambda'} \begin{pmatrix} m & n & l \\ \mu' & \nu' & \lambda' \end{pmatrix} R_{\mu' \mu}^m(0) R_{\nu' \nu}^n(\Omega) R_{\lambda' 0}^l(\hat{\mathbf{r}}) \quad (\text{C.8})$$

The spherical harmonics have property [11, 44]

$$R_{\mu' \mu}^m(0) = \sum_{\mu''} R_{\mu' \mu''}^m(\hat{\mathbf{r}}) R_{\mu'' \mu}^m(\omega_1) \quad (\text{C.9})$$

$$R_{\nu' \nu}^n(\Omega) = \sum_{\nu''} R_{\nu' \nu''}^n(\hat{\mathbf{r}}) R_{\nu'' \nu}^n(\omega_2) \quad (\text{C.10})$$

$$R_{\lambda' 0}^l(\hat{\mathbf{r}}) = \sum_{\lambda''} R_{\lambda' \lambda''}^l(\hat{\mathbf{r}}) R_{\lambda'' 0}^l(0) \quad (\text{C.11})$$

so

$$\begin{aligned} \Phi_{\mu\nu}^{mn l}(0, \Omega, \hat{\mathbf{r}}) &= f^{mn l} \sum_{\mu'' \nu'' \lambda''} R_{\mu'' \mu}^m(\omega_1) R_{\nu'' \nu}^n(\omega_2) R_{\lambda'' 0}^l(0) \times \\ &\quad \left[ \sum_{\mu' \nu' \lambda'} \begin{pmatrix} m & n & l \\ \mu' & \nu' & \lambda' \end{pmatrix} R_{\mu' \mu''}^m(\hat{\mathbf{r}}) R_{\nu' \nu''}^n(\hat{\mathbf{r}}) R_{\lambda' \lambda''}^l(\hat{\mathbf{r}}) \right] \end{aligned} \quad (\text{C.12})$$

According to eq. (4.3.3) in Edmonds [11] or (A.91) in Gray & Gubbins [19]

$$\sum_{\mu' \nu' \lambda'} \begin{pmatrix} m & n & l \\ \mu' & \nu' & \lambda' \end{pmatrix} R_{\mu' \mu''}^{m*}(\hat{\mathbf{r}}) R_{\nu' \nu''}^{n*}(\hat{\mathbf{r}}) R_{\lambda' \lambda''}^{l*}(\hat{\mathbf{r}}) = \begin{pmatrix} m & n & l \\ \mu'' & \nu'' & \lambda'' \end{pmatrix} \quad (\text{C.13})$$

where we can also prove

$$\sum_{\mu' \nu' \lambda'} \begin{pmatrix} m & n & l \\ \mu' & \nu' & \lambda' \end{pmatrix} R_{\mu' \mu''}^m(\hat{\mathbf{r}}) R_{\nu' \nu''}^n(\hat{\mathbf{r}}) R_{\lambda' \lambda''}^l(\hat{\mathbf{r}}) = \begin{pmatrix} m & n & l \\ \mu'' & \nu'' & \lambda'' \end{pmatrix} \quad (\text{C.14})$$

$\Phi_{\mu\nu}^{mn l}$  remains identical in the two cases

$$\begin{aligned} \Phi_{\mu\nu}^{mn l}(0, \Omega, \hat{\mathbf{r}}) &= f^{mn l} \sum_{\mu'' \nu'' \lambda''} \begin{pmatrix} m & n & l \\ \mu'' & \nu'' & \lambda'' \end{pmatrix} R_{\mu'' \mu}^m(\omega_1) R_{\nu'' \nu}^n(\omega_2) R_{\lambda'' 0}^l(0) \\ &= \Phi_{\mu\nu}^{mn l}(\omega_1, \omega_2, 0) \end{aligned} \quad (\text{C.15})$$

Therefore, the projections  $F_{\mu\nu}^{mn l}(r)$  also remain rotational invariant in these two coordinate systems.

### C.3 TRANSFORM IN LOCAL FRAME

In the intermolecular (local) coordinate system, the 2 molecules are both positioned along the  $z$  axis. Using the properties [11, 19, 44] of generalized spherical harmonics:

$$R_{\mu'\mu}^m(\Theta, \Phi, \Psi) = \delta_{\mu'\mu} \quad \text{if } \Theta = \Phi = \Psi = 0 \quad (\text{C.16})$$

and 3j-symbol

$$\begin{pmatrix} m & n & l \\ \mu' & \nu' & \lambda' \end{pmatrix} \neq 0 \quad \text{only if } \mu' + \nu' + \lambda' = 0 \quad (\text{C.17})$$

$\Phi_{\mu\nu}^{mn}( \boldsymbol{\Omega}_1, \boldsymbol{\Omega}_2, \mathbf{r}_{12} )$  in eq. (C.2) can be simplified to

$$\Phi_{\mu\nu}^{mn}( \boldsymbol{\omega}_1, \boldsymbol{\omega}_2, 0 ) = \sum_{\chi} \begin{pmatrix} m & n & l \\ \chi & -\chi & 0 \end{pmatrix} f^m f^n R_{\chi\mu}^m(\boldsymbol{\omega}_1) R_{-\chi\nu}^n(\boldsymbol{\omega}_2) \quad (\text{C.18})$$

Thus eq. (C.1) becomes

$$\begin{aligned} F(\boldsymbol{\omega}_1, \boldsymbol{\omega}_2, r) &= \sum_{mnl\mu\nu} F_{\mu\nu}^{mn}(r) \Phi_{\mu\nu}^{mn}( \boldsymbol{\omega}_1, \boldsymbol{\omega}_2, 0 ) \\ &= \sum_{mnl\mu\nu} F_{\mu\nu}^{mn}(r) f^m f^n \sum_{\chi} \begin{pmatrix} m & n & l \\ \chi & -\chi & 0 \end{pmatrix} R_{\chi\mu}^m(\boldsymbol{\omega}_1) R_{-\chi\nu}^n(\boldsymbol{\omega}_2) \end{aligned} \quad (\text{C.19})$$

and the inverse equation

$$\begin{aligned} F_{\mu\nu}^{mn}(r) &= \int d\boldsymbol{\omega}_1 d\boldsymbol{\omega}_2 F(\boldsymbol{\omega}_1, \boldsymbol{\omega}_2, r) \Phi_{\mu\nu}^{mn*}(\boldsymbol{\omega}_1, \boldsymbol{\omega}_2, 0) \\ &= f^m f^n \sum_{\chi} \begin{pmatrix} m & n & l \\ \chi & -\chi & 0 \end{pmatrix} \times \\ &\quad \int d\boldsymbol{\omega}_1 R_{\chi\mu}^{m*}(\boldsymbol{\omega}_1) \int d\boldsymbol{\omega}_2 R_{-\chi\nu}^{n*}(\boldsymbol{\omega}_2) F(\boldsymbol{\omega}_1, \boldsymbol{\omega}_2, r) \end{aligned} \quad (\text{C.20})$$

The function  $F(\boldsymbol{\omega}_1, \boldsymbol{\omega}_2, r)$  and the projections  $F_{\mu\nu}^{mn}(r)$  can be transformed into each other by 2 simple steps.

#### C.3.1 Transform between $F_{\mu\nu}^{mn}(r)$ and $F_{\mu\nu,\chi}^{mn}(r)$

Suppose

$$F_{\mu\nu,\chi}^{mn}(r) = \sum_l \begin{pmatrix} m & n & l \\ \chi & -\chi & 0 \end{pmatrix} F_{\mu\nu}^{ml}(r) \quad (\text{C.21})$$

Using property of 3j-symbol [44]

$$\sum_{\chi} \begin{pmatrix} m & n & l' \\ \chi & -\chi & 0 \end{pmatrix} \begin{pmatrix} m & n & l \\ \chi & -\chi & 0 \end{pmatrix} = \frac{\delta_{l'l}}{2l+1} \quad (\text{C.22})$$

we have as the inverse transform

$$F_{\mu\nu}^{mn}(r) = (2l+1) \sum_{\chi} \begin{pmatrix} m & n & l \\ \chi & -\chi & 0 \end{pmatrix} F_{\mu\nu,\chi}^{mn}(r) \quad (\text{C.23})$$

Thus Eq. (C.19) becomes

$$\begin{aligned}
F(\omega_1, \omega_2, r) &= \sum_{mn\mu\nu} (2l+1) \sum_{\chi'} \begin{pmatrix} m & n & l \\ \chi' & -\chi' & 0 \end{pmatrix} F_{\mu\nu,\chi'}^{mn}(r) \times \\
&\quad \sum_{\chi} \begin{pmatrix} m & n & l \\ \chi & -\chi & 0 \end{pmatrix} f^m f^n R_{\chi\mu}^m(\omega_1) R_{-\chi\nu}^n(\omega_2) \\
&= \sum_{mn\mu\nu} \sum_{\chi'} \sum_{\chi} F_{\mu\nu,\chi'}^{mn}(r) f^m f^n R_{\chi\mu}^m(\omega_1) R_{-\chi\nu}^n(\omega_2) \times \\
&\quad \sum_l (2l+1) \begin{pmatrix} m & n & l \\ \chi' & -\chi' & 0 \end{pmatrix} \begin{pmatrix} m & n & l \\ \chi & -\chi & 0 \end{pmatrix} \tag{C.24}
\end{aligned}$$

As

$$\sum_l (2l+1) \begin{pmatrix} m & n & l \\ \chi' & -\chi' & 0 \end{pmatrix} \begin{pmatrix} m & n & l \\ \chi & -\chi & 0 \end{pmatrix} = \delta_{\chi'\chi} \tag{C.25}$$

we have

$$F(\omega_1, \omega_2, r) = \sum_{mn\mu\nu\chi} F_{\mu\nu,\chi}^{mn}(r) f^m f^n R_{\chi\mu}^m(\omega_1) R_{-\chi\nu}^n(\omega_2) \tag{C.26}$$

and

$$F_{\mu\nu,\chi}^{mn}(r) = \int d\omega_1 d\omega_2 F(\omega_1, \omega_2, r) f^m f^n R_{\chi\mu}^{m*}(\omega_1) R_{-\chi\nu}^{n*}(\omega_2) \tag{C.27}$$

Thus eq. (C.26, C.27) can be performed either by fast generalized spherical harmonic transform (FGSHT), or being developed into

$$F(\omega_1, \omega_2, r) = \sum_{mn\mu\nu\chi} F_{\mu\nu,\chi}^{mn}(r) f^m f^n r_{\chi\mu}^m(\theta_1) r_{-\chi\nu}^n(\theta_2) e^{-i\chi(\phi_{12}\equiv\phi_1-\phi_2)} e^{-i\mu\psi_1} e^{-i\nu\psi_2} \tag{C.28}$$

and transformed with FFT-3D.

### C.3.2 Rotational invariant transform with FFT-3D

Suppose

$$F_{\mu\nu,\chi}^m(r, \theta_2) = \sum_n F_{\mu\nu,\chi}^{mn}(r) f^n r_{-\chi\nu}^n(\theta_2) \tag{C.29}$$

then we have

$$F(\omega_1, \omega_2, r) = \sum_{m\mu\nu\chi} F_{\mu\nu,\chi}^m(r, \theta_2) f^m r_{\chi\mu}^m(\theta_1) e^{-i\chi\phi_{12}} e^{-i\mu\psi_1} e^{-i\nu\psi_2} \tag{C.30}$$

The inverse transform should be

$$F_{\mu\nu,\chi}^{mn}(r) = \frac{1}{2} \int d(\cos\theta_2) F_{\mu\nu,\chi}^m(r, \theta_2) r_{-\chi\nu}^n(\theta_2) \tag{C.31}$$

In the same way, suppose

$$F_{\mu\nu,\chi}(r, \theta_1, \theta_2) = \sum_m F_{\mu\nu,\chi}^m(r, \theta_2) r_{\chi\mu}^m(\theta_1) \tag{C.32}$$

and the inverse transform

$$F_{\mu\nu,\chi}^m(r, \theta_2) = \frac{1}{2} \int d(\cos\theta_1) F_{\mu\nu,\chi}(r, \theta_1, \theta_2) r_{\chi\mu}^m(\theta_1) \tag{C.33}$$

then we have

$$F(r, \omega_1, \omega_2) = \sum_{\mu\nu\chi} F_{\mu\nu,\chi}(r, \theta_1, \theta_2) e^{-i\chi\phi_{12}} e^{-i\mu\psi_1} e^{-i\nu\psi_2} \tag{C.34}$$

which can be treated as a normal FFT of 3 dimensions.

## C.4 TRANSFORM IN FIXED FRAME

Similarly, in the laboratory coordinate system

$$\Phi_{\mu\nu}^{mn l}(0, \Omega, \hat{\mathbf{r}}) = \sum_{\eta} \begin{pmatrix} m & n & l \\ \mu & \eta & -\mu - \eta \end{pmatrix} f^m f^n R_{\eta,\nu}^n(\Omega) R_{-\mu-\eta,0}^l(\hat{\mathbf{r}}) \quad (\text{C.35})$$

The rotational invariant does not take advantage of the  $\chi$  transform as  $\mu \neq 0$ . The expansion on rotational invariants should be calculated directly.

### c.4.1 Expansion of $F(\mathbf{r}, \Omega)$ on rotational invariants

The total equation of the forward transform is as shown below:

$$F_{\mu\nu}^{mn l}(r) = f^m f^n \sum_{\eta} \begin{pmatrix} m & n & l \\ \mu & \eta & -\mu - \eta \end{pmatrix} \int d\hat{\mathbf{r}} R_{-\mu-\eta,0}^{l*}(\hat{\mathbf{r}}) \int d\Omega F(r, \hat{\mathbf{r}}, \Omega) R_{\eta,\nu}^{n*}(\Omega) \quad (\text{C.36})$$

Firstly, the FGSHT is performed:

$$F_{\eta\nu}^n(\mathbf{r}) = \int d\Omega f^n F(\mathbf{r}, \Omega) R_{\eta,\nu}^{n*}(\Omega) \quad (\text{C.37})$$

Then the spherical harmonic transform by histogram should give

$$F_{\eta\nu,\lambda}^{nl}(r) = \int d\hat{\mathbf{r}} R_{\lambda 0}^{l*}(\hat{\mathbf{r}}) F_{\eta\nu}^n(r, \hat{\mathbf{r}}) \quad (\text{C.38})$$

As  $F_{\eta\nu}^n(\mathbf{r})$  values are tabulated in the Cartesian grid, we cannot use a quadrature approach without interpolation, so the histogram approach is used.

Histogram for a function  $f$  gives:

$$\bar{f}(r) = \int d\theta_r d\phi_r f(x, y, z) \quad (\text{C.39})$$

so if we want to compute

$$\bar{F}(r) = \int d\theta_r d\phi_r R_{\lambda 0}^{l*}(x, y, z) F(x, y, z) \quad (\text{C.40})$$

we just need to propose

$$f(x, y, z) = R_{\lambda 0}^{l*}(x, y, z) F(x, y, z) \quad (\text{C.41})$$

For complex numbers  $F_{\eta\nu}^n(\mathbf{r})$ , the real and imaginary parts can be calculated separately.

The rotational matrices  $R_{\lambda 0}^{l*}(\mathbf{r})$  in Cartesian coordinate system can be pre-generated by recurrence as detailed in appendix D.

Finally, the combination of projections gives:

$$F_{\mu\nu}^{mn l}(r) = f^m \sum_{\eta} \begin{pmatrix} m & n & l \\ \mu & \eta & -\mu - \eta \end{pmatrix} F_{\eta\nu,-\mu-\eta}^{nl}(r) \quad (\text{C.42})$$

**It should be noted that  $F_{\mu\nu}^{mn l}(r)$  is real?**

### C.4.2 Rebuilding of $F(\mathbf{r}, \Omega)$ from projections

and the rebuilding of  $F(\mathbf{r}, \Omega)$  in a certain orientation is as simple as its definition

$$F(\mathbf{r}, \Omega) = \sum_{mnl\mu\nu} F_{\mu\nu}^{mnl}(r) f^m f^n \sum_{\eta} \begin{pmatrix} m & n & l \\ \mu & \eta & -\mu - \eta \end{pmatrix} R_{\eta\nu}^n(\Omega) R_{-\mu-\eta, 0}^l(\hat{\mathbf{r}}) \quad (\text{C.43})$$

## C.5 SYMMETRY

In IEM and MDFT, the rotational invariants are used to describe the solvent. It possess symmetric rules, introduced by the indistinguishability of the two particles, symmetry properties of single particle, and its real number property as a physical quantity. Here we list all the symmetric rules concerning the 2-molecule system.

### C.5.1 Symmetric rules of $F(\omega_1, \omega_2)$ in intermolecular form

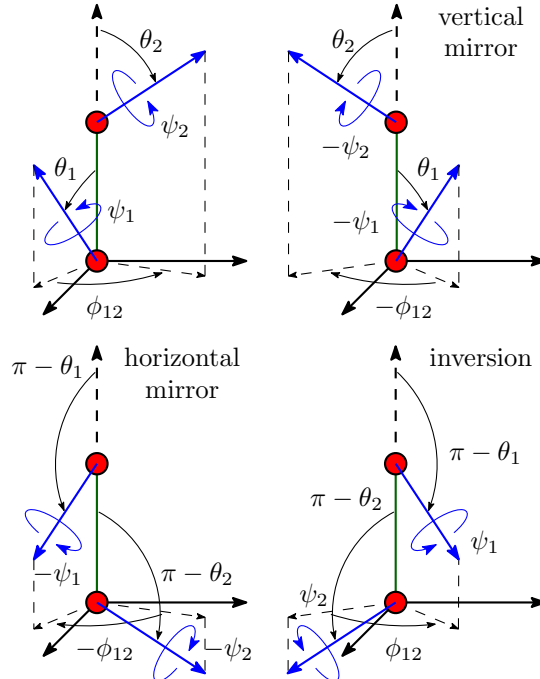


Figure C.1: Symmetry operations of a 2-molecule system

As shown in figure C.1, function in intermolecular coordinate system  $F(\omega_1, \omega_2) \equiv F(\cos \theta_1, \cos \theta_2, \phi, \psi_1, \psi_2)$  possesses symmetry rules:

1. Symmetry of vertical mirror:

$$F(\theta_1, \theta_2, \phi, \psi_1, \psi_2) = F(\theta_1, \theta_2, -\phi, -\psi_1, -\psi_2) \quad (\text{C.44})$$

2. Symmetry of inversion:

$$F(\theta_1, \theta_2, \phi, \psi_1, \psi_2) = F(\pi - \theta_2, \pi - \theta_1, \phi, \psi_2, \psi_1) \quad (\text{C.45})$$

And an additive symmetric rule is possessed by particles having

1. [3.]Symmetry axe C<sub>2n</sub>:

$$F(\theta_1, \theta_2, \phi, \psi_1, \psi_2) = F(\theta_1, \theta_2, \phi, \psi_1 + \pi, \psi_2 + \pi) \quad (\text{C.46})$$

### C.5.2 Symmetric rules of rotational invariant projections

The definition of rotational invariant on  $\chi$ -transform gives

$$c(\theta_1, \theta_2, \phi_{12}, \psi_1, \psi_2) = \frac{1}{2l+1} \sum_{mn\mu\nu\chi} c_{\mu\nu,\chi}^{mn}(r) d_{\chi\mu}^m(\theta_1) d_{\chi\nu}^n(\theta_2) e^{-i\chi\phi_{12}} e^{-i\mu\psi_1} e^{-i\nu\psi_2}$$

Thus

$$\begin{aligned} c(\theta_1, \theta_2, -\phi_{12}, -\psi_1, -\psi_2) &= \frac{1}{2l+1} \sum_{mn\mu\nu\chi} c_{\underline{\mu}\underline{\nu},\underline{\chi}}^{mn}(r) d_{\chi\mu}^m(\theta_1) d_{\chi\nu}^n(\theta_2) e^{-i\chi\phi_{12}} e^{-i\mu\psi_1} e^{-i\nu\psi_2} \\ &= \frac{1}{2l+1} \sum_{mn\mu\nu\chi} (-)^{\mu+\nu} c_{\underline{\mu}\underline{\nu},\underline{\chi}}^{mn}(r) d_{\chi\mu}^m(\theta_1) d_{\chi\nu}^n(\theta_2) e^{-i\chi\phi_{12}} e^{-i\mu\psi_1} e^{-i\nu\psi_2} \\ c(\pi - \theta_2, \pi - \theta_1, \phi_{12}, \psi_2, \psi_1) &= \frac{1}{2l+1} \sum_{mn\mu\nu\chi} c_{\mu\nu,\chi}^{mn}(r) d_{\chi\mu}^m(\pi - \theta_2) d_{\chi\nu}^n(\pi - \theta_1) e^{-i\chi\phi_{12}} e^{-i\mu\psi_2} e^{-i\nu\psi_1} \\ &= \frac{1}{2l+1} \sum_{mn\mu\nu\chi} (-)^{m+n+\mu+\nu} c_{\nu\mu,\chi}^{nm}(r) d_{\chi\mu}^m(\theta_1) d_{\chi\nu}^n(\theta_2) e^{-i\chi\phi_{12}} e^{-i\mu\psi_1} e^{-i\nu\psi_2} \end{aligned}$$

and  $\mu, \nu$  are even.

Thus

$$c_{\mu\nu,\chi}^{mn}(r) = c_{\underline{\mu}\underline{\nu},\underline{\chi}}^{mn}(r) = (-)^{m+n} c_{\nu\mu,\chi}^{nm}(r)$$

(Need proof.)

$$\hat{c}_{\mu\nu,\chi}^{mn}(\mathbf{k}) = (-)^{m+n} \hat{c}_{\mu\nu,\chi}^{*mn}(\mathbf{k})$$

In MDFT, rotational invariant projections are used to describe DCF. The original  $c_{\mu\nu}^{ml}(\mathbf{r})$  collected by IEM is real.

1. With  $r$  and  $l$ : As  $c_{\mu\nu}^{ml}(\mathbf{r})$  is real

$$F_{\underline{\mu}\underline{\nu}}^{ml}(\mathbf{r}) = (-)^{m+n+l} F_{\mu\nu}^{ml}(\mathbf{r}) \quad (\text{C.47})$$

As the two molecules are interchangeable,

$$F_{\nu\mu}^{nl}(\mathbf{r}) = (-)^{m+n} F_{\mu\nu}^{ml}(\mathbf{r}) \quad (\text{C.48})$$

2. [2.]With  $r$  and  $\chi$ :

$$F_{\mu\nu,\chi}^{mn}(\mathbf{r}) = \sum_{\chi} \begin{pmatrix} m & n & l \\ \chi & -\chi & 0 \end{pmatrix} F_{\mu\nu}^{ml}(\mathbf{r}) \quad (\text{C.49})$$

$$F_{\underline{\mu}\underline{\nu},\underline{\chi}}^{mn}(\mathbf{r}) = F_{\mu\nu,\chi}^{mn}(\mathbf{r}) \quad (\text{C.50})$$

$$F_{\nu\mu,\chi}^{nm}(\mathbf{r}) = (-)^{m+n} F_{\mu\nu,\chi}^{mn}(\mathbf{r}) \quad (\text{C.51})$$

3. [3.] With  $k$  and  $l$ :

$$\text{TF}(c_{\mu\nu}^{mnl}(\mathbf{r})) = \hat{c}_{\mu\nu}^{mnl}(\mathbf{k}) \quad (\text{C.52})$$

is real if  $l$  is even, and is purely imaginary if  $l$  is odd.

4. [4.] With  $k$  and  $\chi$ :

$$F_{\mu\nu,\chi}^{mn}(\mathbf{k}) = (-)^{m+n} F_{\mu\nu,\chi}^{*mn}(\mathbf{k}) \quad (\text{C.53})$$

Finally, if the solvent molecule possesses an axe of symmetry  $C_2$ ,  $\mu$  and  $\nu$  is even.

For spherical solutes, the  $\Omega_1$ -dependence vanishes so that  $m = \mu = 0$ , only the terms  $F_{0\nu}^{0nl}(r)$  are not-zero.

# D

## CALCULATION OF ROTATION MATRIX ELEMENTS $R_{\mu\mu'}^m$ BY RECURRENCE

---

$\mathbf{R}^m(\Omega) \equiv \{R_{\mu'\chi}^m(\Omega)\}$  is the rotation matrix of dimension  $(2m+1) \times (2m+1)$ , defined in Messiah and other books [11, 19, 44].

In MDFT, evaluation of  $R_{\mu'\chi}^m(\hat{\mathbf{k}})$  for each  $m, \mu', \chi$  and  $\mathbf{k}$  by its definition:

$$R_{\mu'\chi}^m(\hat{\mathbf{k}}) = r_{\mu'\chi}^m(\theta_k) e^{-i\mu'\phi_k} \quad (\text{D.1})$$

is too costly to be done in iterations; on the other hand, to directly stock the value of every element is heavy in terms of memory. An algorithm of  $R_{\mu\mu'}^m(\hat{\mathbf{k}})$  evaluation by recurrence described by Choi *et al.* [8] suggests an acceptable cost during the computation, by generating the rotation matrix elements from those of lower order to avoid extra calculation.

### d.1 CASE OF $m_{\max} \leq 1$

According to the definition in eq. (D.1), it is easy to find

$$R_{00}^0 = 1 \quad (\text{D.2})$$

For  $m = 1$ ,  $\mathbf{R}^1(\hat{\mathbf{k}})$  depends only on the  $3 \times 3$  orthogonal matrix  $\mathbf{R}$  that defines the rotation from the basis vectors of laboratory frame to those of  $\mathbf{k}$ -frame:

$$\mathbf{R} = \begin{bmatrix} R_{xx} & R_{yx} & R_{zx} \\ R_{xy} & R_{yy} & R_{zy} \\ R_{xz} & R_{yz} & R_{zz} \end{bmatrix} = \begin{bmatrix} \cos \theta_k \cos \phi_k & -\sin \phi_k & \sin \theta_k \cos \phi_k \\ \cos \theta_k \sin \phi_k & \cos \phi_k & \sin \theta_k \sin \phi_k \\ -\sin \theta_k & 0 & \cos \theta_k \end{bmatrix} \quad (\text{D.3})$$

The matrix  $\mathbf{R}$  can be calculated by the cross products of basis vectors as shown in figure 7.3

$$\begin{bmatrix} \mathbf{e}_1'' & \mathbf{e}_2' & \mathbf{e}_3'' \end{bmatrix} = \begin{bmatrix} \mathbf{e}_1 & \mathbf{e}_2 & \mathbf{e}_3 \end{bmatrix} \mathbf{R} = \mathbf{R} \quad (\text{D.4})$$

The rotation matrix  $\mathbf{R}^m$  can be separated into the real  $\mathbf{F}^m$  and imaginary  $\mathbf{G}^m$  parts, which can be given by the relations

$$R_{\chi\chi'}^m = F_{\chi\chi'}^m + iG_{\chi\chi'}^m \quad (\text{D.5})$$

$$\begin{bmatrix} F_{11}^1 & F_{10}^1 & F_{11}^1 \\ F_{01}^1 & F_{00}^1 & F_{01}^1 \\ F_{11}^1 & F_{10}^1 & F_{11}^1 \end{bmatrix} = \begin{bmatrix} (R_{yy} + R_{xx})/2 & R_{xz}/\sqrt{2} & (R_{yy} - R_{xx})/2 \\ R_{zx}/\sqrt{2} & R_{zz} & -R_{xz}/\sqrt{2} \\ (R_{yy} - R_{xx})/2 & -R_{xz}/\sqrt{2} & (R_{yy} + R_{xx})/2 \end{bmatrix} \quad (\text{D.6})$$

$$\begin{bmatrix} G_{11}^1 & G_{10}^1 & G_{11}^1 \\ G_{01}^1 & G_{00}^1 & G_{01}^1 \\ G_{11}^1 & G_{10}^1 & G_{11}^1 \end{bmatrix} = \begin{bmatrix} (R_{yx} - R_{xy})/2 & R_{yz}/\sqrt{2} & -(R_{yx} + R_{xy})/2 \\ -R_{zy}/\sqrt{2} & 0 & -R_{zy}/\sqrt{2} \\ (R_{yx} + R_{xy})/2 & R_{yz}/\sqrt{2} & (R_{xy} - R_{yx})/2 \end{bmatrix} \quad (\text{D.7})$$

## d.2 CASE OF $m_{\max} > 1$

### D.2.1 Recurrence relation for $-m + 1 \leq \chi' \leq m - 1$

The recurrence relation for  $-m \leq \chi \leq m$ ,  $-m + 1 \leq \chi' \leq m - 1$  between matrix elements is:

$$R_{\chi\chi'}^m = a_{\chi\chi'}^m R_{00}^1 R_{\chi\chi'}^{m-1} + b_{\chi\chi'}^m R_{10}^1 R_{\chi-1,\chi'}^{m-1} + b_{-\chi,\chi'}^m R_{-1,0}^1 R_{\chi+1,\chi'}^{m-1} \quad (\text{D.8})$$

where

$$\begin{aligned} a_{\chi\chi'}^m &= \left[ \frac{(m+\chi)(m-\chi)}{(m+\chi')(m-\chi')} \right]^{\frac{1}{2}} \quad (-m+1 \leq \chi \leq m-1) \\ b_{\chi\chi'}^m &= \left[ \frac{(m+\chi)(m+\chi-1)}{2(m+\chi')(m-\chi')} \right]^{\frac{1}{2}} \quad (-m+2 \leq \chi \leq m-2) \end{aligned} \quad (\text{D.9})$$

To separate the real and imaginary parts, suppose

$$H_{\chi\chi'}^m(i, j) = F_{ij}^1 F_{\chi\chi'}^{m-1} - G_{ij}^1 G_{\chi\chi'}^{m-1} \quad (\text{D.10})$$

$$K_{\chi\chi'}^m(i, j) = F_{ij}^1 G_{\chi\chi'}^{m-1} + G_{ij}^1 F_{\chi\chi'}^{m-1} \quad (\text{D.11})$$

therefore

$$F_{\chi\chi'}^m = a_{\chi\chi'}^m H_{\chi\chi'}^m(0, 0) + b_{\chi\chi'}^m H_{\chi-1,\chi'}^m(1, 0) + b_{-\chi,\chi'}^m H_{\chi+1,\chi'}^m(-1, 0) \quad (\text{D.12})$$

$$G_{\chi\chi'}^m = a_{\chi\chi'}^m K_{\chi\chi'}^m(0, 0) + b_{\chi\chi'}^m K_{\chi-1,\chi'}^m(1, 0) + b_{-\chi,\chi'}^m K_{\chi+1,\chi'}^m(-1, 0) \quad (\text{D.13})$$

In the case of  $\chi = \pm m$ , certain terms in eq. (D.8) are out of definition. They are supposed to be zero. Another way is to suppose that

$$\begin{aligned} a_{\chi\chi'}^m &= 0 \quad \text{for } \chi = \pm m \\ b_{\chi\chi'}^m &= 0 \quad \text{for } \chi = \pm m \text{ and } \chi = \mp(m-1) \end{aligned} \quad (\text{D.14})$$

### D.2.2 Recurrence relation for $-m + 2 \leq \chi' \leq m$

For the case  $\chi' = \pm m$  which are not covered in eq. (D.8), another recurrence relation supposes that:

$$R_{\chi\chi'}^m = c_{\chi\chi'}^m R_{0,1}^1 R_{\chi,\chi'-1}^{m-1} + d_{\chi\chi'}^m R_{1,1}^1 R_{\chi-1,\chi'-1}^{m-1} + d_{-\chi,\chi'}^m R_{-1,1}^1 R_{\chi+1,\chi'-1}^{m-1} \quad (\text{D.15})$$

$$F_{\chi\chi'}^m = c_{\chi\chi'}^m H_{\chi,\chi'-1}^m(0, 1) + d_{\chi\chi'}^m H_{\chi-1,\chi'-1}^m(1, 1) + d_{-\chi,\chi'}^m H_{\chi+1,\chi'-1}^m(-1, 1) \quad (\text{D.16})$$

$$G_{\chi\chi'}^m = c_{\chi\chi'}^m K_{\chi,\chi'-1}^m(0, 1) + d_{\chi\chi'}^m K_{\chi-1,\chi'-1}^m(1, 1) + d_{-\chi,\chi'}^m K_{\chi+1,\chi'-1}^m(-1, 1) \quad (\text{D.17})$$

with

$$\begin{aligned} c_{\chi\chi'}^m &= \left[ \frac{2(m+\chi)(m-\chi)}{(m+\chi')(m+\chi'-1)} \right]^{\frac{1}{2}} \quad (-m+1 \leq \chi \leq m-1) \\ d_{\chi\chi'}^m &= \left[ \frac{(m+\chi)(m+\chi-1)}{(m+\chi')(m+\chi'-1)} \right]^{\frac{1}{2}} \quad (-m+2 \leq \chi \leq m-2) \end{aligned} \quad (\text{D.18})$$

and

$$\begin{aligned} c_{\chi\chi'}^m &= 0 \quad \text{for } \chi = \pm m \\ d_{\chi\chi'}^m &= 0 \quad \text{for } \chi = \pm m \text{ and } \chi = \mp(m-1) \end{aligned} \quad (\text{D.19})$$

which is available for  $-m + 2 \leq \chi' \leq m$ .

### D.2.3 Symmetries

The symmetries of  $R_{\chi\chi'}^m$  allow us to calculate only a half of the elements:

$$R_{-m,-m'}^l = (-1)^{m+m'} R_{mm'}^{l*} \quad (\text{D.20})$$

which gives

$$F_{-m,-m'}^l = (-1)^{m+m'} F_{mm'}^l \quad (\text{D.21})$$

$$G_{-m,-m'}^l = -(-1)^{m+m'} G_{mm'}^l \quad (\text{D.22})$$



# E

## PROPERTIES OF WIGNER 3J-SYMBOL AND GSH

---

The properties of Wigner 3j-symbol and Wigner generalized spherical harmonics (GSH, Wigner D-symbol) play a huge role in the reduction of molecular Ornstein-Zernike equation as well as finding the relation between rotational invariant projections. Their main properties, presented in Messiah [44], Gray & Gubbins [19] and Edmonds [11], are listed here.

### e.1 PROPERTIES OF WIGNER 3J-SYMBOL

Wigner 3j-symbols are equivalent to Clebsch-Gordon (CG) coefficients multiplied by the phase factor:

$$\begin{pmatrix} m & n & l \\ \mu & \nu & -\lambda \end{pmatrix} = \frac{(-)^{m-n+\lambda}}{\sqrt{2l+1}} \langle mn\mu\nu | l\lambda \rangle \quad (\text{E.1})$$

and can be calculated with the Racah formula [44].

#### *Reality*

The 3j-symbols are real.

$$\begin{pmatrix} m & n & l \\ \mu & \nu & \lambda \end{pmatrix} = \begin{pmatrix} m & n & l \\ \mu & \nu & \lambda \end{pmatrix}^* \quad (\text{E.2})$$

#### *Selection rules*

$$\begin{pmatrix} m & n & l \\ \mu & \nu & \lambda \end{pmatrix} = 0 \text{ if } \begin{cases} \mu + \nu + \lambda = 0 \\ |m - n| < l < m + n \\ (\text{triangular inequalities}) \end{cases} \text{ are not meet.} \quad (\text{E.3})$$

#### *Permutation*

##### 1. Even permutation

$$\begin{pmatrix} m & n & l \\ \mu & \nu & \lambda \end{pmatrix} = \begin{pmatrix} n & l & m \\ \nu & \lambda & \mu \end{pmatrix} = \begin{pmatrix} l & m & n \\ \lambda & \mu & \nu \end{pmatrix} \quad (\text{E.4})$$

##### 2. Odd permutation

$$\begin{aligned} (-)^{m+n+l} \begin{pmatrix} m & n & l \\ \mu & \nu & \lambda \end{pmatrix} &= \begin{pmatrix} n & m & l \\ \nu & \mu & \lambda \end{pmatrix} \\ &= \begin{pmatrix} m & l & n \\ \mu & \lambda & \nu \end{pmatrix} = \begin{pmatrix} l & n & m \\ \lambda & \nu & \mu \end{pmatrix} \end{aligned} \quad (\text{E.5})$$

3. Simultaneous change of signs of  $\mu$ ,  $\nu$  and  $\lambda$

$$\begin{pmatrix} m & n & l \\ \mu & \nu & \lambda \end{pmatrix} = (-)^{m+n+l} \begin{pmatrix} m & n & l \\ -\mu & -\nu & -\lambda \end{pmatrix} \quad (\text{E.6})$$

*Orthogonality*

$$\sum_{l=|m-n|}^{m+n} \sum_{\lambda=-l}^l (2l+1) \begin{pmatrix} m & n & l \\ \mu & \nu & \lambda \end{pmatrix} \begin{pmatrix} m & n & l \\ \mu' & \nu' & \lambda \end{pmatrix} = \delta_{\mu\mu'} \delta_{\nu\nu'} \quad (\text{E.7})$$

$$\sum_{\mu=-m}^m \sum_{\nu=-n}^n \begin{pmatrix} m & n & l \\ \mu & \nu & \lambda \end{pmatrix} \begin{pmatrix} m & n & l' \\ \mu & \nu & \lambda' \end{pmatrix} = (2l+1)^{-1} \delta_{ll'} \delta_{\lambda\lambda'} \quad (\text{E.8})$$

## e.2 PROPERTIES OF GSH

There are many different definitions of GSH given in lectures. Here we adopt the definition in Messiah:

$$R_{\mu'\mu}^m(\phi\theta\psi) = e^{-i\mu'\phi} r_{\mu'\mu}^m(\theta) e^{-i\mu\psi} \quad (\text{E.9})$$

where  $r_{\mu\mu'}^m$  is the generalized Legendre polynomial (GLP), which is real, and can be evaluated using the Wigner formula:

$$\begin{aligned} r_{\mu'\mu}^m(\theta) = & [(m+\mu')! (m-\mu')! (m+\mu)! (m-\mu)!]^{\frac{1}{2}} \times \\ & \sum_i \frac{(-)^i (\cos \theta/2)^{2m+\mu'-\mu-2i} (\sin \theta/2)^{2i-\mu'+\mu}}{(m+\mu'-i)! (m-\mu-i)! i! (i-\mu'+\mu)!} \end{aligned} \quad (\text{E.10})$$

*Symmetries of  $r_{\mu'\mu}^m(\theta)$*

$$r_{\mu\mu'}^m(\theta) = (-)^{\mu'-\mu} r_{\mu'\mu}^m(\theta) \quad (\text{E.11})$$

$$\underline{r}_{\mu'\mu}^m(\theta) = (-)^{\mu'-\mu} r_{\mu'\mu}^m(\theta) \quad (\text{E.12})$$

$$r_{\mu'\mu}^m(\theta) = r_{\mu\mu'}^m(-\theta) \quad (\text{E.13})$$

$$r_{\mu'\mu}^m(\theta + \pi) = (-)^{m+\mu} \underline{r}_{\mu'\mu}^m(\theta) \quad (\text{E.14})$$

where  $\underline{\mu} \equiv -\mu$ .

*Symmetries of  $R_{\mu'\mu}^m(\phi\theta\psi)$*

$$R_{\mu'\mu}^m(\phi\theta\psi) = (-)^{\mu'-\mu} R_{\mu'\mu}^{m*}(\phi\theta\psi) \quad (\text{E.15})$$

$$R_{\mu'\mu}^m(\phi\theta\psi) = (-)^{\mu'-\mu} R_{\mu\mu'}^{m*}(\phi\theta\psi) \quad (\text{E.16})$$

$$R_{\mu'\mu}^m(\phi\theta\psi) = (-)^{m+\mu'} R_{\mu'\mu}^m(-\phi, \theta + \pi, \psi) = (-)^{m+\mu} R_{\mu'\mu}^m(\phi, \theta + \pi, -\psi) \quad (\text{E.17})$$

*Unitarity and orthogonality*

$$\sum_{\mu'} R_{\mu'\mu}^m(\phi\theta\psi) R_{\mu'\mu''}^{m*}(\phi\theta\psi) = \delta_{\mu\mu''} \quad (\text{E.18})$$

$$\sum_{\mu} R_{\mu'\mu}^m(\phi\theta\psi) R_{\mu''\mu}^{m*}(\phi\theta\psi) = \delta_{\mu'\mu''} \quad (\text{E.19})$$

$$\sum_{m\mu'\mu} R_{\mu'\mu}^m(\phi\theta\psi) R_{\mu'\mu'}^{m*}(\phi'\theta'\psi') = \delta_{\phi\phi'}\delta_{\theta\theta'}\delta_{\psi\psi'} \quad (\text{E.20})$$

$$\frac{1}{8\pi^2} \int d\cos\theta d\phi d\psi R_{\mu'\mu}^m(\phi\theta\psi) R_{\nu'\nu}^{n*}(\phi\theta\psi) = \frac{\delta_{mn}\delta_{\mu'\nu'}\delta_{\mu\nu}}{2n+1} \quad (\text{E.21})$$

$r_{\mu'\mu}^m(\theta)$  in terms of  $\cos\theta$  and  $\sin\theta$

1. If  $(-)^{\mu'+\mu} = +1$ ,  $r_{\mu'\mu}^m(\theta)$  is a polynomial of degree  $m$  in  $\cos\theta$ .
2. If  $(-)^{\mu'+\mu} = -1$ ,  $r_{\mu'\mu}^m(\theta)/\sin\theta$  is a polynomial of degree  $(m-1)$  in  $\cos\theta$ .

*Rotation and product*

$$R_{\mu'\mu}^m(\omega) = \sum_{\chi} R_{\mu'\chi}^m(\omega_2) R_{\chi\mu}^m(\omega_1) \quad (\text{E.22})$$

where  $\omega$  is the result of the successive application of  $\omega_1$  and  $\omega_2$  in order.

$$\begin{aligned} R_{\chi\mu}^m(\omega) &= \sum_{\mu'} R_{\mu'\chi}^{m*}(\hat{k}) R_{\mu'\mu}^m(\Omega) \\ R_{\mu'\mu}^m(\Omega) &= \sum_{\chi} R_{\chi\mu'}^{m*}(\hat{k}^{-1}) R_{\chi\mu}^m(\omega) = \sum_{\chi} R_{\mu'\chi}^m(\hat{k}) R_{\chi\mu}^m(\omega) \end{aligned} \quad (\text{E.23})$$

*Composition relation for GSHs*

$$\sum_{\mu'\nu'\lambda'} \begin{pmatrix} m & n & l \\ \mu' & \nu' & \lambda' \end{pmatrix} R_{\mu'\mu}^m(\phi\theta\psi) R_{\nu'\nu}^n(\phi\theta\psi) R_{\lambda'\lambda}^l(\phi\theta\psi) = \begin{pmatrix} m & n & l \\ \mu & \nu & \lambda \end{pmatrix} \quad (\text{E.24})$$



## ERROR EVALUATION OF INTERPOLATION STRATEGIES FOR DCF IN LOCAL FRAME

The error introduced by the two interpolation orders for a DCF of order  $n_{\max} = 1$  (for which the exact DCF can be computed directly; see details later) is shown in figure F.1.

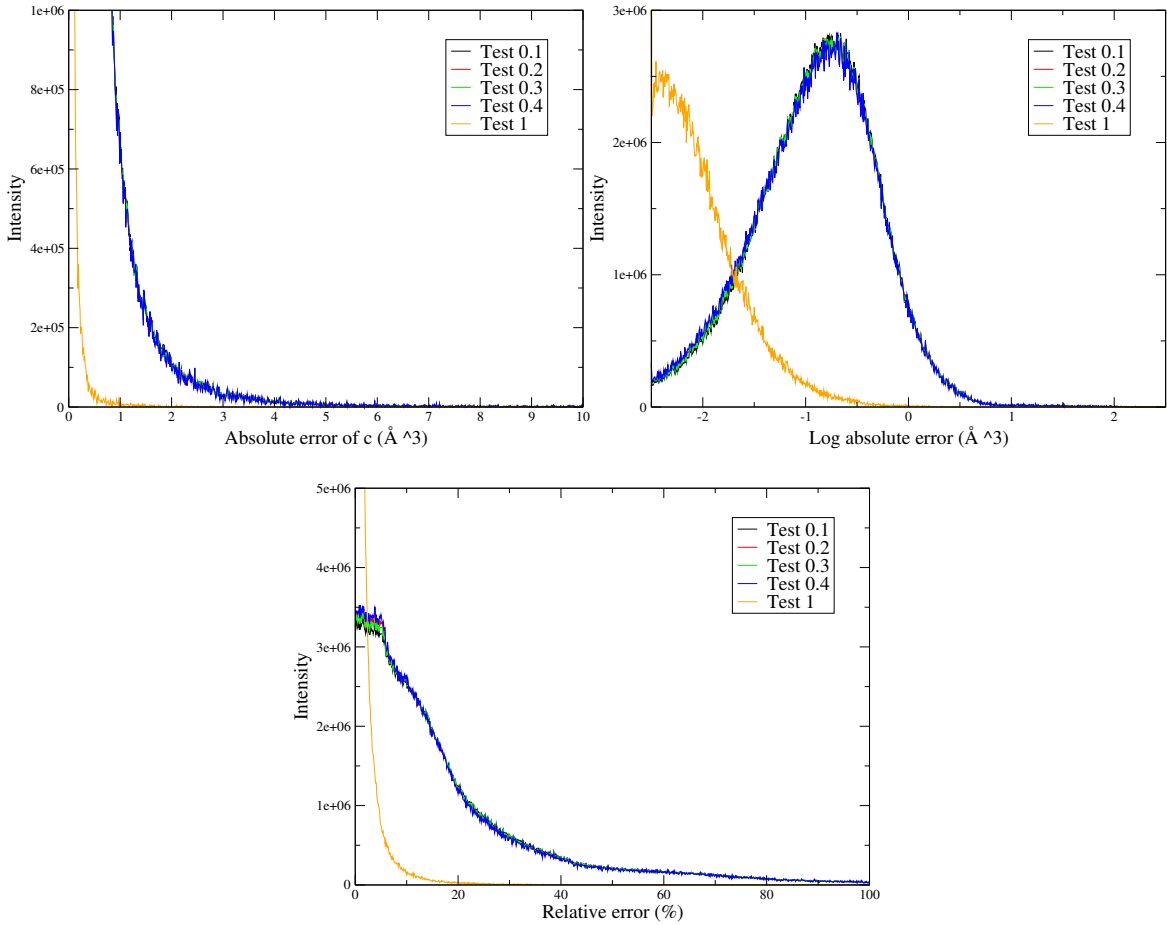


Figure F.1: Error of finding  $\hat{c}(\mathbf{k}, \Omega_1, \Omega_2)$  by interpolation compared to direct calculation: Test 0.1-0.4 is zero order interpolation with  $\phi$  tabulated as in figure 7.4. Test 1 is linear interpolation.

**Absolute error** is the histogram that counts the number of times that the calculated DCF gives the corresponding absolute error  $E_a^i$  with a resolution of 0.01, in range of [0, 10]:

$$E_a^i = |c_k^i - c_k| \quad (\text{F.1})$$

where  $c_k^i$  is any element of  $\hat{c}(\mathbf{k}, \Omega_1, \Omega_2)$  of unity  $\text{\AA}^3$  calculated as described and  $c_k$  is the one calculated directly as the reference.

**Log absolute error** is treated the same way as  $E_a^i$ , with  $E_l^i$  defined as

$$E_l^i = \log |c_k^i - c_k| \quad (\text{F.2})$$

**Relative error** is defined as

$$E_r^i = \left| c_k^i - c_k \right| / |c_k| \quad (\text{F.3})$$

with resolution of 0.1%, in range of [0, 1].

In all three figures, the 4 curves given by zero order interpolation do not diverge a great deal compared with the linear interpolation one. The result of MDFT also shows that zero order interpolation gives large energy error with a DCF of  $n_{\max} = 1$ , and has convergency problems in certain cases. We conclude that the linear interpolation scheme is absolutely necessary. On the other hand, as seen in eq. (7.16), it is computationally much more expensive than the simple histogram scheme, as it requires  $2^5 = 32$  times of operations.

## ORIGINAL DATA OF MDFT IMPLEMENTATION

---

In this appendix, some original implementation data which is thought redundant to put in the main context are put here. These details may contributes to further researches and gives a global image of the parameter and version sensibility of code MDFT.

### **g.1** SERIES OF CHARGED CH<sub>4</sub> CENTER

These tests are done with the sequential code.

#### G.1.1 *Branch “naive” result*

with Lebedev quadrature

#### G.1.2 *Branch “standard” result*



## BIBLIOGRAPHY

---

- [1] Luc Belloni and Ioulia Chikina. “Efficient full Newton - Raphson technique for the solution of molecular integral equations - example of the SPC/E water-like system.” In: *Molecular Physics* 112.9-10 (2014), pp. 1246–1256. DOI: 10.1080/00268976.2014.885612. eprint: <http://dx.doi.org/10.1080/00268976.2014.885612>. URL: <http://dx.doi.org/10.1080/00268976.2014.885612> (cit. on p. 95).
- [2] H. J. C. Berendsen, J. R. Grigera, and T. P. Straatsma. “The missing term in effective pair potentials.” In: *The Journal of Physical Chemistry* 91.24 (1987), pp. 6269–6271. DOI: 10.1021/j100308a038. eprint: <http://dx.doi.org/10.1021/j100308a038>. URL: <http://dx.doi.org/10.1021/j100308a038> (cit. on pp. 13, 14).
- [3] L. Blum. “Invariant Expansion. II. The Ornstein Zernike-Equation for Nonspherical Molecules and an Extended Solution to the Mean Spherical Model.” In: *The Journal of Chemical Physics* 57.5 (1972), pp. 1862–1869. DOI: <http://dx.doi.org/10.1063/1.1678503>. URL: <http://scitation.aip.org/content/aip/journal/jcp/57/5/10.1063/1.1678503> (cit. on pp. 3, 35, 41, 43, 44).
- [4] L. Blum and A. J. Torruella. “Invariant Expansion for Two-Body Correlations: Thermodynamic Functions, Scattering, and the Ornstein-Zernike Equation.” In: *The Journal of Chemical Physics* 56.1 (1972), pp. 303–310. DOI: <http://dx.doi.org/10.1063/1.1676864>. URL: <http://scitation.aip.org/content/aip/journal/jcp/56/1/10.1063/1.1676864> (cit. on pp. 3, 35, 41, 43, 95).
- [5] Richard H. Byrd, Peihuang Lu, Jorge Nocedal, and Ciyou Zhu. “A Limited Memory Algorithm for Bound Constrained Optimization.” In: *SIAM J. Sci. Comput.* 16.5 (Sept. 1995), pp. 1190–1208. DOI: 10.1137/0916069. URL: <http://dx.doi.org/10.1137/0916069> (cit. on p. 28).
- [6] David Chandler and Hans C. Andersen. “Optimized Cluster Expansions for Classical Fluids. II. Theory of Molecular Liquids.” In: *The Journal of Chemical Physics* 57.5 (1972), pp. 1930–1937. DOI: <http://dx.doi.org/10.1063/1.1678513>. URL: <http://scitation.aip.org/content/aip/journal/jcp/57/5/10.1063/1.1678513> (cit. on p. 2).
- [7] Martin Chaplin. *Water Model*. URL: [http://www1.lsbu.ac.uk/water/water\\_models.html](http://www1.lsbu.ac.uk/water/water_models.html) (cit. on p. 13).
- [8] Cheol Ho Choi, Joseph Ivanic, Mark S. Gordon, and Klaus Ruedenberg. “Rapid and stable determination of rotation matrices between spherical harmonics by direct recursion.” In: *The Journal of Chemical Physics* 111.19 (1999), pp. 8825–8831. DOI: <http://dx.doi.org/10.1063/1.480229>. URL: <http://scitation.aip.org/content/aip/journal/jcp/111/19/10.1063/1.480229> (cit. on p. 103).
- [9] Christopher J. Cramer and Donald G. Truhlar. “Implicit Solvation Models: Equilibria, Structure, Spectra, and Dynamics.” In: *Chemical Reviews* 99.8 (1999). PMID: 11849023, pp. 2161–2200. DOI: 10.1021/cr960149m. eprint: <http://dx.doi.org/10.1021/cr960149m>. URL: <http://dx.doi.org/10.1021/cr960149m> (cit. on pp. 1, 7).

- [10] Liem X. Dang, Julia E. Rice, and Peter A. Kollman. “The effect of water models on the interaction of the sodium–chloride ion pair in water: Molecular dynamics simulations.” In: *The Journal of Chemical Physics* 93.10 (1990), pp. 7528–7529. DOI: <http://dx.doi.org/10.1063/1.459714>. URL: <http://scitation.aip.org/content/aip/journal/jcp/93/10/10.1063/1.459714> (cit. on p. 3).
- [11] A. R. Edmonds. *Angular Momentum in Quantum Mechanics*. 1960 (cit. on pp. 95–97, 103, 107).
- [12] R. Evans. “The nature of the liquid-vapour interface and other topics in the statistical mechanics of non-uniform, classical fluids.” In: *Advances in Physics* 28.2 (1979), pp. 143–200. DOI: 10.1080/00018737900101365. eprint: <http://dx.doi.org/10.1080/00018737900101365>. URL: <http://dx.doi.org/10.1080/00018737900101365> (cit. on p. 3).
- [13] Sebastiao Formosinho and Monica Barroso, eds. *Proton-Coupled Electron Transfer. A Carrefour of Chemical Reactivity Traditions*. RSC Catalysis Series. The Royal Society of Chemistry, 2012, P001–157. DOI: 10.1039/9781849733168. URL: <http://dx.doi.org/10.1039/9781849733168> (cit. on p. 1).
- [14] P. H. Fries and G. N. Patey. “The solution of the hypernetted-chain approximation for fluids of nonspherical particles. A general method with application to dipolar hard spheres.” In: *The Journal of Chemical Physics* 82.1 (Jan. 1985), pp. 429–440. DOI: [doi:10.1063/1.448764](https://doi.org/10.1063/1.448764). URL: [http://jcp.aip.org/resource/1/jcpa6/v82/i1/p429\\_s1](http://jcp.aip.org/resource/1/jcpa6/v82/i1/p429_s1) (visited on 01/15/2013) (cit. on pp. 3, 35, 43, 95).
- [15] M. Frigo and S.G. Johnson. “The Design and Implementation of FFTW3.” In: *Proceedings of the IEEE* 93.2 (2005), pp. 216–231. DOI: 10.1109/JPROC.2004.840301 (cit. on pp. 47, 49, 63).
- [16] Peter Gács and László Lovász. *Complexity of Algorithms*. Lecture Notes. 1999 (cit. on p. 89).
- [17] Gaussian 09 keyword: SCRF. 2014. URL: [http://www.gaussian.com/g\\_tech/g\\_ur/k\\_scrf.htm](http://www.gaussian.com/g_tech/g_ur/k_scrf.htm) (cit. on p. 8).
- [18] Lionel Gendre, Rosa Ramirez, and Daniel Borgis. “Classical density functional theory of solvation in molecular solvents: Angular grid implementation.” In: *Chemical Physics Letters* 474.4–6 (June 2009), pp. 366–370. DOI: 10.1016/j.cplett.2009.04.077. URL: <https://acces-distant.upmc.fr/http/www.sciencedirect.com/science/article/pii/S0009261409004175> (visited on 03/01/2012) (cit. on p. 3).
- [19] C.G. Gray and K.E. Gubbins. *Theory of Molecular Fluids: I: Fundamentals*. International Series of Monographs on Chemistry. OUP Oxford, 1984. URL: <http://books.google.de/books?id=3mz2RcnnMGwC> (cit. on pp. 2, 7, 10, 47, 96, 97, 103, 107).
- [20] Georg Hager and Gerhard Wellein. *Formation lecture: Node-Level Performance Engineering*. Dec. 2015. URL: <http://moodle.rrze.uni-erlangen.de/course/view.php?id=274> (cit. on p. 91).
- [21] J. P. Hansen. “Basic Statistical Theory of Liquids.” In: *The Physics and Chemistry of Aqueous Ionic Solutions*. Ed. by M.-C Bellissent-Funel and G. W. Neilson. Dordrecht: Springer Netherlands, 1987, pp. 1–59. DOI: 10.1007/978-94-009-3911-0\_1. URL: [http://dx.doi.org/10.1007/978-94-009-3911-0\\_1](http://dx.doi.org/10.1007/978-94-009-3911-0_1) (cit. on p. 3).
- [22] Jean-Pierre Hansen and Ian R. McDonald. *Theory of Simple Liquids*. Ed. by Jean-Pierre Hansen and Ian R. McDonald. Fourth Edition. Oxford: Academic Press, 2013 (cit. on pp. 2, 10, 26, 27).

- [23] Robert B. Hermann. “Theory of hydrophobic bonding. II. Correlation of hydrocarbon solubility in water with solvent cavity surface area.” In: *The Journal of Physical Chemistry* 76.19 (1972), pp. 2754–2759. DOI: 10.1021/j100663a023. eprint: <http://dx.doi.org/10.1021/j100663a023>. URL: <http://dx.doi.org/10.1021/j100663a023> (cit. on p. 8).
- [24] Fumio Hirata, ed. *Molecular Theory of Solvation*. en. Vol. 24. Understanding Chemical Reactivity. Dordrecht: Kluwer Academic Publishers, 2004. URL: <http://link.springer.com/10.1007/1-4020-2590-4> (visited on 08/10/2016) (cit. on pp. 3, 21).
- [25] MJ Holst. “The Poisson-Boltzmann Equation.” In: () (cit. on pp. 8, 9).
- [26] Laura D. Hughes, David S. Palmer, Florian Nigsch, and John B. O. Mitchell. “Why are some properties more difficult to predict than others? A study of QSPR models of solubility, melting point, and Log P.” In: *Journal of Chemical Information and Modeling* 48.1 (Jan. 2008), pp. 220–232. DOI: 10.1021/ci700307p (cit. on p. 1).
- [27] Philippe Hunenberger and Maria Reif. “Chapter 2 Fundamental Experimental Problems.” In: *Single-Ion Solvation: Experimental and Theoretical Approaches to Elusive Thermodynamic Quantities*. The Royal Society of Chemistry, 2011, pp. 8–38. DOI: 10.1039/9781849732222-00008. URL: <http://dx.doi.org/10.1039/9781849732222-00008> (cit. on p. 53).
- [28] Guillaume Jeanmairet. “A molecular density functional theory to study solvation in water.” Theses. Université Pierre et Marie Curie - Paris VI, July 2014. URL: <https://tel.archives-ouvertes.fr/tel-01067993> (cit. on p. 3).
- [29] Guillaume Jeanmairet, Maximilien Levesque, Rodolphe Vuilleumier, and Daniel Borgis. “Molecular Density Functional Theory of Water.” In: *The Journal of Physical Chemistry Letters* 4 (Jan. 2013), pp. 619–624. DOI: 10.1021/jz301956b. URL: <http://pubs.acs.org/doi/abs/10.1021/jz301956b> (visited on 02/12/2013) (cit. on p. 3).
- [30] Guillaume Jeanmairet, Maximilien Levesque, Volodymyr Sergievskyi, and Daniel Borgis. “Molecular density functional theory for water with liquid-gas coexistence and correct pressure.” In: *The Journal of Chemical Physics* 142.15 (Apr. 2015), p. 154112. DOI: 10.1063/1.4917485. URL: <http://scitation.aip.org/content/aip/journal/jcp/142/15/10.1063/1.4917485> (visited on 04/17/2015) (cit. on p. 3).
- [31] Guillaume Jeanmairet, Nicolas Levy, Maximilien Levesque, and Daniel Borgis. “Molecular density functional theory of water including density–polarization coupling.” In: *Journal of Physics: Condensed Matter* 28.24 (June 2016), p. 244005. DOI: 10.1088/0953-8984/28/24/244005. URL: <http://stacks.iop.org/0953-8984/28/i=24/a=244005?key=crossref.f8479e7e8caf2fba10b27ef710dcc300> (visited on 04/27/2016) (cit. on p. 3).
- [32] Frank Jensen. *Introduction to Computational Chemistry*. John Wiley & Sons, 2006 (cit. on pp. 1, 7–9).
- [33] William L. Jorgensen and Julian Tirado-Rives. “Free energies of hydration for organic molecules from Monte Carlo simulations.” In: *Perspectives in Drug Discovery and Design* 3.1 (1995), pp. 123–138. DOI: 10.1007/BF02174470. URL: <http://dx.doi.org/10.1007/BF02174470> (cit. on p. 2).

- [34] M. A. Kastenholz and Philippe H. Hünenberger. “Computation of methodology-independent ionic solvation free energies from molecular simulations. I. The electrostatic potential in molecular liquids.” In: *The Journal of Chemical Physics* 124.12, 124106 (2006). DOI: <http://dx.doi.org/10.1063/1.2172593>. URL: <http://scitation.aip.org/content/aip/journal/jcp/124/12/10.1063/1.2172593> (cit. on pp. 53, 54).
- [35] Mika A. Kastenholz and Philippe H. Hünenberger. “Computation of methodology-independent ionic solvation free energies from molecular simulations. II. The hydration free energy of the sodium cation.” In: *The Journal of Chemical Physics* 124.22, 224501 (2006). DOI: <http://dx.doi.org/10.1063/1.2201698>. URL: <http://scitation.aip.org/content/aip/journal/jcp/124/22/10.1063/1.2201698> (cit. on p. 53).
- [36] Peter G. Kusalik and Igor M. Svishchev. “The Spatial Structure in Liquid Water.” In: *Science* 265.5176 (1994), pp. 1219–1221. DOI: [10.1126/science.265.5176.1219](https://doi.org/10.1126/science.265.5176.1219). eprint: <http://science.sciencemag.org/content/265/5176/1219.full.pdf>. URL: <http://science.sciencemag.org/content/265/5176/1219> (cit. on p. 14).
- [37] B. Lee and F.M. Richards. “The interpretation of protein structures: Estimation of static accessibility.” In: *Journal of Molecular Biology* 55.3 (1971), 379 –IN4. DOI: [http://dx.doi.org/10.1016/0022-2836\(71\)90324-X](http://dx.doi.org/10.1016/0022-2836(71)90324-X). URL: <http://www.sciencedirect.com/science/article/pii/002228367190324X> (cit. on p. 8).
- [38] Maximilien Levesque, Virginie Marry, Benjamin Rotenberg, Guillaume Jeanmairet, Rodolphe Vuilleumier, and Daniel Borgis. “Solvation of complex surfaces via molecular density functional theory.” In: *The Journal of Chemical Physics* 137.22 (Dec. 2012), pp. 224107–224107–8. DOI: [doi:10.1063/1.4769729](https://doi.org/10.1063/1.4769729). URL: [http://jcp.aip.org/resource/1/jcpsa6/v137/i22/p224107\\_s1?isAuthorized=no](http://jcp.aip.org/resource/1/jcpsa6/v137/i22/p224107_s1?isAuthorized=no) (visited on 12/13/2012) (cit. on p. 3).
- [39] Nicolas Levy, Daniel Borgis, and Massimo Marchi. “A dielectric continuum model of solvation for complex solutes.” In: *Computer Physics Communications* 169.1–3 (2005). Proceedings of the Europhysics Conference on Computational Physics 2004CCP 2004Europhysics Conference on Computational Physics 2004, pp. 69 – 74. DOI: <http://dx.doi.org/10.1016/j.cpc.2005.03.018>. URL: <http://www.sciencedirect.com/science/article/pii/S0010465505001153> (cit. on p. 9).
- [40] Massimo Marchi, Daniel Borgis, Nicolas Levy, and Pietro Ballone. “A dielectric continuum molecular dynamics method.” In: *The Journal of Chemical Physics* 114.10 (2001), pp. 4377–4385. DOI: <http://dx.doi.org/10.1063/1.1348028>. URL: <http://scitation.aip.org/content/aip/journal/jcp/114/10/10.1063/1.1348028> (cit. on pp. 9, 29).
- [41] Lorenzo Maschio, Bernard Kirtman, Roberto Orlando, and Michel Rérat. “Ab initio analytical infrared intensities for periodic systems through a coupled perturbed Hartree-Fock/Kohn-Sham method.” In: *The Journal of Chemical Physics* 137.20, 204113 (2012). DOI: <http://dx.doi.org/10.1063/1.4767438>. URL: <http://scitation.aip.org/content/aip/journal/jcp/137/20/10.1063/1.4767438> (cit. on p. 54).
- [42] A. D. Mcnaught and A. Wilkinson. *IUPAC Compendium of Chemical Terminology*, 2nd ed. (the "Gold Book"). WileyBlackwell; 2nd Revised edition edition (cit. on p. 1).

- [43] N. David Mermin. “Thermal Properties of the Inhomogeneous Electron Gas.” In: *Physical Review* 137.5A (Mar. 1965), A1441–A1443. DOI: 10.1103/PhysRev.137.A1441. URL: <http://link.aps.org/doi/10.1103/PhysRev.137.A1441> (visited on 02/10/2014) (cit. on p. 3).
- [44] Albert Messiah. *Quantum Mechanics*. Quantum Mechanics vol. 2. North-Holland, 1981. URL: <https://books.google.fr/books?id=VR93vUk8d\8C> (cit. on pp. 47, 95–97, 103, 107).
- [45] B. R. A. Nijboer and Th. W. Ruijgrok. “On the energy per particle in three- and two-dimensional Wigner lattices.” In: *Journal of Statistical Physics* 53.1 (), pp. 361–382. DOI: 10.1007/BF01011562. URL: <http://dx.doi.org/10.1007/BF01011562> (cit. on p. 53).
- [46] Trenton H. Parsell, Meng-Yin Yang, and A. S. Borovik. “C-H Bond Cleavage with Reductants: Re-Investigating the Reactivity of Monomeric MnIII/IV-Oxo Complexes and the Role of Oxo Ligand Basicity.” In: *Journal of the American Chemical Society* 131.8 (2009). PMID: 19196005, pp. 2762–2763. DOI: 10.1021/ja8100825. eprint: <http://dx.doi.org/10.1021/ja8100825>. URL: <http://dx.doi.org/10.1021/ja8100825> (cit. on p. 1).
- [47] German L. Perlovich, Tatyana V. Volkova, and Annette Bauer-Brandl. “Towards an understanding of the molecular mechanism of solvation of drug molecules: A thermodynamic approach by crystal lattice energy, sublimation, and solubility exemplified by paracetamol, acetanilide, and phenacetin.” In: *Journal of Pharmaceutical Sciences* 95.10 (), pp. 2158–2169. DOI: 10.1002/jps.20674. URL: <http://dx.doi.org/10.1002/jps.20674> (cit. on p. 1).
- [48] GermanL Perlovich and Annette Bauer-Brandl. “Solvation of Drugs as a Key for Understanding Partitioning and Passive Transport Exemplified by NSAIDs.” In: *Chemical Processes with Participation of Biological and Related Compounds*. CRC Press, 2008, pp. 291–325. DOI: doi:10.1201/b12241-9. URL: <http://dx.doi.org/10.1201/b12241-9> (cit. on p. 1).
- [49] William H. Press, Saul A. Teukolsky, William T. Vetterling, and Brian P. Flannery. *Numerical Recipes 3rd Edition: The Art of Scientific Computing*. 3rd ed. New York, NY, USA: Cambridge University Press, 2007 (cit. on pp. 46, 63, 70, 93).
- [50] Joël Puibasset and Luc Belloni. “Bridge function for the dipolar fluid from simulation.” In: *The Journal of Chemical Physics* 136.15, 154503 (2012), pp. –. DOI: <http://dx.doi.org/10.1063/1.4703899>. URL: <http://scitation.aip.org/content/aip/journal/jcp/136/15/10.1063/1.4703899> (cit. on p. 33).
- [51] R E Raab and O L De Lange. *Multipole theory in electromagnetism: classical, quantum, and symmetry aspects, with applications*. International series of monographs on physics. Oxford: Clarendon Press, 2005. URL: <https://cds.cern.ch/record/859649> (cit. on p. 54).
- [52] Rosa Ramirez and Daniel Borgis. “Density Functional Theory of Solvation and Its Relation to Implicit Solvent Models.” In: *The Journal of Physical Chemistry B* 109.14 (2005), pp. 6754–6763. DOI: 10.1021/jp045453v. URL: <http://dx.doi.org/10.1021/jp045453v> (visited on 07/05/2010) (cit. on p. 3).
- [53] Rosa Ramirez, Ralph Gebauer, Michel Mareschal, and Daniel Borgis. “Density functional theory of solvation in a polar solvent: Extracting the functional from homogeneous solvent simulations.” In: *Physical Review E* 66.3 (2002), pp. 031206–031206–8. DOI: 10.1103/PhysRevE.66.031206. URL: <http://link.aps.org/doi/10.1103/PhysRevE.66.031206> (visited on 03/01/2012) (cit. on p. 3).

- [54] Benoit Roux and Thomas Simonson. “Implicit solvent models.” In: *Biophysical Chemistry* 78.1–2 (Apr. 1999), pp. 1–20. DOI: 10.1016/S0301-4622(98)00226-9. URL: <http://www.sciencedirect.com/science/article/pii/S0301462298002269> (visited on 04/29/2014) (cit. on p. 9).
- [55] V.R. Saunders, C. Freyria-Fava, R. Dovesi, L. Salasco, and C. Roetti. “On the electrostatic potential in crystalline systems where the charge density is expanded in Gaussian functions.” In: *Molecular Physics* 77.4 (1992), pp. 629–665. DOI: 10.1080/00268979200102671. eprint: <http://dx.doi.org/10.1080/00268979200102671> (cit. on p. 54).
- [56] Volodymyr P. Sergiievskyi, Guillaume Jeanmairet, Maximilien Levesque, and Daniel Borgis. “Fast Computation of Solvation Free Energies with Molecular Density Functional Theory: Thermodynamic-Ensemble Partial Molar Volume Corrections.” In: *The Journal of Physical Chemistry Letters* 5.11 (2014), pp. 1935–1942. DOI: 10.1021/jz500428s. URL: <http://dx.doi.org/10.1021/jz500428s> (visited on 07/07/2014) (cit. on p. 3).
- [57] Michiel Sprik and Michael L. Klein. “A polarizable model for water using distributed charge sites.” In: *The Journal of Chemical Physics* 89.12 (1988), pp. 7556–7560. DOI: <http://dx.doi.org/10.1063/1.455722>. URL: <http://scitation.aip.org/content/aip/journal/jcp/89/12/10.1063/1.455722> (cit. on p. 3).
- [58] Jacopo Tomasi, Benedetta Mennucci, and Roberto Cammi. “Quantum Mechanical Continuum Solvation Models.” In: *Chemical Reviews* 105.8 (2005), pp. 2999–3094. DOI: 10.1021/cr9904009. URL: <http://dx.doi.org/10.1021/cr9904009> (visited on 12/13/2012) (cit. on pp. 2, 8).
- [59] Jacopo Tomasi and Maurizio Persico. “Molecular Interactions in Solution: An Overview of Methods Based on Continuous Distributions of the Solvent.” In: *Chemical Reviews* 94.7 (1994), pp. 2027–2094. DOI: 10.1021/cr00031a013. eprint: <http://dx.doi.org/10.1021/cr00031a013>. URL: <http://dx.doi.org/10.1021/cr00031a013> (cit. on pp. 2, 7, 8).
- [60] Samuel Williams, Andrew Waterman, and David Patterson. “Roofline: An Insightful Visual Performance Model for Multicore Architectures.” In: *Commun. ACM* 52.4 (Apr. 2009), pp. 65–76. DOI: 10.1145/1498765.1498785. URL: <http://doi.acm.org/10.1145/1498765.1498785> (cit. on p. 90).
- [61] Shuangliang Zhao, Rosa Ramirez, Rodolphe Vuilleumier, and Daniel Borgis. “Molecular density functional theory of solvation: From polar solvents to water.” In: *The Journal of Chemical Physics* 134.19, 194102 (2011). DOI: <http://dx.doi.org/10.1063/1.3589142>. URL: <http://scitation.aip.org/content/aip/journal/jcp/134/19/10.1063/1.3589142> (cit. on pp. 3, 13, 31, 35).
- [62] Ciyou Zhu, Richard H. Byrd, Peihuang Lu, and Jorge Nocedal. “Algorithm 778: L-BFGS-B: Fortran subroutines for large-scale bound-constrained optimization.” In: *ACM Transactions on Mathematical Software* 23.4 (Dec. 1997), pp. 550–560. DOI: 10.1145/279232.279236. URL: <https://acces-distant.upmc.fr/http/portal.acm.org/citation.cfm?doid=279232.279236> (visited on 06/09/2011) (cit. on p. 28).